QUARTERLY PROGRESS REPORT

OCTOBER 15, 1954

RESEARCH LABORATORY OF ELECTRONICS

MASSACHUSETTS INSTITUTE OF TECHNOLOGY

CAMBRIDGE, MASSACHUSETTS

M 1707 W
HV 1H

The F
mental l
and the

The re
part by
nology,
Army S
Researcl
Researcl
Contract
the Arm

depart-
neering

sible in
Tech-
by the
Naval
ch, Air
Corps
ent of

M.C. MIGEL LIBRARY
AMERICAN PRINTING
HOUSE FOR THE BLIND

MASSACHUSETTS INSTITUTE OF TECHNOLOGY

RESEARCH LABORATORY OF ELECTRONICS

QUARTERLY PROGRESS REPORT

October 15, 1954

Submitted by: J. B. Wiesner
G. G. Harvey
H. J. Zimmermann

TABLE OF CONTENTS

Personnel		v
Publications and Reports		viii
Introduction		x
I.	Physical Electronics	1
	Electron Emission Problems	1
	A Redetermination of the Crystallographic Variation of Electron Field Emission from Tungsten	1
	Growth of Single Crystals of Tantalum	1
	Experimental Studies	2
	Ionization Gauge Control Circuit and Ionization Gauge	2
	Infrared Radiation Pyrometer	3
II.	Microwave Gaseous Discharges	4
	Microwave Breakdown in Hydrogen at High Pressures	4
	Plasma Oscillation	5
	Microwave Determination of the Probability of Collision of Slow Electrons in Neon	6
III.	Solid State Physics	7
	Dynamic Reversibility in the Kinetic Theory	7
	Microwave Study of Semiconductors	7
IV.	Low Temperature Physics	10
	The Viscosity of Liquid Helium	10
	Hall-Effect and Magneto-Resistance Effect Measurements in Resistance Minimum Metals: Discussion of Feasibility	12
V.	Microwave Spectroscopy	14
	A Paramagnetic Resonance Study of Ammonium Chrome Alum	14
	Hindered Rotation in Semisymmetric Molecules	15
VI.	Magnet Laboratory Research	17
	Nuclear Orientation in Mercury Vapor	17
	Nuclear Magnetic Resonance in Gases	18
	Stepwise Excitation of Mercury	20
VII.	Microwave Tube Research	23
	Equivalent Circuit for a Three-Terminal Pair Network	23
	The Minimum Noise Figure of Longitudinal Beam Amplifiers	24
	Beam Noise Measurements	27
	The Internally Coated Cathode	27
VIII.	Atomic Beam Research	30
	Cesium Clock	30
	Well-Collimated Atomic Beam Ovens	34
	Hyperfine Structure Anomalies in Cesium Radioisotopes	38
	Nuclear Magnetic Octupole Moments of the Stable Gallium Isotopes	39

	Hyperfine Structure of Halogens	41
IX.	Multipath Transmission	42
	Narrow-Band Limiting	42
X.	Statistical Communication Theory	48
	A Theorem Concerning Noise Figures	48
	The Wiener Theory of Nonlinear Systems	55
	Properties of Second-Order Autocorrelation Functions	63
	Field Mapping by Crosscorrelation	66
	Correlation Detection of a Periodic Signal Multiplied by Noise	69
	An Improvement in the Digital Electronic Correlator	74
	Measurement of Industrial Process Behavior	75
XI.	Speech Analysis	77
	Recognition of Silences	77
	The Nasal Consonants	79
XII.	Visual Replacement Projects	82
	Acoustic Obstacle Detection	82
	New Step-Down Detector	84
XIII.	Communications Biophysics	87
	A Probabilistic Approach to Certain Neuroelectric Phenomena	87
	Analog Correlator for Electroencephalography	95
XIV.	Analog Computer Research	96
	Time Domain Synthesis by Delay Line Techniques	96
XV.	Network Synthesis	97
	Voltage Transfer Synthesis – RLC Lattice	97
XVI.	Switching Control Systems	100

HV1707
W

PERSONNEL

Administration

Professor J. B. Wiesner, Director
Professor G. G. Harvey, Associate Director
Professor H. J. Zimmermann, Associate Director
Mr. R. A. Sayers, Personnel and Business Manager
Mr. C. B. Leard, Purchasing Agent
Mr. J. H. Hewitt, Librarian

Advisory Committee

Professor G. S. Brown
Professor N. H. Frank
Professor G. G. Harvey
Professor A. G. Hill
Professor J. A. Stratton
Professor J. B. Wiesner
Professor H. J. Zimmermann

Faculty, Instructors, and Research Associates

Adler, R. B.
Allis, W. P.
Barlow, J. S.
Bavelas, A.
Bitter, F.
Bobroff, D. L.
Brazier, Mary A. B.
Brown, G. S.
Brown, S. C.
Caldwell, S. C.
Chu, L. J.
Edgerton, H. E.
Elias, P.
Fano, R. M.
Feld, B. T.
Frank, N. H.
Garland, C. W.
Guillemin, E. A.
Halle, M.
Harvey, G. G.
Haus, H. A.
Herlin, M. A.
Hill, A. G.
Huffman, D. A.
King, J. G.
Kivelson, D.
Lee, Y. W.
Lees, A. B.
Licklider, J. C. R.
Linvill, W. K.
Locke, W. N.
Maffeo, P. D., Jr.
Mason, S. J.
Nottingham, W. B.
Radford, W. H.
Reza, F. M.
Rosenblith, W. A.
Scott, R. E.
Strandberg, M. W. P.
Stratton, J. A.
Thomas, J. E., Jr.
Waugh, J. S.
Wiesner, J. B.
Youngblood, W. A.
Zacharias, J. R.
Zimmermann, H. J.

Electronics Laboratory Staff Members and Guests

Abrams, Fern S.
Andrew, A. M.
Badessa, R. S.
Bowser, Sara E.
Brown, R. M.
Burdine, B. H.
Campbell, Elizabeth J.
Cavileer, R. P.
Davis, C. W.
Dunn, J. M.
Ferretti, E.
Fricker, S. J.
Fried, C.
Ginsburgh, Ethel L.
Gould, D. H.
Graham, J. W.
Handsaker, K.
Hewitt, J. H.
Howland, B.
Hurtig, C. R.
Ingersoll, J. G.
Ingraham, E. C.
Johnson, L. B.
Kent, R. L.
Keyes, R. V., Jr.
Land, Helen R.
Leard, C. B.
Lettvin, J. Y.
Loesch, B.
Long, R. E.
Marill, T. M.
Matheson, A. I.
McCarthy, J. J.
McCulloch, W. S.
Moore, M. H., Jr.
Morgenroth, C.
Nowell, J. C., III
Pitts, W. H.
Raab, D. H.
Rosebury, F.
Rosenbloom, M.
Ryan, L. W.
Sagalyn, P. L.
Sayers, R. A.
Schwartz, C. L.
Searle, C. L.
Smullin, L. D.
Smythe, Miriam C.
Tilley, R. B.
Wall, P. D.
Witcher, C. M.
Yngve, V. H.

PERSONNEL

Research Assistants and Students

Abu-Zeid, M. M.
Adams, N. I., III
Adolph, A. R.
Aisenberg, S.
Armstrong, D. B.
Aubrey, B. B.
Baghdady, E. J.
Bello, P. A.
Bers, A.
Bose, A. G.
Breckenridge, W. G.
Buchsbaum, S. J.
Bullis, W. M.
Capon, J.
Connor, T. J.
Cruz, J. B., Jr.
DeClaris, N.
Dickey, D. H.
Edmonds, D. S., Jr.
Elkan, J.
Folkart, Barbara M.
Freeman, R. F.
Frishkopf, L. S.
Gilardini, A. L.
Gordon, E. I.
Gross, J.
Gruber, S.
Haun, R. D., Jr.
Hayase, J. Y.
Heinzerling, E. W.
Higier, T.
Hilibrand, J.
Hiller, E. R., Jr.
Ho, Y. C.
Holloway, J. H.
Houston, J. M.
Hughes, G. W.
Jennings, L. D., Jr.
Jordan, K. L.
Josephson, B., Jr.
Kleiman, H.
Kolm, H. H.
Kosowsky, D. I.
Krongelb, S.
Lange, W. J.
Lerner, R. M.
Lewis, P. M., II
Lichtenberg, A. J.
Littlefield, K. E.
Lorens, C. S.
Lull, R. E.
Lustig, E.
Macy, J., Jr.
Margolis, S. G.
McCluskey, E. J., Jr.
McElvery, R. M.
McRae, D. D.
McWhorter, A. L.
Murray, G. R., Jr.
Osborne, A. J.
Peter, M.
Pezaris, S. D.
Pinson, J. C.
Powers, K. H.
Pucel, R. A.
Pugh, A. L., III
Radley, J. -P. A.
Savage, D. E.
Schatz, Carol D.
Sciegienny, J.
Shelton, H.
Slutsky, L. J.
Smith, W. B.
Sprenger, T. I.
Stanley, J. R.
Stein, S.
Stern, T. E.
Stirman, J. P.
Stoddard, J. C.
Strieby, M.
Stroke, H. H.
Swan, P. R., Jr.
Thomas, J. B.
Thornton, R. D.
Unger, S. H.
Wennstrom, A.
Wernikoff, R. E.
Weston, B. J.
Whitney, W. M.
Williard, M. W.
Wolga, G. J.
Wright, J. W.
Young, J. E. R.
Yussuf, S. E.

Draftsmen

Navedonsky, C. P., Foreman
Rollins, I. E.
Williams, R. P.
Wittekind, Jean M.

Machine Shop

Keefe, J. B., Foreman
Barnet, F. J.
Beers, N. E.
Bletzer, P. W.
Brennan, J., Helper
Bunick, F. J.
Carter, C. E.
Coyle, J. E.
Fortunato, J. P.
Gibbons, W. D.
Liljeholm, F. H.
Marshall, J. M.
McLean, J. J.
Nickerson, C. R.
O'Brien, F. J.
Papa, D. C.
Sanromá, J. B.
Smart, D. A.
Yena, J. V.

PERSONNEL

Secretaries

Bender, Dorothy L.
Berman, Barbara R.
Charait, Shirley E.
Connell, Rosemarie
Corvino, Nancy A.
Crimmings, Anne F.
D'Amato, Marjorie A.
DeMember, Lucille M.
Grace, Jane C.
Hayes, M. Patricia
Moyer, June
Nicholson, Edith D.
Scanlon, Dorothea C.
Tranfaglia, Angelyn A.
Yelovitz, Diane

Stock Rooms

Hughes, M. F., Foreman
Bella, C. J., Clerk
Boyle, L. E., Clerk
Cloran, H. J.
Haggerty, R. H.
McFarland, T. E.

Technicians and Assistants

Aborjaily, Catherine S.
Ames, S. R.
Barrett, J. W.
Belinski, A. M.
Calileo, D. W.
Caulfield, J. F.
Chetkauskas, L.
Colaruotola, J. F.
Diver, B. J.
Faltin, C. L.
Fralin, E. W.
Goddard, L. W., Jr.
Goodridge, Elizabeth
Hanasik, J. R.
Karas, P.
Kelly, M. A.
Kierstead, J. D.
Konopacki, J. F.
Lewis, R. R.
Lorden, G. J.
Perullo, F. R.
Sears, A. R.
Serini, Ann G.
Sprague, L. E.
Sutherland, L. J.
Washington, L., Jr.
Weiss, R.

Tube Laboratory

Glass Blowers

Smullin, L. D.
Rosebury, F.
Ryan, L. W.
Roman, Ruth R.
Velluto, A. J.

Technicians

Cox, Alice G.
Doucette, W. F.
Johnson, Dorothy B.
MacDonald, A. A.
Ricchio, F. P.

Technicians' Shop

Berg, A. E., Foreman
Fownes, Marilyn R.
Hanasik, Catherine
Joy, C. R.

PUBLICATIONS AND REPORTS

MEETING PAPERS PRESENTED

Spectroscopy Symposium, University of Ohio, Columbus
June 14-18, 1954

D. Kivelson, Theory of the interaction of hindered internal rotation with over-all rotations.

Symposium on Vacuum Technology, Asbury Park, New Jersey
June 17, 1954

W. B. Nottingham, Design and properties of the M.I.T. modified Bayard-Alpert gauge.

Acoustical Society of America, New York
June 23-26, 1954

L. S. Frishkopf and W. A. Rosenblith, Neural responses to clicks: an analysis of masked and unmasked intensity functions.

AIEE-IRE Semiconductor Device Research Conference, University of Minnesota, Minneapolis, June 28-30, 1954

A. L. McWhorter and R. H. Kingston, Channels and excess current in grown junction diodes.

American Physical Society, Electronic Physics Division, University of Minnesota, Minneapolis, June 29, 1954

W. P. Allis, Electrical discharges in microwave cavities (invited paper).

Conference on the Physics of Ionized Gases, Birmingham, England
July 5-6, 1954

S. C. Brown, Low-energy electron collision cross sections in helium (courtesy of The Royal Society).

Gordon Research Conference on Instrumentation, New London, New Hampshire
July 27, 1954

P. Elias, Information theory.

Atomic Beam Conference, Brookhaven National Laboratory, Upton, L.I., New York
Aug. 18-19, 1954

R. T. Daly, Jr., Precision experiments with gallium.

C. L. Schwartz, The theory of nuclear octupole interactions.

H. H. Stroke, Hyperfine structure anomalies in cesium isotopes (invited paper).

Association of Teachers of Mathematics in New England, M.I.T., Cambridge
Aug. 20, 1954

C. M. Witcher, Teaching mathematics to the blind.

MEETING PAPERS PRESENTED (continued)

International URSI Meeting, Amsterdam
Aug. 23 - Sept. 2, 1954

P. Elias, Error-free coding.

International Mathematical Congress, Amsterdam
Sept. 2-9, 1954

F. M. Reza, Some geometrical properties of the root locus curve.

JOURNAL ARTICLES ACCEPTED FOR PUBLICATION

(Reprints of these and previous articles still in print are available from the Document Room, 20-B-221, Research Laboratory of Electronics, Massachusetts Institute of Technology, Cambridge 39, Massachusetts)

E. J. Baghdady, Frequency-modulation rejection with narrow-band limiters (Proc. I.R.E.)

Y. Bar-Hillel, Structural linguistics, logical syntax, and semantics (Language)

F. Bitter, S. P. Davis, B. Richter, and J. E. R. Young, Optical studies of radioactive mercury (Phys. Rev.)

L. Gould and S. C. Brown, Microwave determination of the probability of collision of electrons in helium (Phys. Rev.)

W. Grattidge, A scale expander for a recording potentiometer (Rev. Sci. Instr.) (Laboratory and Shop Notes)

M. Halle, The strategy of phonemics (Word)

M. Halle, Why and how do we study the sounds of speech? (Report of Fifth Annual Round Table Meeting on Linguistics and Language Teaching)

B. Howland, J. Y. Lettvin, W. S. McCulloch, W. H. Pitts, and P. D. Wall, Studies on the nature of reflex inhibition produced by the interaction of volleys running in neighboring dorsal roots (J. Neurophysiol.)

J. G. King and V. Jaccarino, The hyperfine structure and nuclear moments of the stable bromine isotopes (Phys. Rev.)

D. Kivelson, Theory of the interaction of hindered internal rotation with over-all rotations. I. Symmetric rotors: methyl silane (J. Chem. Phys.)

D. H. Looney and S. C. Brown, The excitation of plasma oscillations (Phys. Rev.) (Technical Report No. 273)

Carol D. Schatz, The role of context in the perception of stops (Language)

P. A. Tate and M. W. P. Strandberg, A simple high temperature microwave spectrograph (Rev. Sci. Instr.)

C. M. Witcher, Physics without sight (Physics Today)

C. M. Witcher and L. Washington, Jr., Sonar for the blind? (Electronics)

V. H. Yngve, The machine and the man (Mechanical Translation)

V. H. Yngve, Mechanical translation (Science (Japan))

Introduction

This report, the thirty-fifth in a series of quarterly progress reports issued by the Research Laboratory of Electronics, contains a review of the research activities of the Laboratory for the three-month period ending August 31, 1954. Inasmuch as this is a preliminary report, no results should be considered final.

I. PHYSICAL ELECTRONICS

Prof. W. B. Nottingham
S. Aisenberg
W. M. Bullis
D. H. Dickey
J. D. Hobbs
J. M. Houston
W. J. Lange
L. E. Sprague

A. ELECTRON EMISSION PROBLEMS

1. A Redetermination of the Crystallographic Variation of Electron Field Emission from Tungsten

This work has been completed and will be presented in Technical Report No. 286.

A correction is necessary to the discussion of experimental results given in the Quarterly Progress Report of July 15, 1954. The discontinuity in slope at approximately 800°K noted in the preliminary emission vs. temperature measurements was found to be nonexistent when a more accurate temperature scale was used. The remainder of the discussion is still correct.

J. M. Houston

2. Growth of Single Crystals of Tantalum

Some rather large single crystals of tantalum have been grown by resistance heating and a moving temperature gradient. The moving temperature gradient is achieved by using mercury as the electrode, as shown in Fig. I-1. The tantalum ribbon is fastened to the upper electrode. The lower end of the ribbon is welded to a 5-cm length of 120-mil tungsten rod which is submerged in the mercury and serves to weight the ribbon sufficiently to overcome surface tension and maintain the ribbon vertical.

With the metal high-vacuum valve closed, enough air is admitted to the mercury reservoir through the stopcock to push mercury into the tube containing the ribbon. The metal valve is used as an adjustable slow leak to the forepump, which slowly exhausts the air from the mercury reservoir, thus lowering the level in the tube at the desired rate.

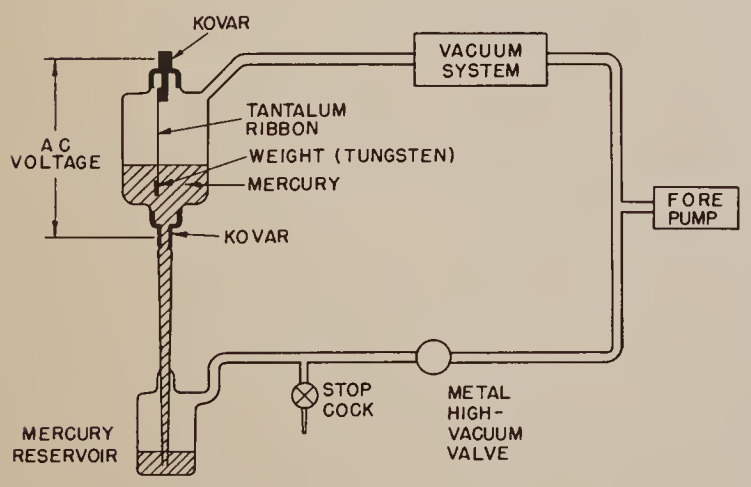

Fig. I-1
Tantalum crystal-growing setup.

The tantalum ribbon is 1 mil thick and 2-3 mm wide. We have obtained the largest crystals after a 3 per cent cold work, as first reported by Mrowca (1). We have cold-worked the tantalum by cold rolling rather than cold stretch. The percentage of cold roll is then measured by the elongation of the ribbon. With a

temperature of about 2400°K and a mercury lowering rate of approximately 8 mm/hr, at least one single crystal of approximately 1 cm in length is obtained on nearly every run of 6 to 8 hours.

W. J. Lange

References

1. B. A. Mrowca, J. Appl. Phys. 14, 684 (1943).

B. EXPERIMENTAL STUDIES

1. Ionization Gauge Control Circuit and Ionization Gauge

The ionization gauge control circuit has been constructed, modified, and used. The modifications include an additional negative feedback loop to reduce the input impedance, the time constant, and the zero drift (caused by line voltage variation). A diode limiter was also included to protect the electron current meter against accidental shorts. The circuit is still free from batteries. When the drawings and operating instructions have been completed, a more detailed description of the circuit will be given.

In order to test the operation of the control circuit, it was used to investigate the variation with geometry of the gauge sensitivity of the screened Bayard-Alpert type of ionization gauge. The sensitivity of the ion gauge is measured by: $K = 1/p\ (i_+/i_-)$, where i_+ and i_- are the ion and electron currents, and p is the pressure. The sensitivity, K, depends upon the nature of the gas, the electrode potentials, the electrode geometry, and is not supposed to depend upon electron current. The Bayard-Alpert ion gauge in our laboratory has two supposedly identical filaments: one used as the electron emitter, and the other as a flash filament and a spare. In operation, the flash filament is at electron collector potential, while the emitting filament is 100 volts negative with respect to the electron collector. Using the modified ion control circuit plus an appropriate switching circuit to quickly interchange the two hot filaments electrically, the relative values of the gauge constants for the two filaments were measured for various identical electron currents. Not only was a discrepancy found between the two gauge constants, where none was expected, but the discrepancy was a function of the electron current, and varied from approximately 20 per cent at 10 μa to 10 per cent at 10 ma for a sealed-off ion gauge. Incomplete measurements on another gauge indicate that the discrepancy can be as great as 40 per cent, and may cause a corresponding error in the pressure measurement. The discrepancy was reduced at high electron currents, probably because the higher space charge influenced the electron orbits more than the electrode geometry and made the difference in geometry less important.

The results indicate that the gauge constant K depends upon the electron current,

and that the ion current is therefore not exactly a linear function of electron current, as is commonly supposed. A method has been developed for measuring the dependence of ion current upon electron current in spite of the changes of pressure caused by changes of current to the electron collector.

S. Aisenberg

2. Infrared Radiation Pyrometer

Preliminary measurements taken with an optical bench model of the revised optical system described in the Quarterly Progress Report, July 15, 1954, indicate that the sensitivity and response are substantially the same as previously reported.

A pilot model of the complete revised optical system has been constructed; the prism has been procured, and when it is prepared this system will be aligned and further tests made.

W. M. Bullis

II. MICROWAVE GASEOUS DISCHARGES

Prof. S. C. Brown
Prof. W. P. Allis
A. L. Gilardini
E. Gordon
Helen R. Land
J. J. McCarthy

A. MICROWAVE BREAKDOWN IN HYDROGEN AT HIGH PRESSURES

In preparation for extending data on the continuous wave breakdown of hydrogen at high pressure by the use of pulse techniques, a study was made of the effect of various pulse widths and pulse repetition frequencies on the breakdown of hydrogen. This was done to determine what combinations of pulse widths and pulse repetition frequencies would give values of breakdown electric field equal to that obtained for the continuous wave. The heavy lines in Fig. II-1 represent the data taken of breakdown for various values of pulse repetition frequency as a function of pulse width for a given value of pressure of hydrogen. In all instances, as the pulse width increases, the value of breakdown electric field approaches that for continuous wave breakdown. This effect, of course, occurs at smaller values of pulse width for large repetition rates than for small repetition rates.

Because the plate dissipation of the magnetron is limited, the increased peak output of the magnetron must be accompanied by an appropriate change in the duty cycle of the pulse. If the peak power is to be twice the continuous wave power, the duty cycle must not exceed 0.5. On the curves of Fig. II-1 the pulse duty cycle is plotted as a dotted line. From these curves it can be seen that there are values of duty cycles which make it impossible to obtain the combinations of pulse width and pulse repetition frequency which would give an equivalent continuous wave breakdown. However, for duty cycles greater than 0.1 there are combinations of pulse width and repetition frequency which give an equivalent continuous wave breakdown. Data obtained at different pressures indicate that the percentage deviation of pulse breakdown from continuous wave breakdown decreases as the pressure increases; thus it is reasonable to assume that a duty cycle that permits equivalent continuous wave breakdown at the pressure indicated in the figure will continue to do so as the pressure increases.

The trend of these constant duty cycle curves can be understood through the realization that the time required to obtain breakdown in the gas is the time required for the electron density in the gas to reach the ambipolar transition density of approximately 10^7 electrons/cm^3. There are, however, an initial number of electrons left over from the previous breakdown which can influence the time required to obtain the necessary build-up of electron density. An equivalent continuous wave breakdown is obtained when the electron density builds up within the limits of a given pulse width to the ambipolar transition density from an original density determined by the time elapsed since the previous breakdown. The build-up of electron density is determined by the free diffusion of electrons in hydrogen; the decay of electron density after a breakdown is determined by

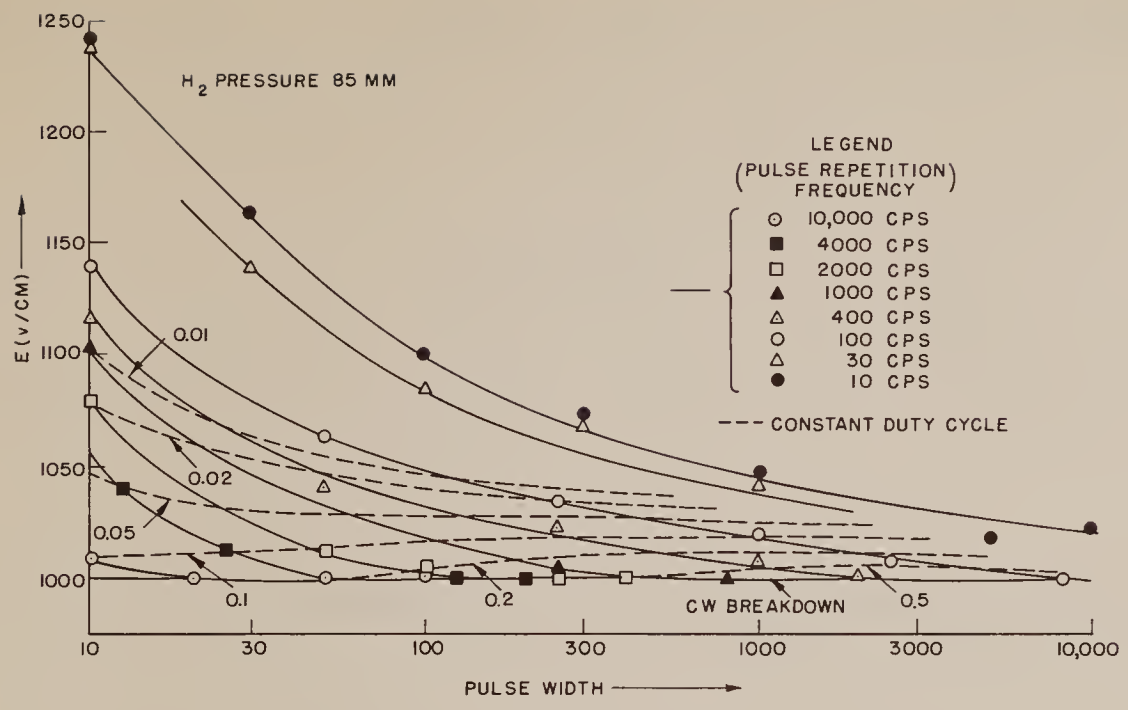

Fig. II-1

The variation of breakdown field as a function of pulse width and pulse repetition frequency showing the effect of the pulse duty cycle.

the ambipolar diffusion of electrons in hydrogen from the breakdown density to the ambipolar transition density. If the pulse repetition frequency is smaller than a critical frequency, practically no influence is felt from the electrons of the previous discharge and the pulse breakdown for a given pulse width should no longer be a function of pulse frequency. The decay of electron density in the ambipolar region is given by

$$n = n_o \exp\left(-\frac{D_a}{\Lambda^2} t\right)$$

where n_o = initial electron density, n = density at time t, D_a = ambipolar diffusion coefficient, Λ = diffusion length of cavity, and t = time. For a pressure of 85 mm of Hg, and values of $(D_a p) = 700$, $\Lambda = 0.4$ cm, $n = 10^7$, and $n_o = 10^{10}$, a diffusion time of 0.13 sec is obtained which corresponds approximately to a repetition frequency of 7 to 8 cycles per second.

J. J. McCarthy

B. PLASMA OSCILLATION

To further the investigations of D. H. Looney (1), a tube has been constructed and put into operation (2); oscillations and a standing-wave pattern have been observed. The plasma-beam interaction region was three times the maximum length used by Looney. The purpose of the new tube is to allow independent measurements of the oscillation frequency, plasma electron density, and standing-wave pattern in the interaction region.

(II. MICROWAVE GASEOUS DISCHARGES)

The variation of phase velocity with electron density can now be determined, and the assumption that the plasma electrons behave as a gas which propagates an acoustical pressure wave can be tested using various models of the electron gas.

E. Gordon

References

1. D. H. Looney and S. C. Brown, Phys. Rev. 93, 965 (1954).
2. Quarterly Progress Report, Research Laboratory of Electronics, M.I.T., July 15, 1954, p. 12.

C. MICROWAVE DETERMINATION OF THE PROBABILITY OF COLLISION OF SLOW ELECTRONS IN NEON

The collision probability for momentum transfer of slow electrons in Ne will be measured with the microwave method of Gould and Brown (1). Cataphoresis will be used to purify neon (spectroscopically pure Airco neon) from the other rare gas impurities, and activated uranium to eliminate the impurities that are not rare gases (2).

A. L. Gilardini

References

1. L. Gould and S. C. Brown, Phys. Rev. 95, 897 (1954).
2. R. Riesz and G. H. Dicke, J. Appl. Phys. 25, 196 (1954).

III. SOLID STATE PHYSICS

Prof. W. P. Allis
Prof. S. C. Brown
Prof. G. G. Harvey
Prof. L. Tisza
J. M. Goldey
J. B. Thomas

A. DYNAMIC REVERSIBILITY IN THE KINETIC THEORY

Boltzmann's integral equation is generally assumed to give a correct account of the kinetic processes in gases when the intermolecular interactions can be described in terms of binary collisions. The purpose of the present investigation is to draw attention to an additional limitation.

The fundamental equations of physics satisfy the principle of dynamic reversibility: the transformation reversing the direction of time $t \rightarrow -t$ carries over every solution into another dynamically admissible solution. In contrast, the phenomenological description of such processes as electrical conductivity or viscous flow is irreversible.

It would be desirable to have a statistical theory that contains both the reversible and irreversible aspects and indicates clearly how the latter arises from the former.

It is easily shown that the Boltzmann equation falls short of this requirement. The theory predicts that any inhomogeneity existing at an initial time in an isolated system decays exponentially until the quiescent state is reached. This prediction is in conflict with the principle of dynamic reversibility that requires spontaneous departures from the quiescent state.

From the experimental point of view the implications of the Boltzmann equation are correct for signals above noise level, but the fluctuations (thermal noise) provide us with a clear indication that spontaneous deviations from equilibrium have been too drastically averaged out from the classical theory.

The origin of this shortcoming has been submitted to a detailed analysis, the results of which may be helpful for the formulation of a more general kinetic theory, in which resistivity and noise are accounted for within the same formalism.

L. Tisza

B. MICROWAVE STUDY OF SEMICONDUCTORS

Measurements of the carrier contribution to the dielectric coefficient of germanium have been completed. The carrier contribution is given by $\sigma_i/\omega\epsilon_o$. In order to obtain an effective mass from these measurements, it is necessary to have an expression for σ_i. The general expression for σ in a crystal, from which σ_i may be obtained, is

$$\sigma = \int \frac{(\nabla_k E)_a}{\hbar^2} \frac{e^2}{(\nu_c + j\omega)} \frac{\partial f_o^o}{\partial E} d^3k \qquad (1)$$

where f_o^o is the equilibrium distribution function and $(\nabla_k E)_a$ is the gradient of the energy along the direction a in k space. In order to obtain an expression for σ, therefore, something must be known about the energy surfaces. We have obtained an

expression for σ for the conduction band by assuming that the band edge occurs along the 111 axis and that the surfaces of constant energy are ellipsoids of revolution about the minimum. This is the model recently proposed by Lax and his associates (1).

For this model we obtain

$$\sigma_i = \frac{ne^2\omega}{m^*\left(\nu_c^2 + \omega^2\right)} \tag{2}$$

where m^* is given by

$$m^* = \frac{3m_1m_2}{2m_1 + m_2} \tag{3}$$

where m_1 is the longitudinal mass, and m_2 the transverse mass.

For the same energy surfaces Herring (2) has recently obtained an expression which differs slightly from Eq. 2. His result may be approximated for the present case to

$$\sigma_i = \frac{n\mu^2m^*\omega}{B}\left[1 - \frac{\omega^2(m^*)^2\mu^2}{Be^2}C\right] \tag{4}$$

where

$$B = \frac{3r(2+r)}{(1+2r)^2}$$

where $r = m_1/m_2$ and

$$C = \frac{\left\langle \frac{E}{\nu_c^4} \right\rangle \langle E \rangle}{\left\langle \frac{E}{\nu_c^2} \right\rangle^2}$$

the angular brackets indicating Maxwellian averages.

The valence band of germanium, according to recent evidence (3), is two-fold degenerate with the band edge occurring at the origin. In this case, the holes are distributed between the two degenerate bands. Here, integration of Eq. 1 leads to Eq. 2 again, but the effective mass is obtained from the relation

$$\frac{n}{m^*} = \frac{n_1}{m_1} + \frac{n_2}{m_2}$$

where $n = n_1 + n_2$, and m_1 and m_2 are suitable averages of the masses in the two bands.

The measurements were made at two temperatures. For the N material the conductivity followed the law

$$\sigma_T = \sigma_{300} \left(\frac{300}{T}\right)^{1.66}$$

This value of the exponent is in agreement with that obtained by other workers (4). For the P type we obtained

$$\sigma_T = \sigma_{300} \left(\frac{300}{T}\right)^{2.17}$$

whereas the accepted value of the exponent is 2.33 (4).

The measured values of the effective mass are as follows. For electrons we obtain $m^* = 0.10 \pm 0.05\ m_o$ where we have used Eq. 2. If we use Eq. 4 we have $m^* = 0.08 \pm 0.04\ m_o$, where we have used a mass ratio r of 17 as obtained by Lax et al. (1) in calculating B. For holes, the measured value of the mass is $m^* = 0.33 \pm 0.05\ m_o$ when we have used a value of 2.17 for the temperature exponent. If the temperature exponent is taken as 2.33, we get for the mass $m^* = 0.28 \pm 0.05\ m_o$.

These results, for both N and P types are in agreement with results obtained by cyclotron resonance experiments (1, 3) and magnetic susceptibility measurements (5). They are not in agreement, however, with the results of an experiment similar to the present one (6, 7).

J. M. Goldey

References

1. B. Lax, H. Zeiger, R. N. Dexter, and E. S. Rosenblum, Phys. Rev. 93, 1418 (1954).
2. C. Herring, personal communication.
3. R. N. Dexter, H. Zeiger, and B. Lax, Phys. Rev. 95, 557 (1954).
4. F. J. Morin, Phys. Rev. 93, 62 (1954).
5. J. H. Crawford and D. K. Stevens, Phys. Rev. 94, 1415 (1954).
6. T. S. Benedict and W. Shockley, Phys. Rev. 89, 1152 (1953).
7. T. S. Benedict, Phys. Rev. 91, 1565 (1953).

IV. LOW TEMPERATURE PHYSICS

Prof. M. A. Herlin
Dr. C. W. Garland
R. P. Cavileer
L. D. Jennings, Jr.
H. H. Kolm
W. M. Whitney
J. W. Wright

A. THE VISCOSITY OF LIQUID HELIUM

Measurements made in liquid helium indicate that thermomechanical flow caused by heat input to the rotor is now entirely responsible for the excessive damping observed; all damping from the magnetic bearing itself has been eliminated. The results of two measurements are shown in Fig. IV-1, which represents rotor speed as a function of angular displacement. It will be seen that the timing points fall on straight lines to within 0.5 per cent.

The first curve, taken at 2.17°K, indicates a viscosity of 41 micropoise, which is about twice the value observed by other investigators. The measurement was continued until the level of liquid helium dropped below the rotor; the slope of the curve is seen to change discontinuously at this point, the new value indicating a viscosity of 5 micropoise, the accepted value for helium gas at this temperature. This observation eliminates the possibility of instrumental damping in the most direct possible way.

Calculations indicate that the excessive damping in liquid helium would be accounted for by a heat input of only 6 mw to the rotor. This same heat input would produce an apparent viscosity of 45.8 micropoise at the lower temperature of 1.97°K (the value observed by other investigators is 12 micropoise), which is seen to be in good agreement with the observed value of 44.4 micropoise. It is of interest to note that the thermomechanical damping mechanism in question, being proportional to 1/TS, increases very rapidly below 1.5°K and might account for the observed discrepancy between all oscillating disk measurements on the one hand, and, on the other, some approximate preliminary results obtained by a static method (1).

Figure IV-2 shows the result of a measurement made at higher speeds in an effort to determine the nature of the nonlinear effects observed by other investigators. It is seen that the damping line does not show curvature but changes its slope nearly discontinuously, indicating a new value of apparent viscosity at higher speeds. This observation is in agreement with the "saturation effect" of the excess decrement observed by other authors using oscillating disk methods (2).

It is clear from measurements made thus far that the major source of heat input is eddy current heating owing to corrections made by the servomechanism to counteract mechanical noise. Major changes are necessary to remedy this situation; most expediently, removal of the apparatus to a more favorable location. Further work will not be undertaken until this difficulty can be overcome.

H. H. Kolm

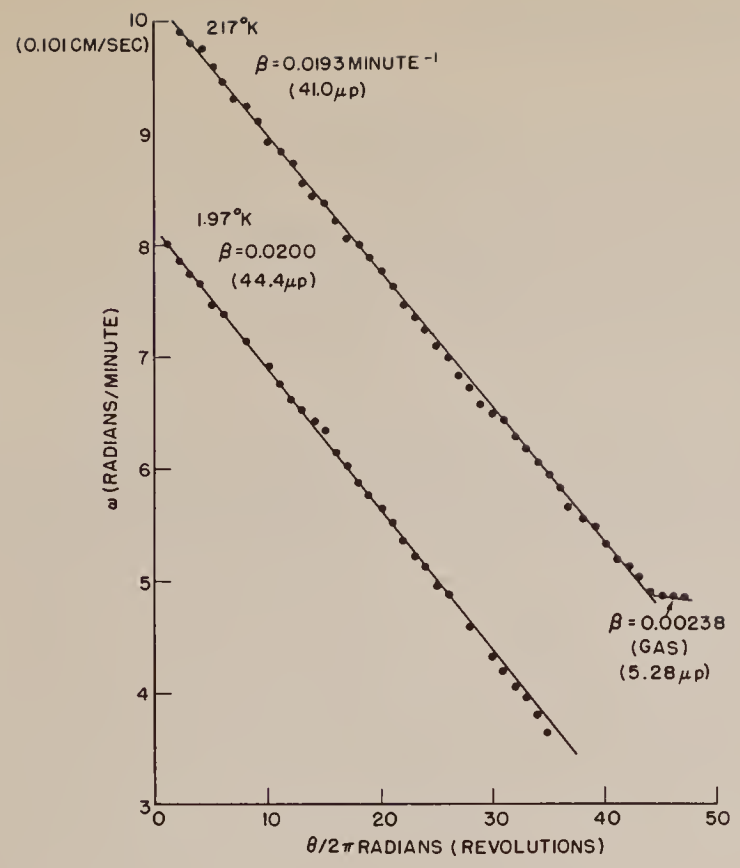

Fig. IV-1

The observed decay of rotation in helium II and in gaseous helium at two temperatures.

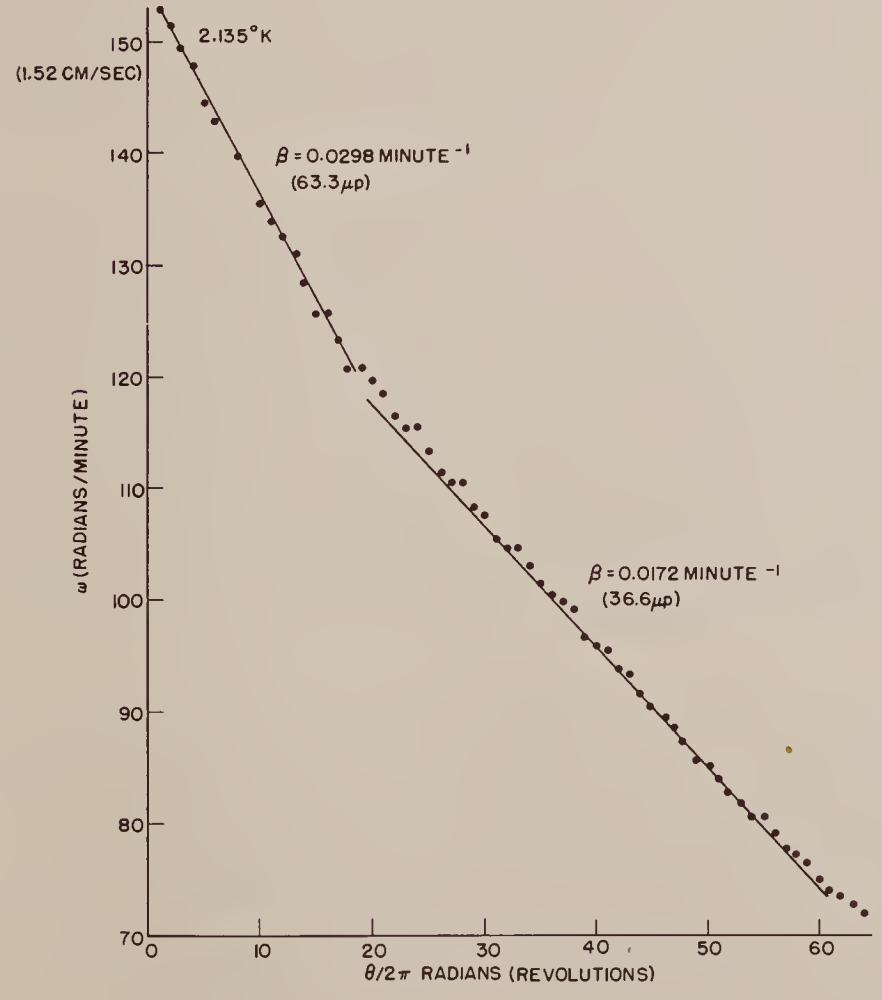

Fig. IV-2

The decay of rotation in helium II at higher speeds.

References

1. J. G. Daunt and R. S. Smith, Revs. Modern Phys. 26, 176 (April 1954).
2. A. C. Hollis-Hallet, Proc. Roy. Soc. (London) A210, 404 (1952).

B. HALL-EFFECT AND MAGNETO-RESISTANCE EFFECT MEASUREMENTS IN RESISTANCE MINIMUM METALS: DISCUSSION OF FEASIBILITY

The "resistance minimum" effect in magnesium has been investigated through measurement of electric and thermal conductivities and thermoelectric power. Electric conductivity has been investigated through a mutual-inductance technique so that bulk samples could be used. In order to separate effects of the mean free path and the electron energy level density, it is desirable to measure the Hall effect. Also, the magneto-resistance effect has already proved enlightening in other resistance minimum metals. Because of the high electrical conductivity, the conventional Hall-effect measurement method requires fine films of metal to provide sufficiently high Hall emfs, and the metallurgical state of the film is difficult to control. It is desirable, therefore, to devise a mutual-inductance method for this measurement, also. Mutual inductance techniques for measurements on magnetic salts have been improved in this laboratory by L. D. Jennings and the writer. It is now possible to apply these methods to Hall-effect measurements with adequate accuracy.

In essence the mutual inductance as a function of applied dc magnetic field for two different coil configurations (described below) determines both the magneto-resistance and Hall coefficients. For mathematical simplicity a spherical sample is chosen. In the first configuration, the axes of the primary and secondary coils are aligned parallel to the applied dc magnetic field. The Hall effect is then radial and contributes nothing to the emf induced in the secondary coil. The effect of unavoidable misalignment of the secondary coil has been computed and is unimportant. This is essentially, then, the experiment of Rorschach and Herlin; the conductivity is obtained as a function of magnetic field.

In the second configuration the primary and secondary coils and the magnetic field are mutually perpendicular. The circulating currents induced by the primary field are diverted by the dc field, producing an induced emf in the secondary. In the conventional Hall experiment, the current lines are constrained to flow parallel to edges of the metal by the Hall field caused by edge charges. In this method the current is actually diverted, and the change in mutual inductance gives the product of the conductivity and the Hall constant. The conductivity measurement is therefore a necessary companion experiment.

In the second configuration, the alignment of the primary with respect to the secondary is critical, but the alignment of either coil with respect to the magnetic field is not. The effect of primary-secondary misalignment may be corrected by rotation of the dc field ninety degrees into the direction of the primary. The mutual inductance thus measured will be that without the Hall effect and will constitute the major correction due to misalignment.

With realizable coils, the anticipated change of mutual inductance over the whole range of magnetic field up to 10,000 gauss is of the order of 0.1 to 1 microhenry. The bridge to be used is sensitive to 0.001 microhenry, so that a precision of one per cent should prevail.

J. W. Wright

V. MICROWAVE SPECTROSCOPY

Prof. M. W. P. Strandberg
Dr. D. Kivelson
C. F. Davis, Jr.
H. Dreicer
J. G. Ingersoll
B. Josephson, Jr.
J. D. Kierstead
S. Krongelb
M. Peter
I. H. Solt, Jr.
P. R. Swan, Jr.
M. Tinkham
G. J. Wolga

A. A PARAMAGNETIC RESONANCE STUDY OF AMMONIUM CHROME ALUM

A detailed solution of the fine structure splitting of the trivalent chromium ground state has been calculated. The effect of the neighbors of the paramagnetic ion was assumed representable by an electric potential of cubic symmetry with a slight trigonal (axial) distortion (1). Matrix elements of the orbital splitting were obtained by the method of Racah (2) assuming only that the expression for the equivalent crystalline potential obeys the same commutation rules with the angular momentum that spherical harmonics do. The effect on energy levels and intensities of spin-orbit coupling and of a magnetic field at an arbitrary angle to the axial distortion was calculated to second order. Otherwise, orientation of the magnetic field in the cubic coordinates does not affect the energy levels, but does alter line intensities for specimen orientations of two-fold (and less) symmetry.

The degeneracy removal by orientation dependent off-diagonal terms and the difficulty in assigning uniformly suitable designations to the energy levels result in three discontinuities in matrix elements and in field derivatives of energy levels as a function of orientation and field.

Line positions and intensities were calculated and checked with experiment. Positions corresponded within 0.2 per cent except where measurement was unusually difficult because of very weak absorptions or interference between two overlapping lines. Intensities generally correlated within a factor of two (within much less when the lines were well separated) and had "regular" shape. In each case, correction was made for linewidth and for observation of absorption at constant frequency instead of constant magnetic field. Linewidths and shapes can be accounted for by assuming a distribution of crystalline electric fields and correcting to a constant field observation. Certain lines have largely the character of $\Delta S_z = 2, 3$. These have been known as "forbidden" (3) or "double-jump" (4) lines. The check included these absorptions, whose intensities were calculated on the basis of the extent of their $\Delta S_z = 1$ character.

The magneto-gyric ratio was studied as a function of crystal dilution and temperature (5). At great dilution (1:50) it was 1.974 ± 0.002; at full strength, 1.988 ± 0.002 independent of temperature within the experimental accuracy. This implies a smaller "cubic field" in the aluminum lattice than in the chromium lattice.

The quartet ground state (three unpaired electrons) can be split only as far as two doublets. A theorem due to Kramers (6) shows that these doublets cannot be

decomposed by an electric field. The separation of these energy levels (zero field splitting, δ) can easily be measured experimentally and amounts to 0.098 cm^{-1} for the very dilute material, 0.135 cm^{-1} for full strength, at 25°C. These values decrease at about the rate of 0.0005 $cm^{-1}/°K$ to 80°K (7). This implies a strong decrease in axial distortion with lower temperature.

At about 80°K, the full strength alum and alums of low dilution undergo a second-order phase transition. Characteristics of this transition have been studied elsewhere in optical, thermodynamic, and other paramagnetic resonance work (8, 9, 10). Powder x-ray diffraction patterns were compared above and below the transition. Line spacing was identical within the resolution of the lines, but intensities changed somewhat. The heavier atoms undoubtedly do not change position appreciably. Below the transition two microwave splittings have been observed which can only be accounted for by the existence of the chromium ions in two possible environments.

The magnet, microwave, control, and presentation apparatus used in this research will be described in two forthcoming Review of Scientific Instruments articles. This problem has been the subject of a thesis submitted to the M. I. T. Department of Physics.

C. F. Davis, Jr.

References

1. J. H. van Vleck, Phys. Rev. 41, 208 (1932).
2. G. Racah, Phys. Rev. 62, 438 (1942).
3. R. Malvano and M. Panetti, Phys. Rev. 78, 826 L (1950).
4. J. Ubbink, J. A. Poulis, and C. J. Gorter, Physica 17, 213 (1951).
5. Quarterly Progress Report, Research Laboratory of Electronics, M.I.T., Jan. 15, 1954, p. 19.
6. H. A. Kramers, Amsterdam K. Akad. Wetenschapen 33, 959 (1930); M. J. Klein, Am. J. Phys. 20, 65 (1952).
7. D. M. S. Bagguley and J. H. E. Griffiths, Proc. Roy. Soc. (London) 204A, 188 (1950).
8. D. L. Kraus and G. C. Nutting, J. Chem. Phys. 9, 133 (1941).
9. H. L. Johnston, Jih-Heng Hu, and W. S. Horton, J. Am. Chem. Soc. 75, 3922 (1953).
10. B. Bleaney, Proc. Roy. Soc. (London) 204A, 203 (1950).

B. HINDERED ROTATION IN SEMISYMMETRIC MOLECULES

A molecule which may be described as a semisymmetric hindered rotor is one that consists of a symmetric top attached at an arbitrary angle to a general asymmetric framework, and allowed to rotate about its symmetry axis relative to the frame.

A well-known example of this type of molecule is methyl alcohol, CH_3-OH. If the two groups are taken as rigid, then the microwave spectrum will be due to the interaction of hindered rotation with over-all rotation.

A theory is being developed for this general type of molecule which will give the Hamiltonian in terms of principal moments of the molecule and the angle of the top relative to principal axes. The pure hindered-rotation spectrum will then be calculated and compared to the experimental results for sample molecules.

P. R. Swan, Jr.

VI. MAGNET LABORATORY RESEARCH

Prof. F. Bitter
Dr. S. P. Davis*
Dr. P. L. Sagalyn
Dr. J. S. Waugh
N. I. Adams III
G. R. Murray, Jr.
H. H. Plotkin
J. R. Stanley
J. E. R. Young

A. NUCLEAR ORIENTATION IN MERCURY VAPOR

A new attempt is being made to obtain nuclear orientation in mercury vapor by "optical pumping" with circularly polarized light (1, 2, 3). Although this has been done in a beam (4, 5), the successful use of a vapor would facilitate the orientation of small amounts of radioactive isotopes.

To prevent condensation of atoms containing oriented nuclei, a hot quartz cell was sealed off with unsaturated vapor at the vapor pressure corresponding to ice temperature. The cell will be irradiated with light from an Hg^{198} arc in a very weak field. In such a field, the transition to the F = 3/2 level of the $^3P_1$ state of Hg^{201} overlaps with the single line of Hg^{198} which can be used, therefore, to orient Hg^{201}. Since a large magnetic field is not needed, the arc can be brought very close to the cell, giving considerably more light intensity than was available in previous attempts. The use of a 198 arc, rather than natural mercury, will considerably reduce the background from the even isotopes. It is planned to detect orientation by the method of Hawkins and Dicke (5), that is, by observing the degree of polarization of the scattered light as a function of a magnetic field parallel to the axis of the light beam. The degree of polarization is a function of the degree of orientation. The component of the earth's field transverse to the light beam axis will cause a disorienting precession of the nuclear magnetic moment which should have a maximum effect when the applied field just cancels the component of the earth's field parallel to the light beam axis. Calculations indicate that with the light intensity available, it should be possible to detect orientation if the thermal relaxation time in the ground state of Hg^{201} is greater than approximately 0.2 sec.

P. L. Sagalyn, J. R. Stanley

References

1. A. Kastler, J. phys. et radium 11, 255 (1950).
2. F. Bitter and J. Brossel, Phys. Rev. 85, 1051 (1952).
3. F. Bitter, R. F. Lacey, and B. Richter, Revs. Modern Phys. 25, 174 (1953).
4. J. Brossel, A. Kastler, and J. Winter, J. phys. et radium 13, 668 (1952).
5. W. B. Hawkins and R. H. Dicke, Phys. Rev. 91, 1008 (1953).

---

*Spectroscopy Laboratory, M.I.T.

B. NUCLEAR MAGNETIC RESONANCE IN GASES

In the nuclear magnetic resonance of B" in BF_3 gas at various pressures with various added gases, simultaneous measurements of linewidth ΔH and signal amplitude vs. applied rf amplitude were made. Theory gives

$$\left(\frac{\text{signal}}{\text{rf}}\right)\Bigg|_{\text{rf}\to 0} \quad \propto \left(\frac{N_B}{\Delta H}\right)$$

where N_B is the number of atoms of B" per cm^3 and ΔH is the linewidth as rf $\to$ 0. In these experiments ΔH was principally due to field inhomogeneity. At an rf value such that

$$\left(\frac{\text{signal}}{\text{rf}}\right) = \frac{1}{2}\left(\frac{\text{signal}}{\text{rf}}\right)\Bigg|_{\text{rf}\to 0}$$

theory gives

$$(\gamma H_1')^2 \, T_1 \, \frac{2}{\gamma \Delta H} = 1$$

In pure BF_3, T_1 is predicted to be proportional to the collision frequency. From kinetic gas theory, in pure BF_3, collision frequency is proportional to N_B. In a mixture one expects a similar dependence on all the types of collisions, although there may be some gas components of greater effectiveness than others.

One can thus define an equivalent B" density N_E such that pure BF_3 of that density would produce the observed T_1.

The following quantities were obtained from measurement:

$$A_o \propto \left(\frac{\text{signal}}{\text{rf}}\right)\Bigg|_{\text{rf}\to 0} \qquad W_o \propto \Delta H \qquad E_c \propto H_1$$

P_B = BF_3 partial pressure, P = total gas pressure

We see from the above that in pure BF_3, T_1 is proportional to N_B but also, in any case,

$$T_1 \propto \frac{\Delta H}{H_1'^2} \propto \frac{W_o}{E_c'^2}$$

Hence we expect that

$$\frac{W_o}{E_c'^2 \, N_B} = \text{constant.} \quad \text{Also, we see that} \quad \frac{A_o W_o}{N_B} = \text{constant.}$$

Taking the ratio, we have $A_o E_c'^2 = C_3$. Now, assuming Boyle's law, N_B is proportional to P_B, we get

$$\frac{W_o}{E_c'^2 P_B} = \text{constant} = C_1 \quad \text{and} \quad \frac{A_o W_o}{P_B} = \text{constant} = C_2.$$

Thus $C_3 = C_2/C_1$.

For mixtures we still have $(A_o W_o)/P_B = C_2$. And by definition,

$$\frac{W_o}{E_c'^2 P_E} = C_1$$

Now

$$C_3 = \frac{C_2}{C_1} = A_o E_c'^2 \frac{P_E}{P_B}$$

We can evaluate C_3 from pure BF_3 runs, that is,

$$C_3 = \overline{\left(A_o E_c'^2\right)}$$

averaged over the pure BF_3 runs. Thus

$$\frac{P_E}{P_B} = \frac{\overline{\left(A_o E_c'^2\right)}}{A_o E_c'^2}$$

We can now compare the effectiveness of an added gas to that of BF_3:

$$\left[\left(\frac{P_E}{P_B} - 1\right) \Big/ \left(\frac{P}{P_B} - 1\right)\right] \equiv \rho$$

We find for

H_2 : $\rho \sim 0.4$: one run, $P_{H_2} \sim 1400$ psi, $P_B \sim 300$ psi

N_2 : $\rho \sim 0.8$: two runs, $P_{N_2} \sim 700$ psi, $P_B \sim 1000$ psi

$P_{N_2} \sim 300$ psi, $P_B \sim 400$ psi

On a purely collision frequency basis, one expects, because of the mass differences for H_2, $\rho \sim 4$; for N_2, $\rho \sim 1.3$. Thus some other effect must be present, perhaps the difficulty of transfer of angular momentum from a light to a heavy rotator.

As a check, the constant C_2 was evaluated for each of eleven runs. In all but one, C_2 fell in the range 1.4 - 2.2. This seems to be the experimental error. In spite of an even larger spread in C_1 obtained from data on pure BF_3, a pressure range of a

factor 3 clearly shows pressure narrowing as expected. The value of T_1 obtained is 2.3 msec/psi for pure BF_3. The pressures used were around 1000 psi (4 runs) and around 300 psi (2 runs). The linewidth was approximately 70 milligauss for all runs, which corresponds to a T_2^* of 3 1/2 msec. One run was made with about 70 psi of O_2 and 1000 psi of BF_3. Oxygen, because of its strong paramagnetism, causes a decrease of T_1 with increase in oxygen pressure. The predicted change was negligible against the experimental error. No change was found. This seems to preclude small traces of air being able to produce variations in the results.

N. I. Adams III

C. STEPWISE EXCITATION OF MERCURY

The structure of the mercury spectral line λ4047A is being studied with methods described in previous reports from this group. This line arises from transitions from the state $^3S_1$ (valence electrons 6s and 7s) down to the metastable state $^3P_0$ (6s, 6p). (See Fig. VI-1.) Our procedure is to measure the absorption of the mercury line λ4047A in mercury vapor containing atoms in the $^3P_0$ state as a function of the frequency of this incident radiation.

To provide a density of metastable atoms sufficient for this experiment, a quartz resonance cell, containing a drop of mercury, is either sealed off with a known pressure of nitrogen, or connected to a vacuum system so that the atmosphere may be controlled. Atoms are excited from the ground state $^1S_0$ (6s, 6s) up to the state $^3P_1$ (6s, 6p) by illuminating with the resonance line λ2537A. Since the energy level $^3P_1$ to $^3P_0$ is in resonance with some vibrational levels of the nitrogen molecule, collisions while the mercury atom is excited knock some mercury atoms into the metastable state. It has been found that the intensities and lifetimes involved are such that a population of metastable atoms which is sufficiently large and constant may be maintained.

A source of λ4047A light of variable frequency is provided by a microwave discharge lamp containing only the isotope Hg^{198}. The light is taken parallel to a variable magnetic field, and one of the Zeeman components is removed. Absorption of the λ4047A beam in the mercury vapor is detected and measured by a photomultiplier that has been filtered to be sensitive only to the line λ5461A. This is one of the possible wavelengths emitted as the atom subsequently falls from the $^3S_1$ level.

The absorption vs. frequency patterns thus observed (Fig. VI-2) show the same qualitative features as have been found by high-resolution spectroscopy. (For a spectral plate of this line, see reference 1.) The even isotopes fall in a broad central peak. Since they do not have nuclear spin, they have no corresponding magnetic hyperfine structure, and the small shift owing to isotopic volumes has not yet been resolved. A tentative identification as hfs components corresponding to the odd isotopes Hg^{199} and Hg^{201} has been made for all of the subsidiary absorption peaks observed. The positions

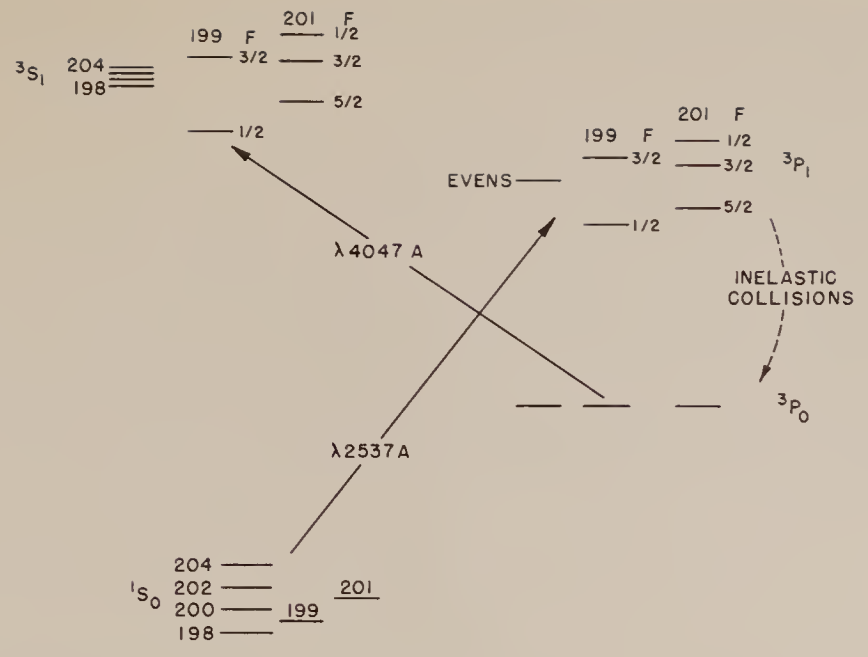

Fig. VI-1

Schematic term diagram of those mercury levels giving rise to the hyperfine structure of the lines λ2537A and λ4047A.

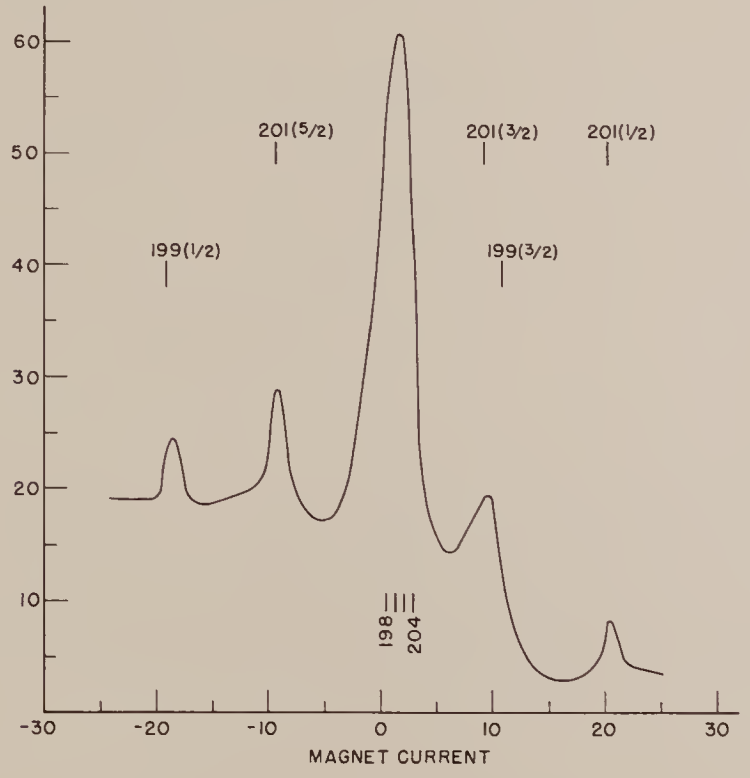

Fig. VI-2

Preliminary determination of the structure of the line λ4047A obtained by magnetic scanning. Vertical markers indicate positions of lines to be expected from previous spectroscopic data. This curve has not been corrected for variation of background signal with the leakage field from the magnet, which may be seen in the curving base line.

of these peaks have been found to satisfy the interval rule and their centers of gravity fall approximately where expected.

An attempt was made to determine which isotopes should be excited into the metastable state, with a pure isotope lamp as the source of the first resonance excitation. However, even if the frequency of the λ2537A radiation brings only atoms of isotopes 198 and 201 into the $^3P_1$ state, absorption peaks are found in the metastable atoms that correspond to the hfs of Hg^{199}. When the mercury pressure is that of the saturated vapor at room temperature, collisions and imprisonment of resonance radiation act to redistribute the excitation energy to all the isotopes.

H. H. Plotkin

References

1. Quarterly Progress Report, Research Laboratory of Electronics, M.I.T., April 15, 1954, p. 28.

VII. MICROWAVE TUBE RESEARCH

L. D. Smullin
Prof. L. J. Chu
Dr. H. A. Haus
A. Bers
D. L. Bobroff
C. Fried
A. J. Lichtenberg
H. Shelton

A. EQUIVALENT CIRCUIT FOR A THREE-TERMINAL PAIR NETWORK

The study of microwave amplifiers of the beam type requires at times (1) an equivalent circuit representation of nonreciprocal three-terminal pair networks. The equivalent circuit is useful if it leads to mathematical simplifications.

A simple equivalent circuit for the most general lossless nonreciprocal three-terminal pair network can be constructed with the aid of a lossless three-terminal pair gyrator. The gyrator is defined by the impedance matrix Z.

$$Z = \begin{bmatrix} 0 & x & y \\ -x & 0 & z \\ -y & -z & 0 \end{bmatrix}$$

The transfer impedances x, y, and z are real quantities.

The most general, lossless, nonreciprocal, three-terminal pair network has an impedance matrix of the form (2)

$$Z = j \begin{bmatrix} X_{11} & X_{12}e^{j\phi_{12}} & X_{13}e^{j\phi_{13}} \\ X_{12}e^{-j\phi_{12}} & X_{22} & X_{23}e^{j\phi_{23}} \\ X_{13}e^{-j\phi_{13}} & X_{23}e^{-j\phi_{23}} & X_{33} \end{bmatrix}$$

The X's are all real quantities. The matrix has thus 9 adjustable parameters. The equivalent circuit shown in Fig. VII-1 also has 9 adjustable parameters. It includes, besides the gyrator and lumped reactances, ideal two-terminal pair phase shifters (2) characterized by the matrix of generalized circuit parameters (3)

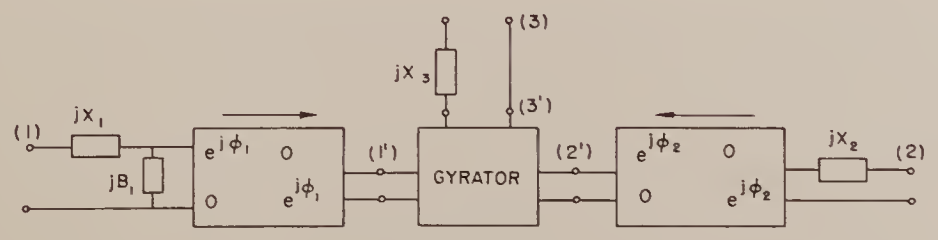

Fig. VII-1
The equivalent circuit.

$$\begin{bmatrix} e^{j\phi} & 0 \\ 0 & e^{j\phi} \end{bmatrix} \tag{1}$$

The arrows above the ideal phase shifters in Fig. VII-1 point from the input to the output terminals of the phase shifters. The voltage and current at the input of a phase shifter with the matrix (Eq. 1) lead the voltage and current at the output by a phase angle ϕ.

Below, the elements of the equivalent circuit are given in terms of the 9 parameters of the three-terminal pair network:

$$X_1 = X_{11} \quad x = X_{12} \quad y = X_{13}$$

$$\phi_1 = \phi_{13} + \frac{1}{2}\pi \quad \phi_2 = \phi_{13} - \phi_{12}$$

$$z = -X_{23} \sin(\phi_{23} + \phi_{12} - \phi_{13}) \quad B_1 = \frac{X_{23}}{X_{12}X_{13}} \cos(\phi_{23} + \phi_{12} - \phi_{13})$$

$$X_2 = X_{22} - \frac{X_{12}X_{23}}{X_{13}} \cos(\phi_{23} + \phi_{12} - \phi_{13})$$

$$X_3 = X_{33} - \frac{X_{13}X_{23}}{X_{12}} \cos(\phi_{23} + \phi_{12} - \phi_{13})$$

H. A. Haus

References

1. Quarterly Progress Report, Research Laboratory of Electronics, M.I.T., Oct. 15, 1954.
2. H. A. Haus, Paper to be published in the Journal of Applied Physics.
3. E. A. Guillemin, Communication Networks (John Wiley and Sons, Inc., New York, 1935) VII, p. 138.

B. THE MINIMUM NOISE FIGURE OF LONGITUDINAL BEAM AMPLIFIERS

Some general relations were derived concerning the minimum noise figure of microwave amplifiers of the beam type. A general model of a microwave amplifier with arbitrary noise smoothing schemes was taken as a starting point. The model assumes that the amplifier can be split into an input and an output section. The rf coupling between the input and output section is provided solely through the electron beam. A klystron, a velocity jump amplifier, and a traveling-wave tube with a severed helix are all special cases of this model. The interaction between the beam and the rf circuit of such

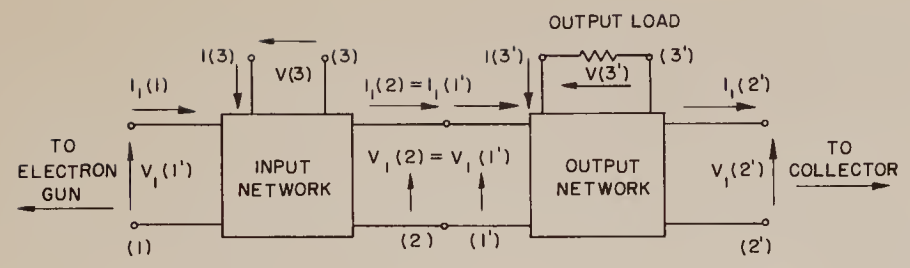

Fig. VII-2
The equivalent circuit of a microwave amplifier.

amplifiers can be represented by an equivalent circuit shown in Fig. VII-2; that is, by two linear nonreciprocal passive three-terminal pair networks connected in cascade. (The reader is referred to reference 1 for the definitions and concepts used in this section.) The terminals marked (1), (2), (1'), and (2') are the "beam terminals." The voltage and current at those terminals are the ac beam voltage and beam current. The terminals marked (3) and (3') are the input and output terminals of the amplifier.

A nonreciprocal passive three-terminal pair network is characterized by 9 complex quantities. However, for our purpose it is sufficient to characterize the output network by two complex quantities, a and b. They are defined as follows: When an ac beam voltage $V_1(1')$ and an alternating beam current $I_1(1')$ are applied to the terminal pair 1' of the output circuit, the voltage across the output load is because of linearity

$$V(3') = aV_1(1') + bI_1(1') \tag{1}$$

The subscript "1" of the voltage and current indicates small signal beam voltages and currents.

One of the relations derived concerns the general form of the minimum noise figure of the amplifier described above. The following definition of the noise figure is used:

$$F = 1 + \frac{\text{Noise power output per unit frequency from beam noise}}{\text{Noise power output per unit frequency from input circuit noise}} \tag{2}$$

The above definition is applicable if the input circuit noise and the beam noise are uncorrelated. The denominator of Eq. 2 is proportional to kT, where T is the temperature of the input circuit.

The numerator of Eq. 2 can be evaluated by techniques of four-terminal network transformations of beam noise. The Thévenin impedance of the input circuit is connected across the terminal pair 3 of Fig. VII-2 with the result that the three-terminal pair input network can be treated as a two-terminal pair network so far as its action upon the beam noise is concerned. Under the assumption that a lossless four-terminal beam transducer between the cathode and the amplifier is optimized for lowest noise figure, we find for the noise figure the general expression

$$F_{min} = 1 + \frac{2\pi}{kT} |K| \left[S_o - \frac{K}{|K|} \Pi_o \right] \tag{3}$$

where

$$S_o = \left(\Phi_o \Psi_o - \Lambda_o^2 \right)^{1/2}$$

S_o and Π_o are two parameters of the beam noise at a plane beyond the potential minimum in the electron gun. K is a constant dependent upon the characteristic parameters of the amplifier. The constant K can be greater or less in magnitude than unity. It is of great interest to find the dependence of K upon the particular amplifying structure used. This has been done under the assumption that the input three-terminal pair network of Fig. VII-2 is lossless. The equivalent circuit for the three-terminal pair network of the preceding section has been used. It is found that two cases have to be distinguished

$$\text{Case A:} \quad \mathrm{Re}(ab^*) < 0 \tag{4}$$

Inequality 4 can be interpreted as follows: Eq. 1 shows that a modulation on the beam at the point (1') with a small signal impedance

$$\frac{V_1(1')}{I_1(1')} = -\frac{b}{a} \tag{5}$$

does not deliver any power to the output circuit. According to inequality 4, the critical impedance 5 must have a positive real part for case A to apply. A long helix terminated in a matched load is a known example of such an output structure.

If case A applies, it can be shown that the minimum possible value of K, K_{min}, is

$$K_{min} = 1 \tag{6}$$

$$\text{Case B:} \quad \mathrm{Re}(ab^*) > 0$$

The critical impedance 5 for case B has a negative real part. A cavity with a long gap (a transit angle θ in the range $0 < \theta < 2\pi$) is a known example of such a structure.

If case B applies

$$K < 1 \tag{7}$$

and indeed can be zero or become negative.

It is obviously of great interest to determine whether any useful amplifier structures exist with a K appreciably less than unity. This question has been investigated under the additional assumption that the output three-terminal pair network of Fig. VII-2 is lossless. Under this assumption it was possible to show that the available power gain G of the amplifier is limited by the magnitude of K by

$$G \leq \frac{1}{1 - K} \tag{8}$$

Thus, a structure with a K appreciably less than unity and a correspondingly low noise figure would be useless as an amplifier because of its low gain. It should be emphasized that relations 6, 7, and 8 have been obtained under the restrictive assumptions that either the input three-terminal pair network or the input and output networks are lossless. A generalization of the proof to include loss encounters great mathematical difficulties.

H. A. Haus

References

1. Quarterly Progress Report, Research Laboratory of Electronics, M.I.T., April 15, 1954, p. 32.

C. BEAM NOISE MEASUREMENTS

Some measurements were made on a gun of higher perveance than was heretofore used. This gun had a convergence half angle of 13°, a perveance of 0.35×10^{-6}, and produced a beam about 0.08 inch in diameter. The heater construction was such as to produce an observable magnetic field at the cathode surface (a few gauss). As with the previous gun, a strong growing noise wave was observed; however, when viewed on an oscilloscope, it fluctuated violently at 60 cps. This was soon traced to the heater. It was observed that the growing noise wave might vary by about 10 db, depending upon the polarity of the heater current, and that this bore a definite relation to the direction of the main focusing field; reversing one required reversing the other to produce a given effect. Previous measurements had indicated that the main focusing field of several hundred gauss produced a leakage field of a few gauss at the cathode, outside the magnetic field.

In order to pin this down more specifically, an auxiliary winding was wrapped around the steel tube surrounding the gun. With this it was possible to produce fields of a few gauss at the cathode, and with the proper polarity the growing noise wave could be eliminated. Subsequent tests, when the gun was removed from the system, indicated that the noise was reduced when the two fields at the cathode were aiding, and the noise was enhanced when they were opposing.

A more careful experiment is being prepared in order to get a better picture of this phenomenon.

C. Fried, L. D. Smullin

D. THE INTERNALLY COATED CATHODE

Previous investigation of internally coated cathodes made from thin (less than 0.005 inch) nickel with holes approximately 0.015 inch in diameter has shown that the electrons

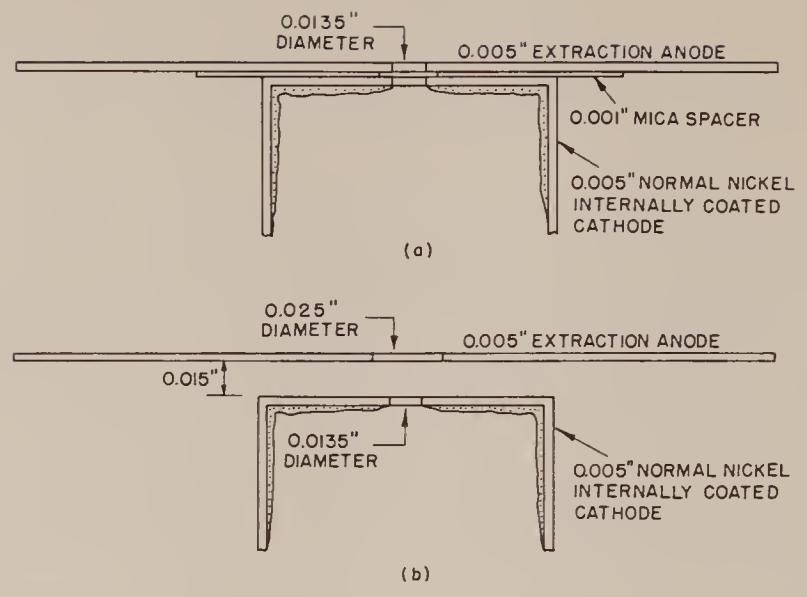

Fig. VII-3

Simple electron sources with internally cooled cathodes.

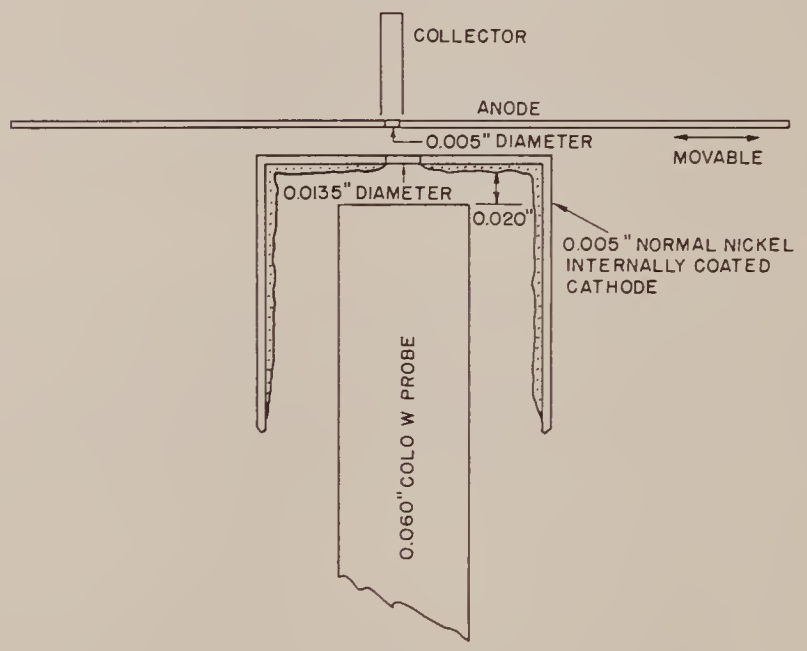

Fig. VII-4

Tube allowing determination of regions of emission.

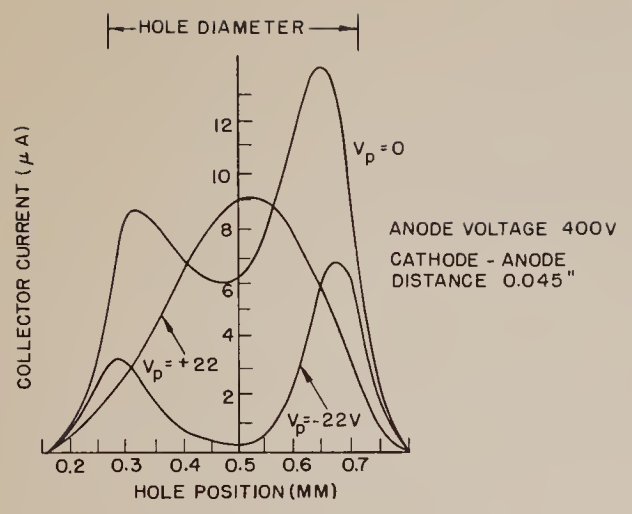

Fig. VII-5

Current density across beam a few hole diameters in front of the cathode.

originate from the coating and are drawn through the hole by the applied anode voltage. The more field that can be made to penetrate the hole, the greater the emission. If such cathodes, then, are to be used as electron sources, we must have "extraction" anodes similar to the simple guns shown in Fig. VII-3(a) and (b).

The source shown in Fig. VII-3(a) has produced current densities of approximately 1 amp/cm^2 at moderate temperatures and less than 100 volts with about 10 per cent interception current. The source in Fig. VII-3(b) shows no interception current, and the construction and operation are not so critical. The presence of the extraction anode necessarily produces a lens combination that is divergent, and a strong field on the outside of this anode is necessary to remove this divergence. A magnetic field might then hold together a hollow beam, or a strongly convergent lens might produce a crossover point to be imaged by conventional means in a cathode-ray tube.

Investigation of the cathode shown in Fig. VII-4 with a small movable anode hole backed by a collector gives us an insight into the origin of the electrons by letting us see the effect of the probe voltage on the amount and pattern of the emission. The significant results are illustrated in Fig. VII-5. Here, the sampled current through the anode hole to the collector is plotted as a function of the distance the anode hole has moved across a diameter of the cathode hole. The results of this experiment seem to be the same as those of a previous similar experiment; the electrons originate behind the hole, but the lens action of the cathode hole is uncertain.

During this investigation, one cathode showed a surprising increase in emission (about ten times) after the coating had been bombarded by electrons of approximately 50 volts from an emitter inside the cavity. This state of activity occurred instantly and has persisted. Possible reasons for this phenomenon were the production of free barium by the bombardment or excessive temperature of the coating (without excessive temperature of nickel).

H. Shelton

VIII. ATOMIC BEAM RESEARCH

Prof. J. R. Zacharias
Prof. J. G. Yates
Dr. V. Jaccarino
Dr. J. G. King

S. J. Buchsbaum
R. T. Daly, Jr.
D. S. Edmonds, Jr.
R. D. Haun, Jr.
J. H. Holloway

K. H. Powers
C. L. Schwartz
H. H. Stroke
R. Weiss

A. CESIUM CLOCK

During the last quarter the cesium beam apparatus which has been under construction to provide a primary frequency standard for the Atomic Beam laboratory has been in successful operation. Much useful information has been obtained showing that such a system can be expected to provide a long term stability approaching 1 part in 10^{10}.

The system uses the field insensitive resonance line of Cs^{133}, occurring at approximately 9192.63197 Mc/sec, as the frequency standard. By exploiting the molecular beam techniques developed for measurements on scarce isotopes, which involve the use of a narrow beam and sensitive detector, an apparatus has been designed to give a good signal-to-noise ratio using only one microgram of cesium per day. The expected linewidth was about 200 cps, making possible a stability of 1 part in 10^{10} by splitting the linewidth to $\pm$1 per cent.

For those not familiar with the principles involved, the following brief description is provided.

There are a number of magnetic resonance lines associated with a cesium (or other) atom, resulting from transitions between two quantum states. There exists a pair of states for which the energy is independent (to the first order) of the external magnetic field, so that the associated frequency is similarly field insensitive. (There is, however, a small term proportional to the square of the field.) The resonance is excited by applying a magnetic field at the appropriate frequency, the width of the resonance curve being inversely proportional to the time the atom spends in the field. With a beam of atoms a long path without collision can be obtained with a high density of atoms, because of the ordered nature of their paths. The transition in question is associated with a reversal in the magnetic moment of the atom. If the beam of atoms is passed through a transverse inhomogeneous magnetic field, a deflection is produced in a direction determined by the sign of the magnetic moment. If a pair of such fields is placed on either side of the rf field (A and B magnets), a distinction can be made between atoms which have made the transition (or "flopped") and the others, by observing whether the two deflections have added or cancelled. A detector placed to measure the number of atoms on one or the other of the two paths will record a resonance curve as the frequency is varied. If the rf field is applied uniformly over a given length, a single peak is obtained. If two separated fields are used as in Ramsey's method, a typical interference pattern is obtained whose spacing depends on the velocity of the atom. If a

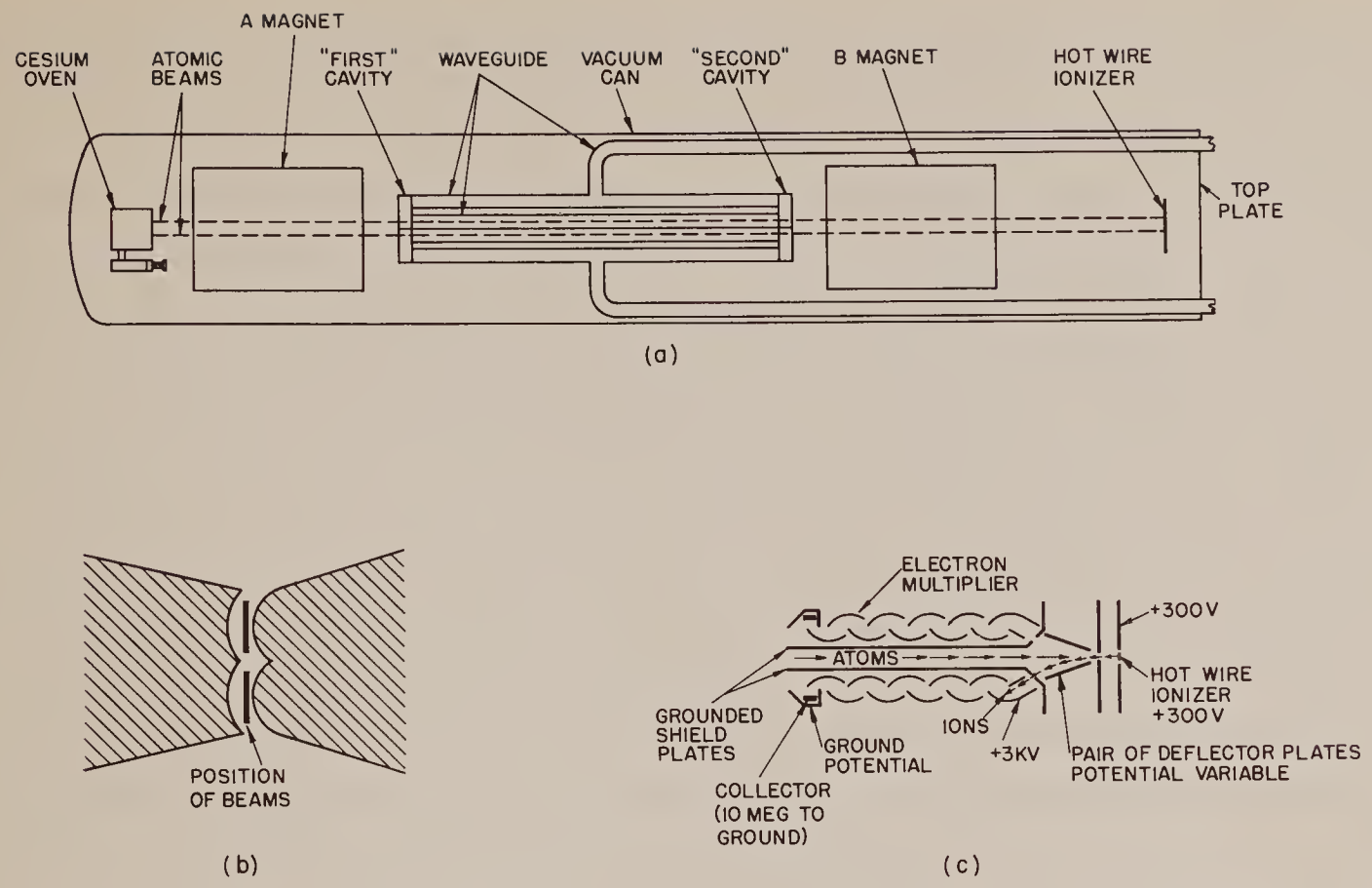

Fig. VIII-1

(a) Schematic diagram of apparatus. The apparatus actually operates in a vertical position with the top plate up. (b) Cross sectional view of deflecting magnets. (c) Schematic view of detector system. This assembly goes in the space at the top of the can in (a).

range of velocities is used, only the central peak is reinforced; the side peaks tend to average out. The use of a surface ionization detector (hot wire) serves to change neutral atoms into charged ions which may be detected electrically. With an electron multiplier as amplifier, the arrival of individual atoms can be recorded.

The general arrangement of the beam apparatus is indicated in the simplified form of Fig. VIII-1. The apparatus is housed in a stainless steel can 6 feet long and 10 inches in diameter into which it is lowered vertically. All connections are brought out through the top plate.

The oven produces two narrow beams of cesium atoms, each of initial cross section 0.020 inch by 3/8 inch with a total divergence in angle of less than 1°. Details of the oven construction and performance are given in the following section, but with a total emission of 10^{-6} gm of cesium per day ($5 \cdot 10^{11}$ atoms/sec) it was expected to provide 10^{7} atoms/sec reaching the detector, of which one-eighth can provide the desired transition.

The A and B magnets, which are identical, produce a transverse inhomogeneous magnetic field. With an Alnico core, and circular section pole pieces (Fig. VIII-1(a)), a field strength of 6000 gauss and a gradient of more than 10,000 gauss/cm is obtained

in a gap of 1/8 inch. The present magnet length is 10 inches, which produces a deflection of 0.025 radian on atoms of the most probable velocity. This is excessive; the magnet length will be reduced in the future to 3 1/2 inches and the gap increased to 1/4 inch. Magnetizing coils are incorporated so that the magnets can be set to the desired strength. The rf field system is designed to use the Ramsey method of separated fields. For each beam, two rectangular cavities each a half wavelength long and spaced 66 cm apart, produce a transverse rf field (parallel to the A and B fields), using the transverse component of the TE_{01} field pattern. The cavities are fed symmetrically with a waveguide feed. To get a symmetrical resonance curve it is essential that the phase of the fields in the two cavities should be the same. This is obtained by providing a second waveguide running between the cavities which is loosely coupled to the cavities by the slots through which the cesium beam passes. If a probe is inserted at its middle point, a null signal is obtained if the phase and amplitude in the cavities are identical. The phase adjustment is made by a tuning screw in each cavity. This measurement can be checked during normal operation, but in general an initial adjustment is adequate.

The steady field in the rf region is made up of the earth's field and the leakage field from the A and B magnets, with provision for some control by small coils near the cavities. It has been found that the maximum field is below 1 gauss. In the final form some magnetic screening will be provided to reduce the contribution of the earth's field, and the desired field will be provided by a suitable coil system.

The detector is a 0.040-inch tungsten ribbon. Cesium atoms falling on this are ionized and are then pulled off and deflected electrostatically to one or the other of two electron multipliers, each having a gain of about 3×10^6.

The apparatus is evacuated by a 2 1/2-inch oil diffusion pump; with liquid air traps a pressure of $5 \cdot 10^{-7}$ mm is regularly maintained.

A considerable amount of apparatus, which is described briefly below, has been constructed for use with the beam tube.

The most important item is the signal source at 9192 Mc/sec. This is produced in a silicon crystal tripler driven by an S-band cavity oscillator (1). The oscillator, with a cavity with a Q of about 50,000 and a triode amplifier, has proved to have a short term stability better than 1 part in 10^9. For convenience in the experimental operation of the beam tube, the long term frequency stability has been improved by fitting a thermostat to the cavity of the oscillator. The thermostat uses a temperature sensitive resistance wound over the whole cylindrical surface of the cavity. This is connected in a sensitive bridge circuit that provides a continuous control of the power supplied to a heater winding outside the cavity, giving rapid and precise control of temperature. Changes of the thermostat setting provide a convenient means of frequency adjustment; they also provide a convenient method of producing a frequency changing linearly with time.

Other facilities available include an automatic frequency sweep circuit that sweeps

the oscillator over a predetermined range by switching the oscillator cavity heating power between two levels. In addition, provision is made for the time of the occurrence of the resonance curve (or any other event, such as a frequency marker from a crystal standard) in the sweep to control automatically the frequency limit desired so that it continues to cover the required range.

The frequency of the S-band oscillator can be compared with the laboratory crystal standard, using the beat frequency between the S-band signal (3064 Mc/sec) and the 17th harmonic of 180 Mc/sec (3060 Mc/sec) derived from a 5 Mc/sec crystal. An audio frequency discriminator (with its peaks located at 1000 and 1500 cps) has proved very convenient for recording small frequency variations. If a small amount of frequency modulation at about 30 cps is applied to the S-band oscillator, the beam current has a 30 cps component which is proportional to the derivative of the resonance curve. When this is applied to a phase sensitive detector, an output having the characteristic of a frequency discriminator is obtained with a zero value at the resonant frequency.

A Sanborn two-channel recorder has been used for recording the data and has proved of great value in a number of different types of measurement.

As soon as the apparatus was assembled with magnets of the quoted specifications, resonance curves of the Ramsey pattern were obtained. Detailed measurements are much too numerous to quote but the important conclusions are as follows.

Resonance curves of the Ramsey pattern with good signal-to-noise ratios were obtained (Fig. VIII-2). The oscillator proved to have more than adequate short-term stability for the purpose, and can produce more than enough power at 9192 Mc/sec. The oscillator was successfully locked to the beam frequency, by using the beam output as an error signal for frequency control. With a very simple control system, a peak frequency deviation of ± 1 part 10^9 was reached and the mean over longer periods would be much smaller.

Probably of greatest importance is the fact that the whole apparatus worked very much according to plan. The oven has run for two extended periods, one of 6 weeks,

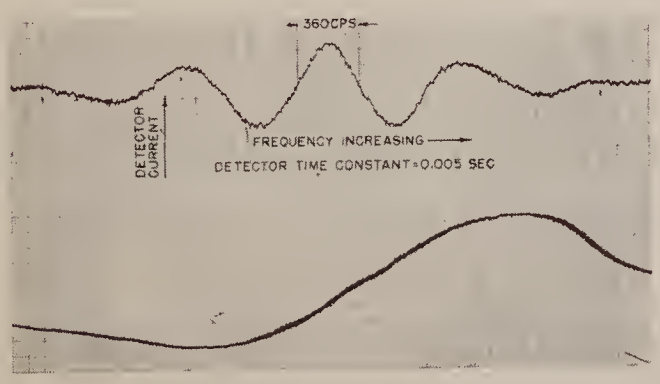

Fig. VIII-2
Resonance curve; axial layout.

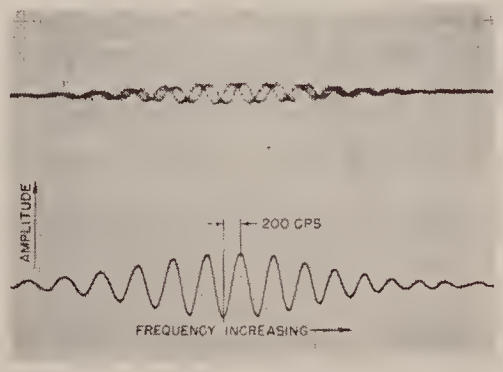

Fig. VIII-3
Discriminator curve; offset layout.

and in each instance the run was ended because the apparatus had to be opened to allow other unrelated changes to be made.

The main feature requiring modification was that the linewidth obtained, of 300 cps, corresponds to using atoms of twice the most probable velocity. If the magnet strength was reduced to allow the use of lower velocity atoms, the background of "unflopped" atoms, already high, was further increased because of certain features of the geometry of the apparatus. For a number of reasons, a more effective arrangement is a layout in which the oven is offset to one side of the axis and the detector is offset to the other. This gives a loss of half the available atoms but can give a much lower background. An experiment with an excessive amount of displacement to suit the large magnet deflections available gave the expected results, shown in Fig. VIII-3. This curve is an example of the discriminator type of characteristic obtained by applying a small amount of frequency modulation to the oscillator. A linewidth of 200 cps with negligible background and very good signal-to-noise ratio was obtained. The total available signal can be increased by using the optimum deflection angle. The large number of peaks was expected from the narrow velocity range used in this experiment. Information available from the present tests provides the essential information for the engineering design of molecular beam tubes of various sorts. The tube construction is simple and has proved very satisfactory. For the immediate future, the beam apparatus will be set up to provide a frequency standard by direct reference to the cesium resonance line with an accuracy of a single observation of about 1 in 10^9. As soon as any greater precision is required, the necessary circuits for locking the oscillator continuously will be provided.

J. R. Zacharias, J. G. Yates

References

1. Quarterly Progress Report, Research Laboratory of Electronics, M.I.T., Jan. 15, 1954.

B. WELL-COLLIMATED ATOMIC BEAM OVENS

To make possible the development of atomic beam clocks which would run for long periods of time without maintenance, it was necessary to develop atomic beam sources (ovens) that would conserve as much material as possible without reducing, significantly, the usable number of atoms. This report describes the construction and test of such ovens.

The number of atoms per second that will leave an oven canal and reach a distant detector which subtends an infinitesimal solid angle located on the axis of the slit is dependent only on the cross sectional area of the slit and on the pressure inside the oven. (In this discussion, the slit is assumed to be some sort of a closed cylindrical surface;

this does not restrict the argument.) On the other hand, the total number of atoms per second that leave the slit is determined by the solid angle which one end of the slit subtends as seen from the other end. This is so because most of the atoms entering the long canal will hit the walls on the oven end of the slit, and the smaller this solid angle, the greater the probability that atoms which hit the walls of the slit will go back into the oven instead of going out the far end of the slit.

Thus, to save material one is led to the use of a cylindrical slit whose length is large relative to its diameter. However, an upper limit is placed on the length by the condition that the length be short compared with the mean free path for atoms in the oven exit canal. If this condition is not fulfilled, then atoms will collide with each other and the point at which such collisions are most probable will serve as a new source – so that the entire length of the slit will not be contributing to the material savings. Since the forward intensity is proportional to a positive power of the pressure in the oven and since one is usually interested in obtaining as great a forward intensity as possible, one obviously wants to operate the oven at as high a pressure as possible. But the mean free path is inversely proportional to the pressure. Therefore, one is forced to make the slit as short as possible. This in turn requires the slit diameter to be very small. To obtain usable forward intensities one must use a large number of such slits with their axes parallel and with as thin boundary walls as possible.

The oven slits now in use were constructed by rolling 0.001 inch thick nickel foil between two interlocking bronze rolls. The width of sheet having the best rolling properties was found to be 0.5 inch. This implies a canal length of 0.5 inch. The length of the sheet is completely arbitrary. The resulting sheet (nicknamed "crinkly sheet") looks very much like miniature corrugated iron. The corrugations are about 0.002 inch deep and about 0.007 inch from peak to peak. The sheet can be cut to the desired length with a pair of kitchen scissors. By alternately stacking these "crinkly sheets" and sheets of flat 0.001-inch nickel foil, one can obtain canal assemblies of arbitrary dimensions.

For the small clock, the dimensions of the slit assembly are 0.025 inch by 1.0 inch, and the length of each slit is 0.5 inch.

In the tests analyzing the directivity of this oven, a charge of cesium carbonate and potassium was placed in the oven. The beam of cesium atoms obtained on heating the oven was detected using a surface ionization detector (hot wire). The oven temperature was measured with an iron-constantan thermocouple bolted on the outside of the oven. The surface ionization detector was a heated tungsten wire, 0.005 inch in diameter, located 12 inches from the oven slit. The useful length of the hot wire was about two inches. The oven was mounted so that it could be turned about a vertical axis parallel to the long dimension (one inch) of the slit assembly and perpendicular to the axes of the slits. The angle through which the oven was turned was read from a micrometer

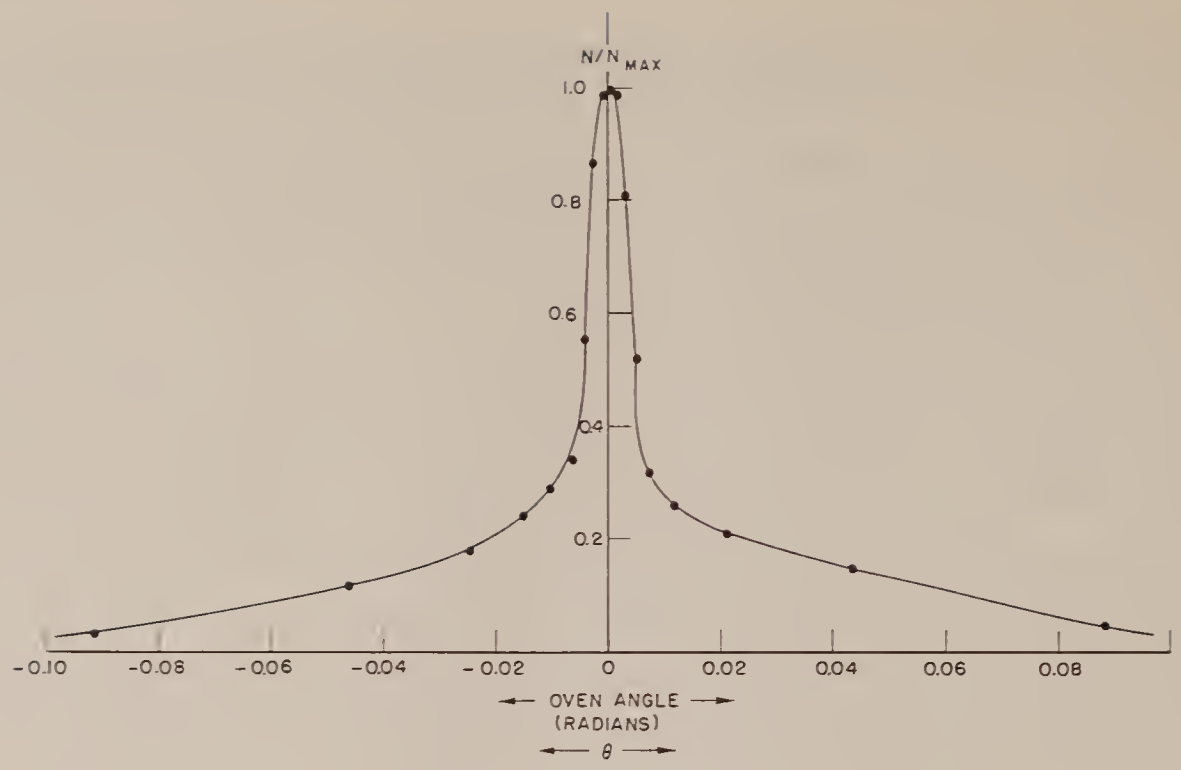

Fig. VIII-4

Plot of beam intensity N vs. oven angle (θ). N is plotted in units of N_{max}, the intensity in the forward direction. The oven temperature was 341°K. The value of N_{max} was 1.1×10^{7} atoms/sec hitting the hot wire.

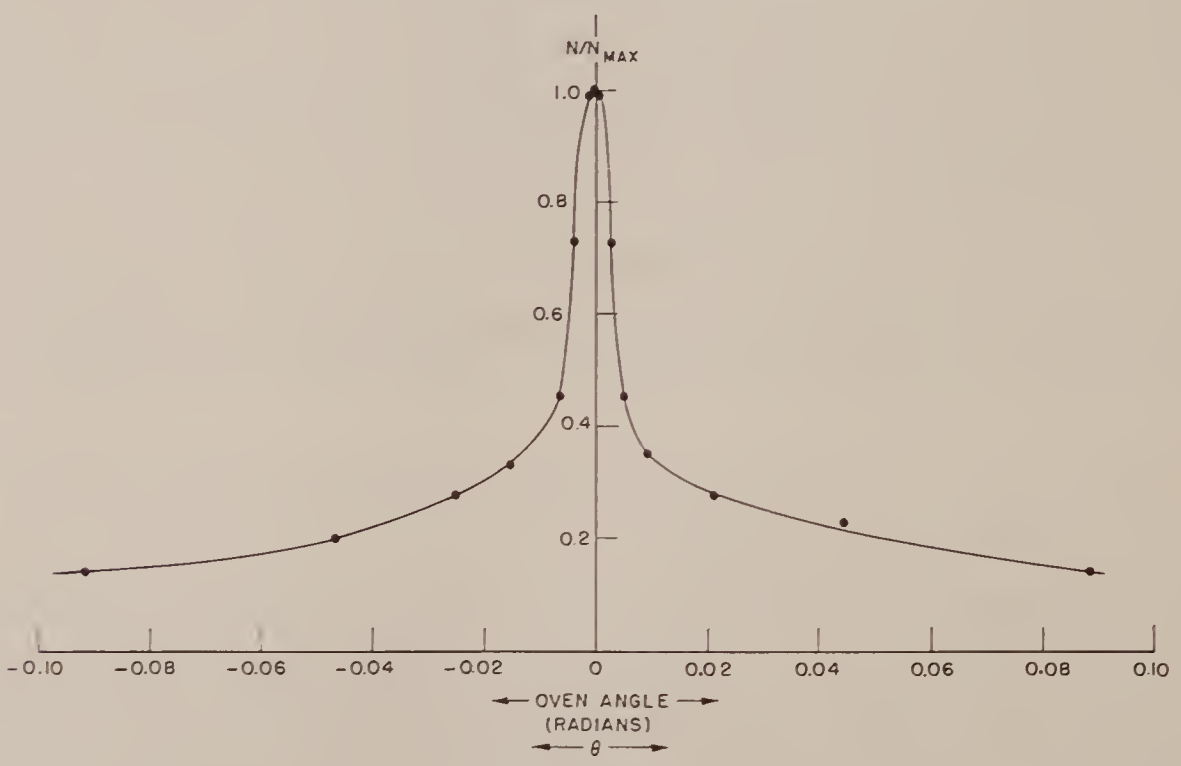

Fig. VIII-5

Plot of beam intensity N vs. oven angle (θ). N is plotted in units of N_{max}, the intensity in the forward direction. The oven temperature was 417°K. The value of N_{max} was 1.9×10^{9} atoms/sec hitting the hot wire.

screw which actuated the turning lever. The number of cesium atoms which hit the hot wire in a second was measured as a function of oven temperature and angle. Two of the curves which were obtained are Fig. VIII-4 and Fig. VIII-5. In both of these curves, the ordinate of the curve has been normalized to unity at an angle of zero radian. Since a linear assembly of slits was used and the detector was also linear, one should interpret these curves as the measurement of angular spread in one direction only. Since each slit is approximately circular in cross section, the curve of angular spread for one slit would be approximately the figure of revolution obtained by rotating Figs. VIII-4 and VIII-5 about the $\theta = 0$ axis. From these figures we see that, in so far as one dimension is concerned, the amount of material within the half intensity angle is about 10 per cent of the total amount of material at a temperature of 341°K. However, from Fig. VIII-5, the amount of material in the central peak is only about 5 per cent of the total for a temperature of 417°K. The material savings in the other direction will depend on the angle which the long dimension of the detector subtends at the source. With Fig. VIII-4 as a guide, we see that if this angle is 0.010 radian, about 10 per cent of the beam in that direction will be useful at a temperature of 341°K. In the experiments described above, the detector subtended an angle of approximately 0.2 radian so that very little material was wasted in this direction.

The major conclusions of the experiments that have been completed are:

1. A definite material saving results from the use of collimated slits. The curves obtained show this when compared with the cosine distribution for N/N_{max} vs. θ which would be obtained for an infinitely short slit or when compared with the curves given by Davis (1). At low temperatures (see below) this material saving seems to be roughly that expected on the basis of considerations of solid angle alone.

2. The source is equivalent to an assembly of about 300 canals each giving about 10^5 atoms/sec at 341°K and 10^7 atoms/sec at 417°K – all going into the solid angle within the cone $\theta = 0.010$ radian. The width at half intensity for a single canal is about 0.010 radian for both temperatures. The proportion of atoms going outside the cone $\theta = 0.010$ radian is a function of temperature.

3. The material saving is a function of temperature. The higher the temperature, the greater the ratio of total material leaving the oven to "forward intensity." (That is, the "wings" of the curves in Figs. VIII-4 and VIII-5 become larger as the temperature is increased.) This temperature dependence is probably due to scattering in the slit (1).

J. R. Zacharias, R. D. Haun, Jr.

References

1. L. Davis, Technical Report No. 88, Research Laboratory of Electronics, M.I.T., Dec. 1, 1948, pp. 10-15.

C. HYPERFINE STRUCTURE ANOMALIES IN CESIUM RADIOISOTOPES

The ratios of the nuclear g values of the four cesium isotopes – Cs^{133} (stable), and Cs^{134}, Cs^{135}, and Cs^{137} (radioactive with half lives of 2.3, 3×10^6, and 37 years, respectively) – have been measured by the atomic beam method, by observing the doublet transitions $\Delta F = 0$, $m = -1 \longleftrightarrow -2$ in the odd-even isotopes, and $m = -3/2 \longleftrightarrow m = -5/2$ in the odd-odd isotope in fields of 8300 to 9500 gauss. The results are:

$$\frac{g_{135}}{g_{133}} = 1.05817 \pm 0.00006$$

$$\frac{g_{137}}{g_{135}} = 1.04004 \pm 0.00005$$

$$\frac{g_{137}}{g_{133}} = 1.10047 \pm 0.00008$$

$$\frac{g_{134}}{g_{133}} = 1.01447 \pm 0.0003$$

When these results are compared with those obtained from the ratios of the $\Delta\nu$'s (1) by means of the Fermi formula (2),

$$\Delta\nu = \frac{8}{3} \pi \mu_I \mu_o \psi^2(0) \frac{2I + 1}{I}$$

derived on the assumption that the nuclear magnetic moment is a point dipole, it is found (3) that there is a discrepancy Δ. The experimental values are

$\Delta(135\text{-}133) = +0.034 \pm 0.006$ per cent

$\Delta(137\text{-}135) = -0.022 \pm 0.005$ per cent

$\Delta(137\text{-}133) = +0.006 \pm 0.008$ per cent

$\Delta(134\text{-}133) = +0.17 \pm 0.03$ per cent

When these values are compared with the results of a detailed treatment of the hfs interaction according to reference 3, in which a departure from a nuclear point dipole theory is considered, one finds, on the basis of a strict independent particle model with quenched intrinsic magnetic moments, agreement with experiment for the three isotopes Cs^{133}, Cs^{134}, and Cs^{135}. Cs^{137} has an hfs anomaly which has a sign opposite to the one predicted with respect to Cs^{135}, as well as one smaller by a factor of 10 with respect to Cs^{133}. This result may be related to the fact that Cs^{137} is a magic nucleus with a closed shell of 82 neutrons. A detailed description of the experiment and theory will be presented in a separate report.

H. H. Stroke, V. Jaccarino, D. S. Edmonds, Jr., R. Weiss

References

1. Quarterly Progress Report, Research Laboratory of Electronics, M.I.T., July 15, 1954.
2. E. Fermi, Z. Physik 60, 320 (1930).
3. A. Bohr and V. F. Weisskopf, Phys. Rev. 77, 94 (1950).

D. NUCLEAR MAGNETIC OCTUPOLE MOMENTS OF THE STABLE GALLIUM ISOTOPES

The three zero-field hyperfine structure intervals of the metastable $^2P_{3/2}$ state of Ga^{69} and Ga^{71} have been remeasured (1) to higher precision to establish the existence of a nuclear magnetic octupole moment.

The atomic beam magnetic resonance method was employed; the transitions were induced by the Ramsey technique (2) of separated oscillating fields. One oscillating field was phase-modulated at 93 cps with respect to the other so that the oscillating fields were alternately in phase and 180° out of phase. The alternately in-phase and out-of-phase Ramsey patterns produced were electronically subtracted by a synchronous detector and displayed on an oscilloscope (see Fig. VIII-6).

The intervals were measured in several external fields ranging from 0.2 gauss to 1 gauss, extrapolated to zero field, and corrected (3) for the perturbing effects of the

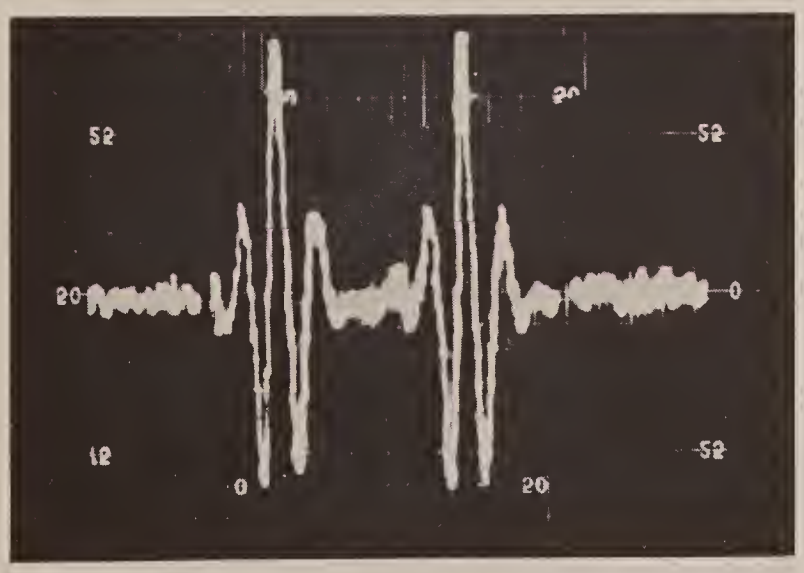

Fig. VIII-6

Typical oscilloscope photograph showing the quadratic Zeeman splitting of the $(F = 2,\ m_F = 0) \leftrightarrow (1, 0)$ and $(2, 1) \leftrightarrow (1, 1)$ transitions in an external magnetic field of 0.4 gauss. The Ramsey technique (2) of separated oscillating fields was used. The two blank portions of the trace calibrate the picture in frequency. The width at half maximum of each central peak is 500 cps.

Table I

Measured and Corrected HFS Intervals of the Metastable $^2P_{3/2}$ State of Ga^{69} and Ga^{71}.

	Ga^{69} (Mc/sec)	Ga^{71} (Mc/sec)
	Measured	
F = 0 ⟷ F = 1	128.27730 ± 0.00020	203.04340 ± 0.00020
F = 1 ⟷ F = 2	319.06706 ± 0.00020	445.46960 ± 0.00020
F = 2 ⟷ F = 3	634.90183 ± 0.00020	766.69580 ± 0.00020
	Corrected	
F = 0 ⟷ F = 1	128.27650 ± 0.00030	203.04133 ± 0.00040
F = 1 ⟷ F = 2	319.06373 ± 0.00050	445.46566 ± 0.00060
F = 2 ⟷ F = 3	634.90597 ± 0.00060	766.70181 ± 0.00080

neighboring $^2P_{1/2}$ ground state as well as the admixture of (4s) (4p) (5s) electronic configuration (see Table I).

The magnetic dipole, electric quadrupole, and magnetic octupole interaction constants (4), a, b, and c, are calculated from the corrected intervals to be:

	Ga^{69}	Ga^{71}
a:	190.794280 ± 0.000150 Mc/sec	242.433950 ± 0.000200 Mc/sec
b:	62.522470 ± 0.000300 Mc/sec	39.399040 ± 0.000400 Mc/sec
c:	84 ± 6 cps	115 ± 7 cps

where the uncertainty is the root-sum-square of the uncertainties in each of the terms of the equations that yield the interaction constants in terms of the intervals.

The data cannot be explained by the mechanism of off-diagonal terms in the interaction matrix giving rise to octupole-like $(I \cdot J)^3$ terms, since $(ab)^{69}/(ab)^{71}$ and $(b^{69})^2/(b^{71})^2$ are greater than unity, and c^{69}/c^{71} is less than unity. To within the quoted uncertainty $a^{69}/a^{71} = c^{69}/c^{71}$.

Schwartz has evaluated the nuclear octupole moment, Ω, and finds

$$\Omega^{69} = (0.107 \pm 0.02) \times 10^{-24} \text{ nuclear magneton cm}^2$$

$$\Omega^{71} = (0.146 \pm 0.02) \times 10^{-24} \text{ nuclear magneton cm}^2$$

Here, as in the corrected intervals, the quoted uncertainty includes the experimental error and the uncertainty in theoretical evaluation.

R. T. Daly, Jr., J. H. Holloway

References and Footnotes

1. P. Kusch and G. E. Becker, Phys. Rev. 73, 584 (1948).
2. N. F. Ramsey and H. B. Silsbee, Phys. Rev. 84, 506 (1951).
3. We are indebted to C. L. Schwartz for the calculation of the interval corrections.
4. For the interaction Hamiltonian, as well as an explicit definition of the constants a, b, and c, see V. Jaccarino et al., Phys. Rev. 94, 1798 (1954). For gallium, the definition of b given should be taken with opposite sign.

E. HYPERFINE STRUCTURE OF HALOGENS

V. Jaccarino and the author have remeasured the hyperfine structure of the stable bromine isotopes to higher precision and have found an octupole interaction that is well outside the experimental uncertainties. Further experimental work must be done before the final results are published.

The hyperfine structure of the long-lived radioactive isotope I^{129} is to be investigated. Since a large octupole interaction was found in the hfs of I^{127} previously studied at this laboratory, there is considerable interest in the proposed experiment. Apparatus for handling the small sample available and for improving the signal-to-noise ratio is being designed.

J. G. King

IX. MULTIPATH TRANSMISSION

Prof. J. B. Wiesner
E. J. Baghdady

NARROW-BAND LIMITING

A study of the behavior of the plots relating the minimum requirement in discriminator bandwidth (to reject two-path FM interference) to the ideal limiter filter bandwidth used (Quarterly Progress Report, April 15, 1954, Fig. VIII-2) sheds some interesting light on the nature of a set of curves that may be associated with those plots. We refer here to the smooth curves that may be drawn to connect the values of minimum required $(BW)_{disc}/(BW)_{if}$ at the odd integral values of $(BW)_{lim}/(BW)_{if}$ used. These curves are identified as the smooth curves shown in Fig. IX-1 superimposed on the calculated broken-curve plots. We will call these smooth curves the envelopes of the calculated plots since Fig. IX-1 shows that as $(BW)_{lim}/(BW)_{if}$ grows large, the broken-curve plots tend to be bounded by the smooth curves.

If we make the definitions

$$x \equiv \frac{(BW)_{lim}}{(BW)_{if}}$$

$$y \equiv \frac{(BW)_{disc}}{(BW)_{if}} \text{ at odd values of } x$$

$$= \text{"envelope" value of } \frac{(BW)_{disc}}{(BW)_{if}}$$

then the semilogarithmic plots of Fig. IX-2 show that

$$\ln\left[\frac{1+a}{1-a} - y\right]$$

is linearly related to x. We recall that a is the ratio of the undesired to the desired signal amplitude at the input to the ideal limiter. Simple calculations show that the plots of Fig. IX-2 lead to the expression

$$y(a,x) = \frac{1+a}{1-a}\left[1 - \zeta(a)\, e^{-k(a)x}\right] \qquad (1)$$

where values of k(a) and $\zeta(a)$ are plotted in Figs. IX-3(a) and (b). Figure IX-3(a) shows k(a) plotted against ln a and shows that the plotted points fit rather closely into a straight line given by

$$k(a) = -0.395 \ln a \qquad (2)$$

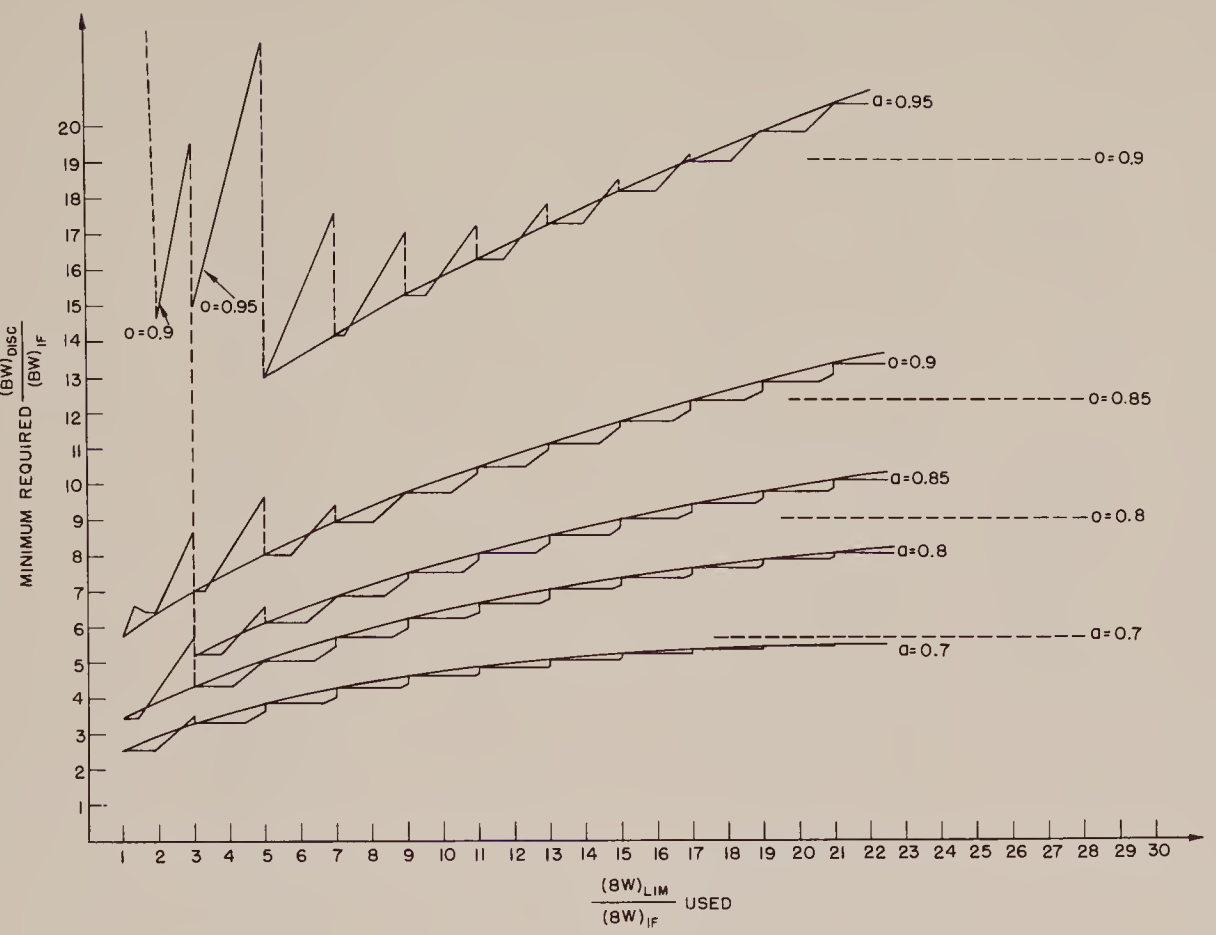

Fig. IX-1

Variation of the minimum discriminator bandwidth requirements with the limiter bandwidth used for various capture ratios, a. The broken curves connecting the calculated plots tend to be bounded by the superimposed smooth curves as the limiter bandwidth grows large.

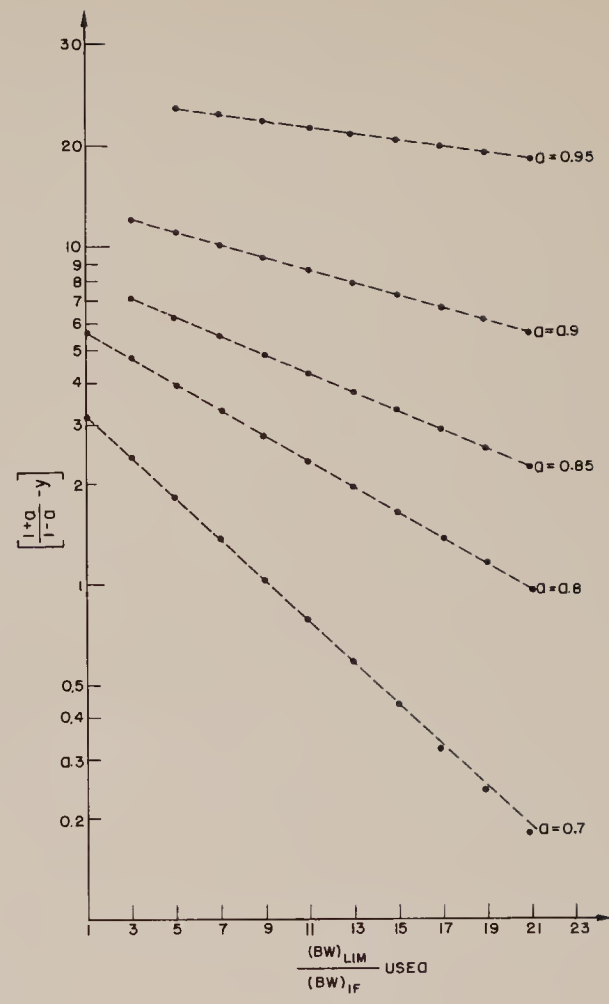

Fig. IX-2

Deviations from the asymptotic values (shown by the dashed horizontal lines in Fig. IX-1) of the discriminator bandwidth required at odd integral values of $(BW)_{lim}/(BW)_{if}$.

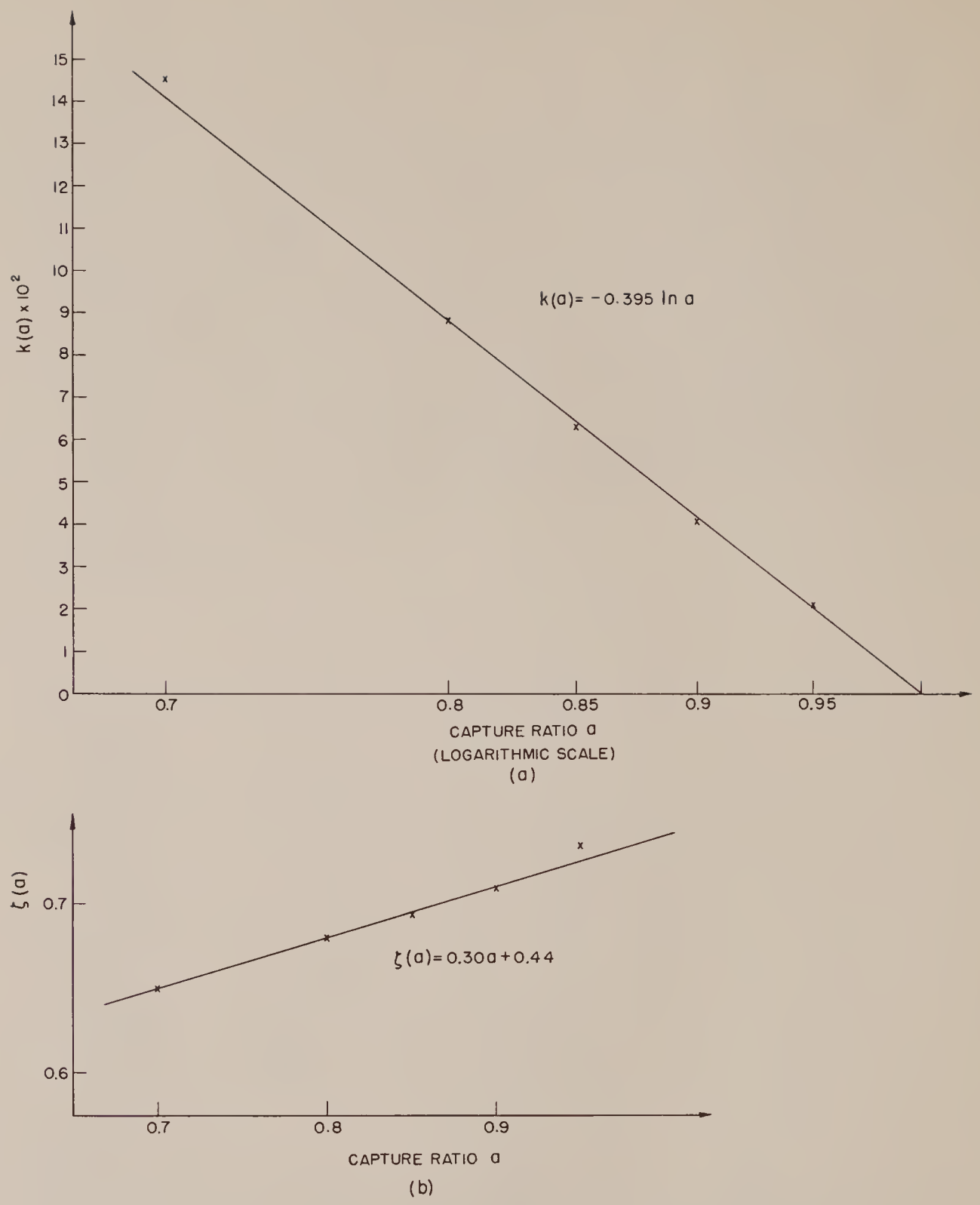

Fig. IX-3

Calculated values of the constants in Eq. 1, resulting from the plots of Fig. IX-2. The deviations of the plotted points from the straight line values may be attributed to small cumulative errors in computation.

The plot of $\zeta(a)$ shown is based on $k(a)$ as given by Eq. 2, with the reasonable assumption that the small deviations of the calculated values of $k(a)$ from the values given by Eq. 2 may be attributed to small cumulative errors in the computations. Figure IX-3(b) shows that the plotted values of $\zeta(a)$ fit into a straight line given by

$$\zeta(a) = 0.30\,a + 0.44 \tag{3}$$

Equation 1 may be normalized into the form

$$\psi(a) \equiv y(a, x) \Big/ \left[\frac{1 + a}{1 - a}\right]$$

$$= 1 - \zeta(a)\, e^{-k(a)x} \tag{4}$$

which is plotted in Fig. IX-4. Clearly, the second term in the right member of Eq. 4 gives the fractional reduction in the minimum required discriminator bandwidth that results from passing the resultant two-path signal through an ideal limiter whose bandwidth is an odd multiple, x, of the bandwidth of the intermediate-frequency section.

Now, at the odd values of x, it is recalled that (1)

$$\frac{(BW)_{disc}}{(BW)_{if}} = 2\,\frac{[\Delta\omega]}{(BW)_{if}} + 1 \tag{5}$$

where $[\Delta\omega]$ is the magnitude of the maximum deviation in the instantaneous frequency of the resultant signal at the output of the ideal limiter filter from the frequency of the desired carrier. It is clear from Fig. IX-1 that Eq. 5 also gives the value of $(BW)_{disc}/(BW)_{if}$ over the horizontal segment following the odd value of x for which $[\Delta\omega]$ is calculated. A combination of Eq. 1 and Eq. 5 yields

$$\frac{[\Delta\omega]}{(BW)_{if}} = \frac{1}{2}(y-1)$$

$$= \frac{a}{1 - a} - \frac{1}{2}\left(\frac{1 + a}{1 - a}\right)\zeta(a)\, e^{-k(a)x} \tag{6}$$

Further normalization yields

$$[\Delta\Omega] \equiv \frac{[\Delta\omega]}{(BW)_{if}} \cdot \frac{1 - a}{a}$$

$$= 1 - \frac{1 + a}{2a}\,\zeta(a)\, e^{-k(a)x} \tag{7}$$

The second term on the right of Eq. 7 yields the fractional amount by which the magnitude of the maximum deviation in instantaneous frequency has been reduced by passing

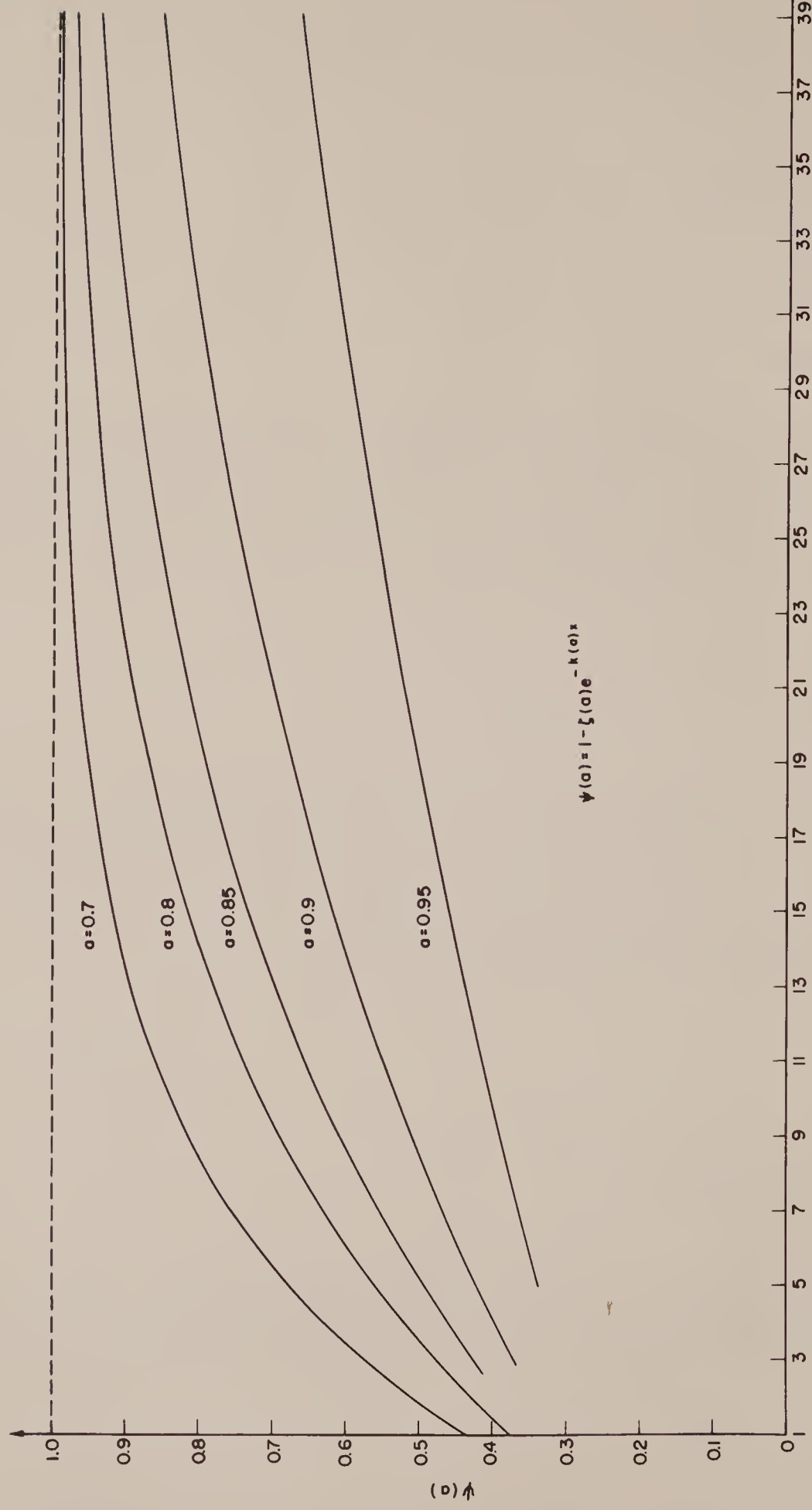

Fig. IX-4

Normalized plots of the envelopes of the broken curves in Fig. IX-1. ψ(a) equals the normalized minimum required discriminator bandwidths at the odd integral values of x.

the resultant two-path signal through an ideal limiter whose bandwidth is an odd multiple, x, of the bandwidth of the intermediate frequency.

Equation 1 is a useful supplement to the calculated plots of Fig. IX-1. It can be used to extrapolate the correct values of the minimum required discriminator bandwidth when the values of limiter bandwidth used are odd integral multiples, x, of the i-f bandwidth, that lie beyond the range covered by the calculated plots. At other values of x, Eq. 1 will yield an approximate answer. Equation 1 may also be used for the same purpose when the capture ratio, a, is required to assume a value that lies in the range $0.7 \leqslant a \leqslant 0.95$, but is not covered by the plots of Fig. IX-1. The indicated restriction in the range is given because the behavior of $\zeta(a)$ outside this range is not completely obvious from the plot of Fig. IX-3(b).

E. J. Baghdady

References

1. E. J. Baghdady, M. Sc. Thesis, Department of Electrical Engineering, M.I.T., August 1953.

X. STATISTICAL COMMUNICATION THEORY

Prof. Y. W. Lee
A. G. Bose
J. Y. Hayase
S. G. Margolis
C. E. McGinnis
S. D. Pezaris
W. B. Smith
R. E. Wernikoff

A. A THEOREM CONCERNING NOISE FIGURES

An expression is obtained for the greatest lower bound of the noise figure of a system consisting of n identical tubes whose plate signals are directly added and whose inputs are obtained through a linear passive coupling network from a source having an internal impedance R_s. It is found that the optimum attainable noise figure of such a system is equal to the optimum noise figure of a circuit consisting of one such tube and an appropriate coupling network.

Introduction

The electron tube, while providing amplification, is a source of noise. Thus, for the detection of weak signals it is advantageous to design the circuitry associated with the amplifier to maximize the signal-to-noise ratio at the output of the amplifier when it is fed from a given source. That is, it is advantageous to minimize the noise figure of the circuit. In the past, attempts have been made to obtain smaller noise figures than obtainable with one tube by using circuits involving more tubes; the plate signal of each tube was added directly to the plate signals of the other tubes to form the output of the circuit. Such attempts have been motivated by the hope that smaller noise figures could be obtained by taking advantage of the incoherency of noise voltages from different noise sources. (The signal at the output of each tube adds coherently while the noise arising from different tubes adds incoherently.) It is the purpose of this work to prove that the noise figure of a circuit involving n identical tubes, connected as indicated above, is at best equal to the optimum noise figure attainable with the use of only one tube and an appropriate coupling network.

Proof

The noise figure calculations are based on a unit bandwidth centered about a frequency f. It is assumed that each tube may be represented, as far as noise figure calculations are concerned, by a shunt resistance R_g and a series equivalent resistance R_{eq} followed by an ideal noiseless tube. According to this assumption, the equivalent circuit is shown in Fig. X-1. Associated with each resistance is a series thermal noise voltage source. For a resistance R the open circuit mean square voltage per unit bandwidth is $4KT\rho R$, where: K = Boltzmann's constant;

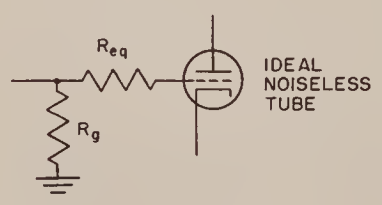

Fig. X-1
Noise equivalent circuit of conventional amplifier tube.

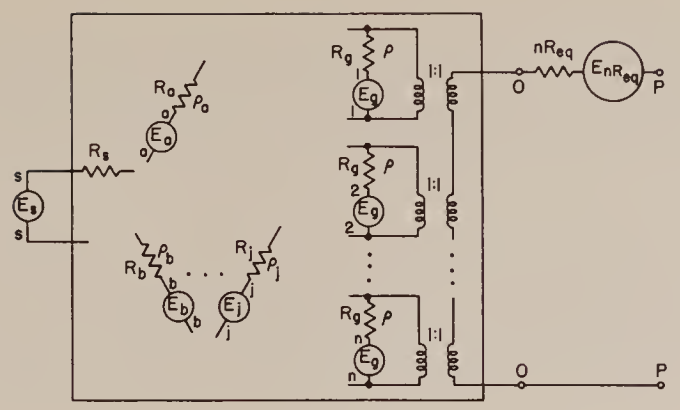

Fig. X-2

Equivalent circuit (for noise figure calculation) of a source coupled through a general coupling network to n tubes whose plate signals are directly added.

T = temperature in degrees Kelvin; ρ = a positive factor used to take into account the equivalent noise temperature of the resistance. We shall call it the equivalent temperature factor.

An equivalent circuit (as far as noise figure calculations are concerned) of a system consisting of n identical tubes whose plate signals are added directly and whose grid signals are obtained through a general linear passive coupling network from a source with impedance R_s is shown in Fig. X-2. The ideal noiseless tubes of Fig. X-1 have been replaced by ideal transformers whose turns ratios have conveniently been chosen to be unity. There is no loss of generality in this choice since a change in the output level affects both signal and noise and thus leaves the signal-to-noise ratio unaltered. The circuit shown in Fig. X-2, with the terminals p-p open circuited, has the same noise figure as the system of n tubes under consideration. The resistances R_a through R_j represent all the resistors in the coupling network. The sources in series with each resistor are the equivalent noise voltage sources. The equivalent temperature factor of each R_g is ρ. The equivalent temperature factor of each of the resistors in the coupling network is arbitrary and is denoted in Fig. X-2 by the symbol ρ with a subscript corresponding to the resistor with which it is associated.

For a linear system, the ratio of the open circuit voltage response at terminals k-k to a voltage excitation at terminals j-j can be expressed in terms of the short circuit admittance parameters as:

$$G(\omega) = -\frac{y_{kj}}{y_{kk}} \qquad (1)$$

The noise figure of a system is defined as

$$F = 1 + \frac{\text{"noise power" at the output caused by noise sources in the system}}{\text{"noise power" at the output caused by noise generated in the source impedance}} \qquad (2)$$

The term "noise power" denotes the integral of the power spectrum of the open circuit voltage over a unit bandwidth centered about a frequency f. Making use of Eqs. 1 and 2, the noise figure for the system shown in Fig. X-2 can be written as

$$F = 1 + \frac{n R_{eq} + \frac{\rho R_g}{|y_{oo}|^2}\left(|y_{01}|^2 + |y_{02}|^2 + \ldots + |y_{on}|^2\right) + \frac{1}{|y_{oo}|^2}\left(\rho_a R_a |y_{oa}|^2 + \ldots + \rho_j R_j |y_{oj}|^2\right)}{R_s \frac{|y_{os}|^2}{|y_{oo}|^2}} \qquad (3)$$

Certainly the right-hand side of this equation will not increase if we assume, for the purpose of calculation, that each of the resistors R_a through R_j in the coupling network has an equivalent temperature factor equal to zero. Equation 3 then becomes

$$F \geq 1 + \frac{n R_{eq} |y_{oo}|^2 + \rho R_g \left(|y_{01}|^2 + |y_{02}|^2 + \ldots + |y_{on}|^2\right)}{R_s |y_{os}|^2} \qquad (4)$$

Notice that the equality sign holds in Eq. 4 if R_a through R_j in Eq. 3 are zero.

Let g_{oo} be the real part of the output admittance y_{oo}. As a consequence of the relation $|y_{oo}| \geq g_{oo}$ we can write

$$F \geq 1 + \frac{n R_{eq} g_{oo}^2 + \rho R_g \left(|y_{01}|^2 + |y_{02}|^2 + \ldots + |y_{on}|^2\right)}{R_s |y_{os}|^2} \qquad (5)$$

Notice that the equality sign in Eq. 5 holds when the condition stated under Eq. 4 holds and, at the same time, the output admittance is real.

In order to reduce the number of variables in this expression for F (Eq. 5) let us make use of power relations at the output terminals 0-0. Let P be the power absorbed by the system when one volt is applied at the output terminals and all other voltage sources are shorted.

Then

$$P = R_s |y_{so}|^2 + R_g \left(|y_{10}|^2 + |y_{20}|^2 + \ldots + |y_{no}|^2\right) + P_1 \qquad (6)$$

where P_1 is the power absorbed in the coupling circuit resistors R_a through R_j and is therefore equal to or greater than zero. Furthermore, for the particular excitation mentioned above, P is just equal to g_{oo}. Using this fact and the relation $y_{ik} = y_{ki}$ for a bilateral network we obtain the equation

$$g_{oo} = R_s|y_{os}|^2 + R_g\left(|y_{01}|^2 + |y_{02}|^2 + \ldots + |y_{on}|^2\right) + P_1 \tag{7}$$

Using Eq. 7 in Eq. 5 we have

$$F \geq 1 - \rho + \frac{n R_{eq} g_{oo}^2 + \rho g_{oo} - \rho P_1}{R_s|y_{so}|^2} \tag{8}$$

In order to simplify this expression further let us again consider the system shown in Fig. X-2. We shall excite the system at the terminals 0-0 with a unit voltage source. For convenience Fig. X-2 is redrawn in Fig. X-3 with the resistances R_g referred to the secondary of the ideal one-to-one ratio transformers. We desire to find a relation between g_{oo} and $|y_{os}|$. In obtaining this relation it is convenient to make use of the following inequality (the proof of this inequality is given in the following subsection):

$$\sum_{k=1}^{n} |e_k|^2 \geq \frac{1}{n}\left|\sum_{k=1}^{n} e_k\right|^2 \tag{9}$$

For a one-volt excitation at terminals 0-0 it is seen, from power considerations and the use of Eq. 7, that

$$g_{oo} = \frac{1}{R_g}\left(|e_1|^2 + |e_2|^2 + \ldots + |e_n|^2\right) + R_s|y_{so}|^2 + P_1$$

$$\geq R_s|y_{so}|^2 + \frac{1}{n R_g} + P_1 \tag{10}$$

Notice that the equality sign holds if the coupling network is symmetrical with respect to its n outputs. Substitution of the expression for $|y_{so}|^2$, obtained from Eq. 10, in Eq. 8 yields

$$F \geq 1 - \rho + \frac{n R_{eq} g_{oo}^2 + \rho g_{oo} - \rho P_1}{g_{oo} - \frac{1}{n R_g} - P_1} = A \tag{11}$$

The quantity A is thus expressed as an explicit function of the two variables g_{oo} and P_1. We desire to minimize A with respect to these two variables. It can be seen from

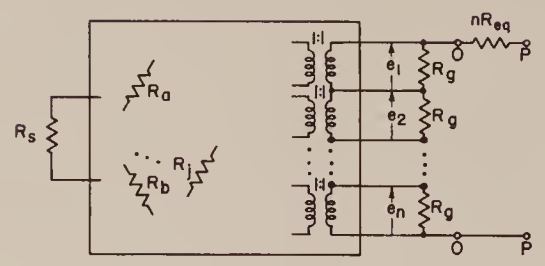

Fig. X-3

Redrawn with all the noise voltage sources set to zero and with the resistances R_g referred to the secondary of the ideal transformers.

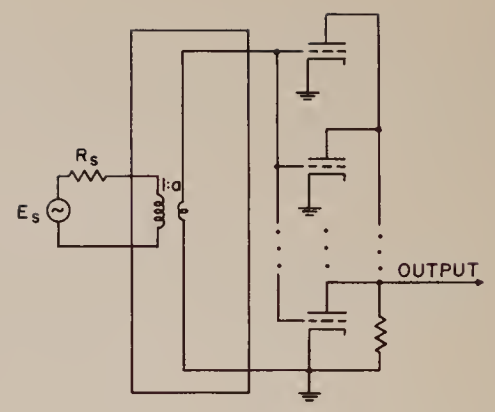

Fig. X-4

Example of a circuit using n tubes and having the minimum obtainable noise figure of one tube.

Eq. 7 that g_{oo} and P_1 are, in general, dependent quantities. If A is minimized with respect to g_{oo} and P_1, considered as independent variables, the minimum value thus obtained will certainly be equal to, or less than, the minimum obtained when the constraints are imposed. Further, it will be seen that in this particular case the minimums are equal since a coupling network corresponding to the minimum A will be physically realizable.

Proceeding with the minimization, Eq. 11 yields

$$\frac{\partial A}{\partial P_1} = \frac{\frac{\rho}{n R_g} + n R_{eq} g_{oo}^2}{\left(g_{oo} - \frac{1}{n R_g} - P_1\right)^2} > 0 \qquad (12)$$

A justification of the inequality symbol in this equation is necessary. Referring to Eq. 10 we see that the denominator in Eq. 12 is always positive and greater than zero. (It can be zero only for the trivial case in which $R_s |y_{so}|^2$ is zero, a case which clearly is of no interest since it implies either a zero impedance source or no transmission from input to output, that is, $y_{so} = 0$.) Since ρ is a positive quantity, it is clear that the numerator of Eq. 12 is greater than zero and that the inequality symbol is valid as shown.

Since $(\partial A/\partial P_1) > 0$ and since $P_1 \geq 0$, the minimum value of A occurs for $P_1 = 0$. We next find the optimum g_{oo} which gives the minimum A for $P_1 = 0$.

$$A_{(P_1=0)} = 1 - \rho + \frac{n R_{eq} g_{oo} + \rho}{1 - \frac{1}{n R_g g_{oo}}} \qquad (13)$$

$$\frac{\partial A_{(P_1=0)}}{\partial g_{oo}} = \frac{n R_{eq} - \dfrac{2 R_{eq}}{R_g g_{oo}} - \dfrac{\rho}{n R_g g_{oo}^2}}{\left(1 - \dfrac{1}{n R_g g_{oo}}\right)^2} = 0 \tag{14}$$

For the same reasons discussed earlier relative to Eq. 12, the denominator of Eq. 14 is always greater than zero. Thus by setting the numerator equal to zero we obtain the optimum value of g_{oo}.

$$g_{oo_{opt}} = \frac{1}{n R_g}\left[1 + \left(1 + \frac{\rho R_g}{R_{eq}}\right)^{1/2}\right] \tag{15}$$

Substituting this optimum value of g_{oo} into Eq. 13 we obtain the minimum value of A.

$$A_{min} = 1 + 2\frac{R_{eq}}{R_g}\left[1 + \left(1 + \frac{\rho R_g}{R_{eq}}\right)^{1/2}\right] \tag{16}$$

The fact that the value of A obtained by this procedure is a minimum can be verified by considering Eqs. 10 and 13.

In view of Eqs. 11 and 15 we can write

$$F \geqslant 1 + 2\frac{R_{eq}}{R_g}\left[1 + \left(1 + \frac{\rho R_g}{R_{eq}}\right)^{1/2}\right] \tag{17}$$

The fact that the equality sign in this inequality is valid is most readily demonstrated by presenting an example in which it holds. The construction of an example is facilitated by noting the sufficient conditions for the validity of the equality sign in the relations of Eqs. 4, 5, and 10. These conditions are stated immediately following their respective equations. Such an example is shown in Fig. X-4. All of the n tubes are in parallel, and the general coupling network is just an ideal transformer with an appropriate turns ratio. A straightforward calculation shows that this circuit has the noise figure given by Eq. 17 with the equality sign when each tube has the input resistance R_g (with an equivalent temperature factor ρ) and the equivalent shot noise resistance R_{eq}.

The interesting result is that the right-hand member of Eq. 17 is independent of n and is exactly the optimum noise figure attainable using a single tube. For $R_{eq}/R_g \ll 1$,

Eq. 17 reduces to the more familiar form for the noise figure of a single stage (1):

$$F \geq 1 + 2\left(\frac{\rho R_{eq}}{R_g}\right)^{1/2} \tag{18}$$

Derivation of Inequality 9

Derivation of the inequality:

$$\sum_{k=1}^{n} |e_k|^2 \geq \frac{1}{n}\left|\sum_{k=1}^{n} e_k\right|^2 \tag{9}$$

Since the magnitude of the sum of complex numbers is less than or equal to the sum of the magnitudes we can write

$$\frac{1}{n}\left|\sum_{k=1}^{n} e_k\right|^2 \leq \frac{1}{n}\left(\sum_{k=1}^{n} |e_k|\right)^2 \tag{19}$$

But

$$\frac{1}{n}\left(\sum_{k=1}^{n} |e_k|\right)^2 = \sum_{k=1}^{n} |e_k|^2 - \frac{1}{n}\left\{(n-1)\sum_{k=1}^{n} |e_k|^2 - \sum_{\substack{i,k \\ i\neq k}} |e_i e_k|\right\}$$

$$= \sum_{k=1}^{n} |e_k|^2 - \frac{1}{2n}\sum_{\substack{i,k \\ i\neq k}} \left(|e_i| - |e_k|\right)^2 \leq \sum_{k=1}^{n} |e_k|^2 \tag{20}$$

Thus, combining Eq. 19 and Eq. 20 we have the desired result:

$$\sum_{k=1}^{n} |e_k|^2 \geq \frac{1}{n}\left|\sum_{k=1}^{n} e_k\right|^2$$

A. G. Bose, S. D. Pezaris

References

1. G. E. Valley, Jr. and H. Wallman, M.I.T. Radiation Laboratory Series, Vol. 18 (McGraw-Hill Book Company, Inc., New York, 1948) p. 640.

B. THE WIENER THEORY OF NONLINEAR SYSTEMS

Introduction

Briefly stated, the objectives of Dr. Wiener's method are to characterize nonlinear systems independent of their input and to present a method for synthesizing the systems from their characterizing parameters. An operator relating the input and output of the nonlinear system is defined in such a way that the parameters which characterize the system can be evaluated experimentally.

The method is confined to those nonlinear systems in which the remote past becomes less and less relevant to the behavior of the system as we push it back in time. It is further restricted to those systems in which fast changes in the output, relative to the input, do not occur. The reason for these restrictions, as will become apparent, is to avoid an excessive number of terms in the Laguerre and Hermite expansions respectively.

As Dr. Wiener has shown, the proper probe for the general investigation of nonlinear systems is the output of a shot-effect generator (gaussian noise with a flat power spectrum). The shot effect is the most general probe and enables nonlinear systems to be classified for all inputs (1).

Definitions

To simplify the description of the method, it is convenient at this point to define certain quantities and relations that are useful in the development of the method.

A. The nth Laguerre polynomial,

$$L_n(x) = \frac{1}{n!} e^x \frac{d^n}{dx^n} (x^n e^{-x})$$

B. The normalized Laguerre functions $h_n(x)$ are defined

$$h_n(x) = e^{-x/2} L_n(x) \tag{1}$$

The following orthogonality relation exists for these functions:

$$\int_0^\infty h_m(x)\, h_n(x)\, dx = \begin{cases} 1 \text{ if } m = n \\ 0 \text{ if } m \neq n \end{cases} \tag{2}$$

C. The nth Hermite polynomial

$$H_n(x) = (-1)^n e^{x^2} \left(\frac{d}{dx}\right)^n e^{-x^2}$$

D. The normalized Hermite polynomials $\phi_n(x)$ are defined

$$\phi_n(x) = \frac{H_n(x)}{\left(2^n\, n!\, (\pi)^{1/2}\right)^{1/2}} \tag{3}$$

E. The normalized Hermite functions are defined

$$\psi_n(x) = e^{-x^2/2}\, \phi_n(x) \tag{4}$$

These functions form a normal orthogonal set over the interval $-\infty$ to ∞. Consequently, we have the relation

$$\int_{-\infty}^{\infty} \phi_m(x)\, \phi_n(x)\, e^{-x^2}\, dx = \begin{cases} 1 & m = n \\ 0 & m \neq n \end{cases} \tag{5}$$

Description of the General Method of Characterization and Synthesis

Now let us consider a nonlinear system whose input and output are the stationary time series x(t) and y(t), respectively. In general, y(t) is some function of the past of x(t). Consequently, it is of interest to obtain a set of parameters which characterize the past of x(t). The past of x(t) can be expanded in a series of Laguerre functions as indicated in Eq. 6

$$x(-t) = \sum_n u_n\, h_n(t) \tag{6}$$

The Laguerre functions form a complete set over the interval zero to infinity and the coefficients u_n form a set of variables which characterize the past of x(t).

These Laguerre coefficients of the past of a time function x(t) are easily generated in practice. They are simply the output of a Laguerre network (a network whose impulse response is $h_n(t)$) whose input is x(t). This can be seen as follows. Referring to Fig. X-5, the output at the present time (t=0) is given by the convolution of x(t) with $h_n(t)$. That is,

$$y(0) = \int_{-\infty}^{0} x(z)\, h_n(0-z)\, dz = \int_{0}^{\infty} x(-z)\, h_n(z)\, dz \tag{7}$$

Let us compare this expression for $y_n(0)$ with the expression for u_n which is obtained

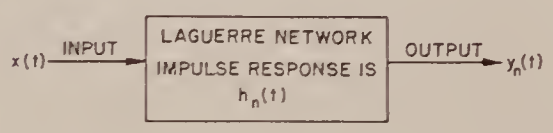

Fig. X-5
Block diagram of Laguerre network.

from Eq. 6 by making use of the orthogonality property of Eq. 2. The latter expression is

$$u_n = \int_0^\infty x(-t)\, h_n(t)\, dt \tag{8}$$

Comparison of Eqs. 7 and 8 shows that $y_n(0) = u_n$. Thus we have demonstrated that the coefficients u_n can be generated by the method shown in Fig. X-5. The actual form of the Laguerre network and the method of synthesis of this network will not be discussed here. For a complete discussion of these topics the reader is referred to reference 2.

Since the set of coefficients u_n characterize the past of x(t), any quantity dependent only on the past of x(t) may be represented as a function of these coefficients. Thus for the nonlinear system with input x(t) and output y(t) we can write

$$y(t) = F\left[u_1, u_2, \ldots, u_s\right] \tag{9}$$

For reasons that will soon become apparent it is convenient to express this function F as a Hermite function expansion of the variables u_1 through u_s. We then have

$$y(t) = \sum_i \sum_j \cdots \sum_h a_{i,j,\ldots,h}\, \phi_i(u_1)\, \phi_j(u_2) \cdots \phi_h(u_s)\, e^{-\frac{u_1^2+u_2^2+\ldots+u_s^2}{2}} \tag{10}$$

In order to simplify this equation let $\Phi(\alpha)$ represent the polynomial $\phi_i(u_1) \ldots \phi_h(u_s)$, and A_α represent the corresponding value of $a_{i,j,\ldots,h}$. Then Eq. 10 becomes

$$y(t) = \sum_\alpha A_\alpha\, \Phi(\alpha)\, e^{-\frac{u_1^2+\ldots+u_s^2}{2}} \tag{11}$$

If, in Eq. 10, the indices i, j, . . . , h range from 0 to N - 1, then α ranges from 0 to $N^s - 1$.

To characterize the nonlinear system, it is necessary to evaluate the coefficients A_α in Eq. 11. To this end, consider the time average

$$\overline{y(t)\, \Phi(\beta)} = \sum_\alpha A_\alpha\, \overline{\Phi(\alpha)\, \Phi(\beta)\, e^{-\frac{u_1^2+\ldots+u_s^2}{2}}} \tag{12}$$

Let us take advantage of the ergodic theorem in evaluating the right-hand member of

this equation. We then have

$$\overline{y(t)\,\Phi(\beta)} = \sum_{a} A_a \int_{-\infty}^{\infty} \cdots \int_{-\infty}^{\infty} \Phi(a)\,\Phi(\beta)\, e^{-\frac{u_1^2+\ldots+u_s^2}{2}} P(u_1, \ldots, u_s)\, du_1 \ldots du_s \tag{13}$$

As mentioned earlier, the probe for the investigation of the nonlinear system is the output of a shot-effect generator. Thus, for the evaluation of the coefficients A_a in Eq. 13, the input x(t) to the nonlinear system is a gaussian signal with a flat power spectrum. Now recall that the parameters u_1 through u_s which characterize the past of x(t) can be obtained as the outputs of the linear passive Laguerre network whose input is x(t). Thus, if x(t) has a gaussian distribution, then u_1 through u_s all have gaussian distributions. In fact, it can be shown from the properties of the Laguerre network, or from the definition of the Laguerre functions, that u_1 through u_s all have independent normalized gaussian distributions when x(t) is gaussian with a flat power spectrum and the proper variance. Thus we have

$$P(u_1, \ldots, u_s) = (2\pi)^{-s/2}\, e^{-\frac{u_1^2+\ldots+u_s^2}{2}} \tag{14}$$

so that Eq. 13 becomes

$$\overline{y(t)\,\Phi(\beta)} = (2\pi)^{-s/2} \sum_{a} A_a \int_{-\infty}^{\infty} \cdots \int_{-\infty}^{\infty} \Phi(a)\,\Phi(\beta)\, e^{-(u_1^2+\ldots+u_s^2)}\, du_1 \ldots du_s \tag{15}$$

The reason for the choice of Hermite functions for the expansion of Eq. 9 now becomes apparent. The joint gaussian probability density (Eq. 14) supplies the necessary exponential factor in the Hermite function expansion (Eq. 12) to enable us to take advantage of the orthogonality relation of Eq. 5 in evaluating the coefficients A_a. Taking advantage of this orthogonality we have:

$$A_\beta = (2\pi)^{s/2}\, \overline{y(t)\,\Phi(\beta)} \tag{16}$$

The A_a's, together with a knowledge of the number of Laguerre coefficients used, serve to characterize the nonlinear system under test. The setup for the experimental evaluation of the coefficients A_a is shown in Fig. X-6.

Now let us consider the problem inverse to that discussed above. Suppose we are given a set of coefficients A_a and asked to find a nonlinear system corresponding to these coefficients. Equation 11 is the guide for the synthesis problem. This equation tells us that, for each a, we must form $\Phi(a)$ and multiply it by A_a and the exponential

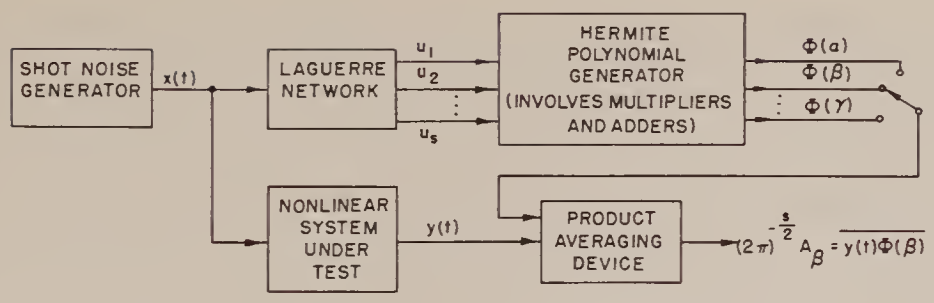

Fig. X-6

Block diagram of the circuitry for the classification of nonlinear systems.

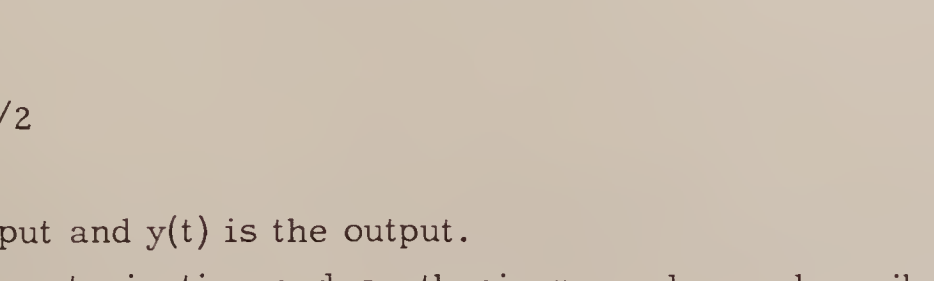

Fig. X-7

Block diagram for the synthesis of nonlinear systems.

$\exp -\left(u_1^2 + \ldots + u_s^2\right)/2$. Then each such product must be added. In practice, the number of multipliers is reduced if we first form the sum of the products $A_\alpha\ \Phi(\alpha)$ and then multiply by the exponential function.

The exponential function, $\exp -\left(u_1^2 + \ldots + u_s^2\right)/2$, can be obtained as the product of s exponential function generators whose inputs are respectively u_1 through u_s. Such generators give an output of $\exp -(x^2/2)$ when the input is x. They are realizable, among other ways, in the form of a small cathode-ray tube with a special target to generate the $\exp -(x^2/2)$ function.

The block diagram of the circuitry used for the synthesis procedure is shown in Fig. X-7.

Example

In order to fix ideas, let us consider a simple example which is particularly suited to characterization and synthesis by Dr. Wiener's method. Let the given nonlinear system contain no storage elements. Further let its input-output characteristic be given by the equation

$$y(t) = e^{-x^2(t)/2} \tag{17}$$

where x(t) is the input and y(t) is the output.

In both the characterization and synthesis procedures described, the Laguerre

network is used to introduce dependence of the output upon the past of the input. The nonlinearity is brought about by the Hermite polynomial generator. For the simple example under consideration, there is no dependence upon the past and thus we can by-pass the Laguerre network. In the experimental procedure, the fact that this nonlinear system has no storage can easily be determined from the results of a priori tests made on the system.

To proceed with the characterization of the simple example, we notice that as a result of by-passing the Laguerre network (Fig. X-6) the variables u_1 through u_s are replaced by the single variable x(t). Equation 10 then becomes:

$$y(t) = \sum_i a_i \, \phi_i(x) \, e^{-x^2/2} \tag{18}$$

Equation 16 becomes

$$a_i = (2\pi)^{1/2} \, \overline{y(t) \, \phi_i(x)} \tag{19}$$

Let us make use of the ergodic theorem to evaluate this time average as an ensemble average. Using Eq. 17 we can write

$$a_i = (2\pi)^{1/2} \int_{-\infty}^{\infty} \phi_i(x) \, e^{-x^2/2} \, p(x) \, dx \tag{20}$$

But since, in the test setup, x(t) is the output of an ideal shot-effect generator, the probability density of x is

$$p(x) = \frac{1}{(2\pi)^{1/2}} \, e^{-x^2/2} \tag{21}$$

Thus

$$a_i = \int_{-\infty}^{\infty} \phi_i(x) \, e^{-x^2} \, dx \tag{22}$$

Referring to Eq. 3 and the definition of the Hermite polynomial, it is seen that

$$\phi_o(x) = \pi^{-1/4} \tag{23}$$

With this result, Eq. 22 becomes

$$a_i = \pi^{1/4} \int_{-\infty}^{\infty} \phi_i(x) \, \phi_o(x) \, e^{-x^2} \, dx \tag{24}$$

As a consequence of the orthogonality relation of Eq. 5 we have the result

$$a_o = \pi^{1/4}$$
$$a_i = 0 \quad i \neq 0 \tag{25}$$

The relations of Eq. 25 together with the knowledge that the Laguerre network has been by-passed serve to characterize the given nonlinear system.

Now let us consider the inverse problem with respect to the same example. Suppose we are given the coefficients of Eq. 25 along with the associated information in the preceding paragraph. Our job is to synthesize the corresponding nonlinear system.

The guide for the synthesis is Eq. 18 which corresponds to Eq. 11 in the more complicated case. Following the general procedure for the synthesis described earlier it is readily seen that the resulting system is that shown in Fig. X-8. Figure X-8(a) shows how the synthesis takes form according to the formal dictates of Eq. 18. The simplified equivalent system obtained from Fig. X-8(a) by inspection is shown in Fig. X-8(b). We see that for the simple example considered the synthesized system consists solely of the "function generator," a component which in the more complicated case will form only a part of the synthesized system.

At this point it is of interest to note that we have at our disposal the two scale factors of the Laguerre and Hermite functions. For simplicity in the presentation of the basic concepts of Dr. Wiener's method, these scale factors have been chosen to be unity. In practice, they can be used to reduce the number of parameters, A_a, necessary to characterize the system. They are to be judiciously chosen on the basis of a priori knowledge of, or tests made on, the nonlinear system.

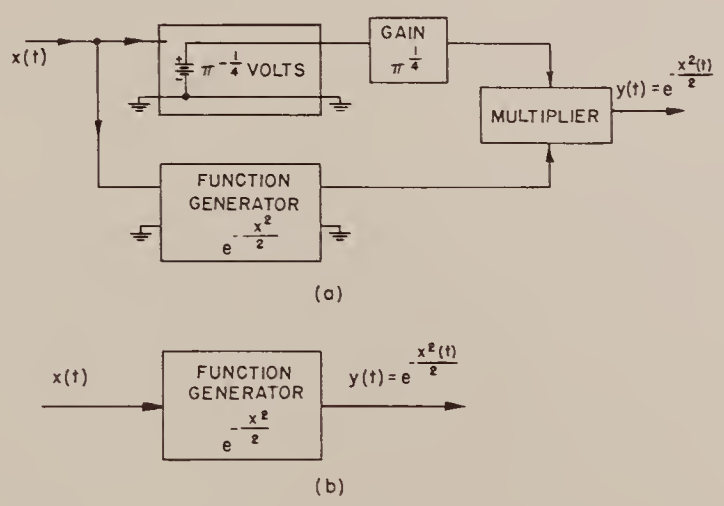

Fig. X-8

(a) Synthesis of the nonlinear characteristic $y = \exp -(x^2/2)$ according to the general procedure of Fig. X-7. (b) Equivalent reduced form of part (a).

In concluding this discussion of Dr. Wiener's method of nonlinear systems the question naturally arises as to the number of parameters, A_α, that may be necessary to characterize a practical system. In the simple example worked earlier, only one parameter was necessary. However, suppose we have a system which requires s Laguerre coefficients to sufficiently characterize that portion of the past of x(t) which influences the behavior of the system. Further suppose we decide that a sufficient approximation to the performance of the system is obtained by letting the indices i, j, . . . , h in Eq. 10 range from 0 to N - 1. Then there are N^s parameters (A_α) necessary to characterize the system. Without a doubt this number can become quite large in many practical cases. However, with the freedom that exists in nonlinear systems, one can hardly expect to apply such a general approach without considerable effort.

A. G. Bose

References

1. N. Wiener, Mathematical problems of communication theory, summer session lecture notes, M.I.T., 1953-1954, unpublished.

2. Y. W. Lee, J. Math. Phys. 11, 83-113 (1932).

C. PROPERTIES OF SECOND-ORDER AUTOCORRELATION FUNCTIONS

In the study of second-order autocorrelation functions the following two definitions are used:

$$\phi_{111}(\tau_1, \tau_2) = \overline{f_1(t)\, f_1(t+\tau_1)\, f_1(t+\tau_1+\tau_2)} \tag{1}$$

$$\phi^*_{111}(\tau_1, \tau_2) = \overline{f_1(t)\, f_1(t+\tau_1)\, f_1(t+\tau_2)} \tag{2}$$

where $f_1(t)$ is a stationary time series.

By shifting the time origin in Eq. 1 we obtain the following relations between the two definitions:

$$\left.\begin{aligned} \phi_{111}(\tau_1, \tau_2) &= \phi^*_{111}(\tau_2, -\tau_1) && \text{(a)} \\ \phi_{111}(-\tau_1, \tau_2) &= \phi^*_{111}(\tau_1, \tau_2) && \text{(b)} \\ \phi_{111}(\tau_1, -\tau_2) &= \phi^*_{111}(-\tau_1, -\tau_2) && \text{(c)} \\ \phi_{111}(-\tau_1, -\tau_2) &= \phi^*_{111}(-\tau_2, \tau_1) && \text{(d)} \end{aligned}\right\} \tag{3}$$

From the definition of $\phi^*_{111}(\tau_1, \tau_2)$ it is clear that

$$\phi^*_{111}(\tau_1, \tau_2) = \phi^*_{111}(\tau_2, \tau_1) \tag{4}$$

Making use of this relation, we obtain from 3(a) and 3(d) the relations

$$\phi_{111}(\tau_1, \tau_2) = \phi^*_{111}(-\tau_1, \tau_2) \tag{3a'}$$

$$\phi_{111}(-\tau_1, -\tau_2) = \phi^*_{111}(\tau_1, -\tau_2) \tag{3d'}$$

The relations between $\phi_{111}(\tau_1, \tau_2)$ and $\phi^*_{111}(\tau_1, \tau_2)$ as given by Eqs. 3b, c, a', and d' are illustrated in Fig. X-9. From these relations it can be shown that the $\phi_{111}(\tau_1, \tau_2)$ plane is the $\phi^*_{111}(\tau_1, \tau_2)$ plane rotated about the τ_2 axis by 180°. That is, the $\phi_{111}(\tau_1, \tau_2)$ plane is the mirror image of the $\phi^*_{111}(\tau_1, \tau_2)$ plane about the τ_2 axis. Consequently, given the properties of $\phi^*_{111}(\tau_1, \tau_2)$, we can easily establish the corresponding properties of $\phi_{111}(\tau_1, \tau_2)$ and vice versa.

By a process similar to that used to derive Eq. 3, we obtain from Eq. 1 the relation

$$\phi_{111}(\tau_1, \tau_2) = \phi_{111}(-\tau_2, -\tau_1) = \phi_{111}(-\tau_1, \tau_1+\tau_2) = \phi_{111}(\tau_2, -\tau_1-\tau_2) \tag{5}$$

This shows that a knowledge of one quadrant of $\phi_{111}(\tau_1, \tau_2)$ is sufficient to determine the

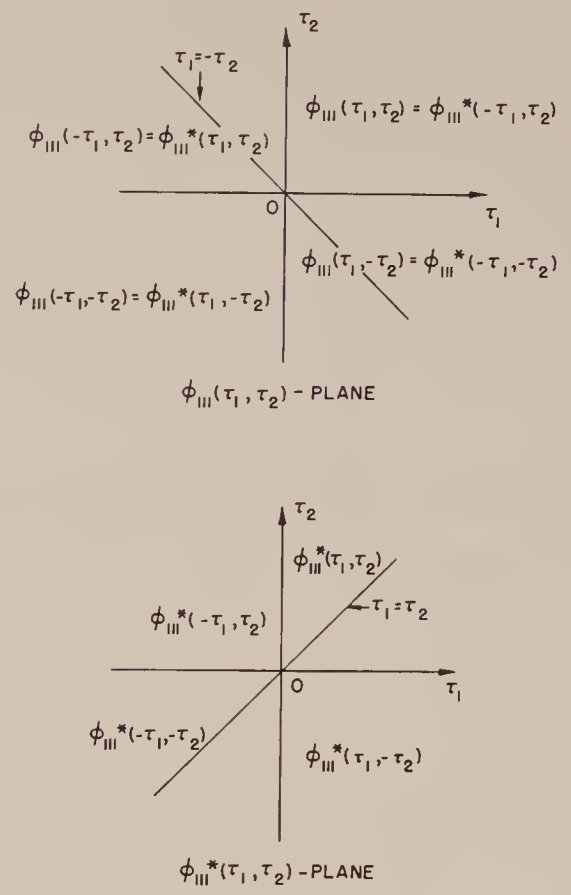

Fig. X-9

Relation between $\phi_{111}(\tau_1,\tau_2)$ and $\phi_{111}^*(\tau_1,\tau_2)$.

The $\phi_{111}(\tau_1,\tau_2)$ plane is the $\phi_{111}^*(\tau_1,\tau_2)$ plane rotated 180° about the τ_2 axis.

remaining three quadrants, although such a procedure as indicated by this equation would not, in general, be the most practical method for constructing the remaining quadrants.

Now let us consider symmetry properties of second-order correlation functions. From Eq. 4 we see that $\phi_{111}^*(\tau_1,\tau_2)$ is always symmetrical about the line $\tau_1=\tau_2$. It follows from this fact, and the mirror image relationship between the $\phi_{111}(\tau_1,\tau_2)$ and $\phi_{111}^*(\tau_1,\tau_2)$ planes, that $\phi_{111}(\tau_1,\tau_2)$ is always symmetrical about the line $\tau_1=-\tau_2$.

It is of interest to show that if f(t) is a stationary time series such that the statistical behavior of f(t) is identical with the statistical behavior of the time series f(-t), then $\phi_{111}(\tau_1,\tau_2)$ is symmetrical about the line $\tau_1=\tau_2$ in addition to being symmetrical about the line $\tau_1=-\tau_2$. Symmetry about the line $\tau_1=\tau_2$ means that $\phi_{111}(\tau_1,\tau_2)=\phi_{111}(\tau_2,\tau_1)$. Sufficient conditions for this equality can be established by expressing $\phi_{111}(\tau_1,\tau_2)$ as an ensemble average.

$$\phi_{111}(\tau_1,\tau_2)=\int_{-\infty}^{\infty}\int_{-\infty}^{\infty}\int_{-\infty}^{\infty} xyz\ P\left(x, y_{\tau_1}, z_{\tau_1+\tau_2}\right) dx\ dy\ dz \qquad (6)$$

In this expression $P\left(x, y_{\tau_1}, z_{\tau_1+\tau_2}\right)$ is the third probability density of f(t). The subscripts of the variables denote the time of observation relative to the time $\tau=0$ when the variable with no subscript (x in this particular expression) is observed. Using this notation we can write

$$\phi_{111}(\tau_2,\tau_1)=\int_{-\infty}^{\infty}\int_{-\infty}^{\infty}\int_{-\infty}^{\infty} x'y'z'\ P\left(x', y'_{\tau_2}, z'_{\tau_1+\tau_2}\right) dx'\ dy'\ dz' \qquad (7)$$

Now, in Eq. 7 let us change the dummy variables of integration. Let x' =z, y' = y,

and $z' = x$. Then Eq. 7 becomes:

$$\phi_{111}(\tau_2, \tau_1) = \int_{-\infty}^{\infty} \int_{-\infty}^{\infty} \int_{-\infty}^{\infty} xyz\, P\left(x_{\tau_1+\tau_2}, y_{\tau_2}, z\right) dx\, dy\, dz \tag{8}$$

To put this equation into a form convenient for comparison to Eq. 6, let us translate the τ axis to establish the reference axis (τ=0) at the time when the variable x is observed. The result is:

$$\phi_{111}(\tau_2, \tau_1) = \int_{-\infty}^{\infty} \int_{-\infty}^{\infty} \int_{-\infty}^{\infty} xyz\, P\left(x, y_{-\tau_1}, z_{-\tau_1-\tau_2}\right) dx\, dy\, dz \tag{9}$$

Comparing Eqs. 6 and 9 we see that a sufficient condition for the existence of symmetry about the line $\tau_1 = \tau_2$ is

$$P\left(x, y_{\tau_1}, z_{\tau_1+\tau_2}\right) = P\left(x, y_{-\tau_1}, z_{-\tau_1-\tau_2}\right) \tag{10}$$

This relation clearly holds for all stationary time series f(t) which have the same statistical behavior as the corresponding time series f(-t). If f(t) is a periodic function, Eq. 10 will hold, and thus there will be symmetry about the line $\tau_1 = \tau_2$ for all functions having a time origin about which the function is symmetrical.

It has been shown that $\phi_{111}(\tau_1, \tau_2)$ is always symmetrical about the line $\tau_1 = -\tau_2$ and is sometimes symmetrical about the line $\tau_1 = \tau_2$. The question naturally arises as to the existence of symmetry about the τ_1 and τ_2 axes. It is next shown that, with the exception of functions which give a constant second-order autocorrelation function, symmetry about the τ_1 and τ_2 axes is not present. This result will be proved by the method of contradiction.

By performing a translation of the time origin in Eqs. 1 and 2, it can be shown that if symmetry exists about either the τ_1 or τ_2 axis, then it exists about both axes. Hence, for the proof it is sufficient to show that the assumption of symmetry about the τ_2 axis leads to a contradiction.

The assumption is

$$\phi_{111}(\tau_1, \tau_2) = \phi_{111}(-\tau_1, \tau_2) \tag{11}$$

Using this relation and Eq. 3a' we obtain the relation

$$\phi_{111}(-\tau_1, \tau_2) = \phi^*_{111}(-\tau_1, \tau_2) \tag{12}$$

Expressing $\phi_{111}(-\tau_1, \tau_2)$ in terms of definition 2,

$$\phi_{111}(-\tau_1, \tau_2) = \phi^*_{111}(-\tau_1, \tau_2 - \tau_1) \tag{13}$$

Hence, from Eqs. 12 and 13

$$\phi^*_{111}(-\tau_1, \tau_2) = \phi^*_{111}(-\tau_1, \tau_2 - \tau_1) \tag{14}$$

If τ_1 is held fixed in Eq. 14, $\phi^*_{111}(-\tau_1, \tau_2)$ is periodic with respect to τ_2 with a period equal to the value of τ_1. This result is a contradiction when $f_1(t)$ is a random stationary time series, for the second-order autocorrelation function of a random function is not periodic with respect to either τ_2 or τ_1. The result is also a contradiction when $f_1(t)$ is a periodic function, for the second-order autocorrelation of a periodic function is periodic with respect to τ_2 for a given τ_1 but the period is independent of τ_1. Hence assumption 11 leads to a contradiction. This proves that $\phi_{111}(\tau_1, \tau_2)$ is not symmetrical with respect to the τ_1 or τ_2 axes except for the degenerate case in which $\phi_{111}(\tau_1, \tau_2)$ is a constant.

Y. W. Lee, A. G. Bose, J. Y. Hayase

D. FIELD MAPPING BY CROSSCORRELATION

The problem of determining the location of n sources of independent random stationary time series by the method of crosscorrelation has been considered under restricted conditions.

The sources lying on a plane are designated by S_j, where $j = 1, \ldots, n$, as shown in Fig. X-10. On the same plane, three points, L_i, $i = 1, 2, 3$, forming an equilateral triangle, are chosen as listening posts. The separation between these points is d. The signals received at L_i are

$$g_i(t) = \sum_{j=1}^{n} f_j(t - k d_{ij}) \tag{1}$$

where $f_j(t) \geq 0$ is the signal generated by S_j, d_{ij} is the distance between the points S_j and L_i, and k is the reciprocal of the velocity of light. The second-order crosscorrelation function of $g_i(t)$ is*

---

*The definition of the crosscorrelation function is similar to the definition of the autocorrelation function, $\phi^*_{111}(\tau_1, \tau_2)$, discussed in subsection C.

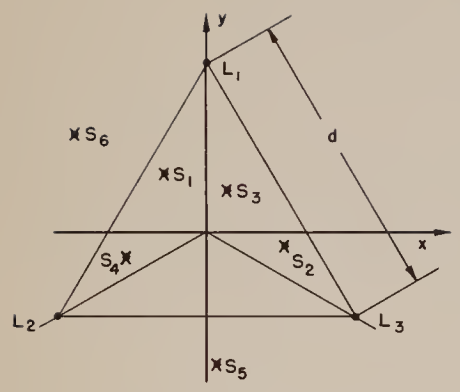

Fig. X-10

Distribution of sources and the location of listening posts.

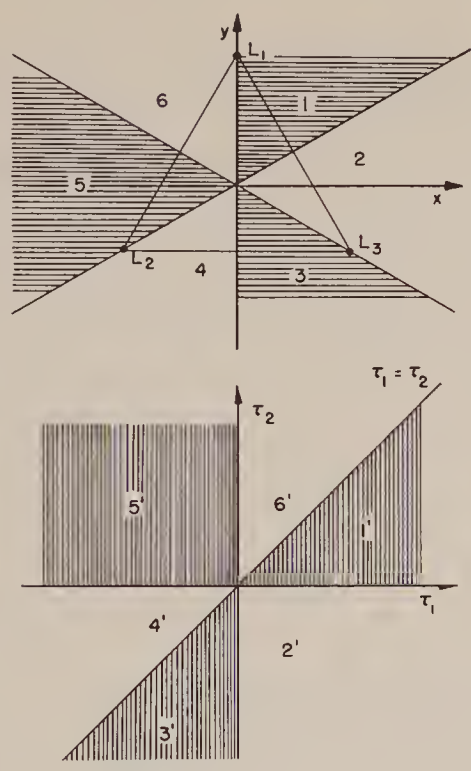

Fig. X-11

Relation between the areas in which sources S_i lie and the areas in which points $\left(\tau_1^{(i)}, \tau_2^{(i)}\right)$ lie.

$$\phi^*_{123}(\tau_1, \tau_2) = \overline{g_1(t)\, g_2(t+\tau_1)\, g_3(t+\tau_2)}$$

$$= \sum_{j=1}^{n} \sum_{\ell=1}^{n} \sum_{p=1}^{n} \overline{f_j(t - k d_{1j})\, f_\ell(t + \tau_1 - k d_{2\ell})\, f_p(t + \tau_2 - k d_{3p})} \qquad (2)$$

As a consequence of the independence of the sources, Eq. 2 is equivalent to

$$\phi^*_{123}(\tau_1, \tau_2) = \sum_{j=1}^{n} \overline{f_j(t - k d_{1j})\, f_j(t+\tau_1 - k d_{2j})\, f_j(t+\tau_2 - k d_{3j})}$$

$$+ \sum_{j=1}^{n} \sum_{\substack{\ell=1 \\ \ell \neq p}}^{3} \sum_{p=1}^{3} a_{j\ell p}\, \overline{f_j(t+\tau_{\ell-1} - k d_{\ell j})\, f_j(t+\tau_{p-1} - k d_{pj})}$$

$$+ \text{constant terms} \quad (n > 1) \qquad (2a)$$

where $\tau_0 = 0$. The value of $\phi^*_{123}(\tau_1, \tau_2)$ at

$$\left.\begin{aligned} \tau_1^{(i)} &= k(d_{2i} - d_{1i}) \\ \tau_2^{(i)} &= k(d_{3i} - d_{1i}) \end{aligned}\right\} \qquad (3)$$

is

$$\phi^*_{123}\left(\tau_1^{(i)}, \tau_2^{(i)}\right) = \overline{f_i^3\,(t - k d_{1i})} + A\,\overline{f_i^2(t - k d_{1i})}$$

$$+ \sum_{\substack{j=1 \\ j\neq i}}^{n} \overline{\left\{f_j(t - k d_{ij})\, f_j\left(t + \tau_1^{(i)} - k d_{2j}\right) f_j\left(t + \tau_2^{(i)} - k d_{3j}\right)\right\}}$$

$$+ \sum_{\substack{j=1 \\ j\neq i}}^{n} \sum_{\substack{\ell=1 \\ \ell\neq p}}^{3} \sum_{p=1}^{3} a_{j\ell p}\, \overline{f_j\left(t + \tau_{\ell-1}^{(i)} - k d_{\ell j}\right) f_j\left(t + \tau_{p-1}^{(i)} - k d_{pj}\right)}$$

$$+ \text{other constant terms} \quad (n > 1) \tag{4}$$

In the simple case where n = 1,

$$\phi^*_{123}\left\{k(d_{21} - d_{11}),\quad k(d_{31} - d_{11})\right\} = \overline{f_1^3(t - k d_{11})} \tag{5}$$

Since it can be shown that

$$\overline{f_j^3(t)} \geq \overline{f_j(t)\, f_j(t + \tau_1)\, f_j(t + \tau_2)} \tag{6}$$

the time displacements $\tau_1^{(1)}$ and $\tau_2^{(1)}$, which are related to the distances d_{11}, d_{21}, and d_{31} by

$$\tau_1^{(1)} = k(d_{21} - d_{11}), \quad \tau_2^{(1)} = k(d_{31} - d_{11}) \tag{7}$$

can be determined by plotting $\phi^*_{123}(\tau_1, \tau_2)$ vs. τ_1, τ_2 with the aid of a correlator.

When n > 1, the summation terms in Eq. 4 may introduce an error in the measured $\tau_1^{(i)}$ and $\tau_2^{(i)}$. It can be shown that this error depends on the relative position of the points S_j, and the nature of the random function $f_j(t)$. If the summation terms introduce negligible error on the measured $\tau_1^{(i)}$ and $\tau_2^{(i)}$, then those determine the location of S_i.

The difference in the distances $d_{2i} - d_{1i}$, $d_{3i} - d_{1i}$, and $d_{2i} - d_{3i}$ can be expressed in terms of $\tau_1^{(i)}$ and $\tau_2^{(i)}$ by the equations

$$\left.\begin{aligned} d_{2i} - d_{1i} &= \frac{\tau_1^{(i)}}{k} \\ d_{3i} - d_{1i} &= \frac{\tau_2^{(i)}}{k} \\ d_{2i} - d_{3i} &= \frac{\tau_1^{(i)} - \tau_2^{(i)}}{k} \end{aligned}\right\} \tag{8}$$

Three families of hyperbolas, whose respective foci are L_1 and L_2, L_1 and L_3, and L_2 and L_3, are available for determining the location of S_i. Any two families of hyperbolas are sufficient to determine the location of S_i which is given by the intersection of a branch from each family. The choice of the two families is dictated by the geometrical configuration of S_i and the fixed points, L_1, L_2, and L_3. The differences in the distances from the two foci to S_i for a given family are given by Eq. 8. This hyperbolic grid system is the same as that of Loran.

With the restriction that

$$\left.\begin{aligned} &|\tau_1^{(i)}| \leqslant k\,d \\ \text{and}\quad &|\tau_2^{(i)}| \leqslant k\,d \end{aligned}\right\} \tag{9}$$

the relation between the areas in which the sources, S_i, and the points, $\left(\tau_1^{(i)}, \tau_2^{(i)}\right)$, lie can be shown as in Fig. X-11. The correspondence between the areas in the xy plane and the $\tau_1\tau_2$ plane is shown by primed integers and unprimed integers.

J. Y. Hayase

E. CORRELATION DETECTION OF A PERIODIC SIGNAL MULTIPLIED BY NOISE

If a periodic signal S'(t) is multiplied by statistically stationary random noise, the product may be written

$$S'(t)\,N'(t) = \left[S(t) + \bar{S}\right]\left[N(t) + \bar{N}\right] \tag{1}$$

where S and N are the mean values of S'(t) and N'(t), respectively. If $\bar{N}$ is not zero, the periodic signal can be detected by autocorrelation, but if it is zero, detection by autocorrelation alone is not possible.

By filtering in the frequency domain, Eq. 1 may be reduced to S(t) N(t). For this case, the autocorrelation function of the product is the product of the autocorrelation functions

$$\phi_{SN}(\tau) = \phi_S(\tau)\,\phi_N(\tau) \tag{2}$$

Although $\phi_S(\tau)$ is periodic, $\phi_N(\tau)$ tends to zero for τ large, so that, in general, the periodic signal may not be detected by autocorrelation. If the factors of Eq. 2 are separated, or, if $\phi_N(\tau)$ is made to approach a constant other than zero, detection by autocorrelation is possible.

The factors may be separated by taking the logarithm, thus

$$\log|SN| = \log|S| + \log|N| \tag{3}$$

$$\phi(\tau) = \phi_{\log S}(\tau) + \phi_{\log N}(\tau) + 2\,\overline{\log N(t)}\;\overline{\log S(t)} \tag{4}$$

The periodic signal is revealed by the first term of Eq. 4; the other terms approach constants for τ large.

The noise factor of Eq. 2 may be made nonzero for τ large by a nonlinear operation on the product S(t) N(t). If the product S(t) N(t) is applied as an input to a nonlinear device the transfer characteristic of which may be written

$$f(x) = \sum_{0}^{\infty} A_n x^n \tag{5}$$

then the output autocorrelation function may be written

$$\phi(\tau) = \overline{\sum_{n=0}^{\infty} A_n \left[S(t)\,N(t)\right]^n \sum_{j=0}^{\infty} A_j \left[S(t+\tau)\,N(t+\tau)\right]^j}$$

$$= \sum_{n=0}^{\infty} A_n^2 \,\overline{\left[S(t)\,S(t+\tau)\right]^n}\;\overline{\left[N(t)\,N(t+\tau)\right]^n}$$

$$+ \sum_{\substack{n=0 \\ n\neq j}}^{\infty} \sum_{j=0}^{\infty} A_n\,A_j\,\overline{S(t)^n\,S(t+\tau)^j}\;\overline{N(t)^n\,N(t+\tau)^j} \tag{6}$$

Some noise terms having nonzero means are multiplied by signal terms. Since it is not possible for a random function raised to an even power to have a zero mean, any nonlinear device having even-power terms in the power series expansion of its transfer characteristic permits the detection of the periodic signal. If the probability density function of N(t) has even symmetry about the origin, then the odd-power terms of Eq. 5 do not aid in the detection of the periodic signal; but if not, the odd-power terms may aid.

A commercially available logarithmic device and a full-wave linear rectifier provided the more interesting transfer characteristics for the experimental work. The characteristics are

Limiter (odd)

$$y = \begin{cases} k_1 \log k_2 x & a \leqslant x \leqslant b \\ k_3 x & -a \leqslant x \leqslant a \\ -k_1 \log(-k_2 x) & -b < x \leqslant -a \end{cases} \tag{7}$$

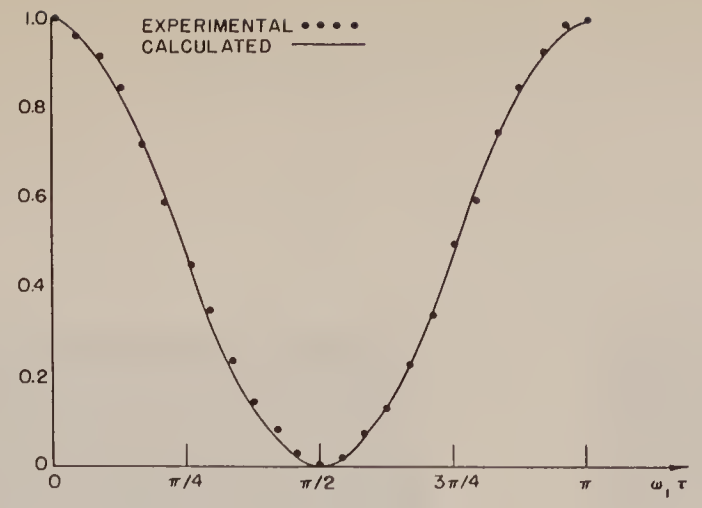

Fig. X-12
$\phi(\tau)$ for full-wave S.

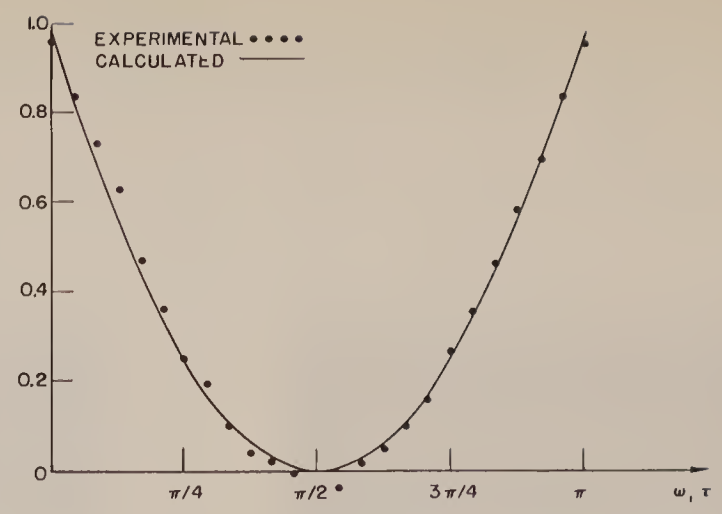

Fig. X-13
$\phi(\tau)$ for full-wave log S.

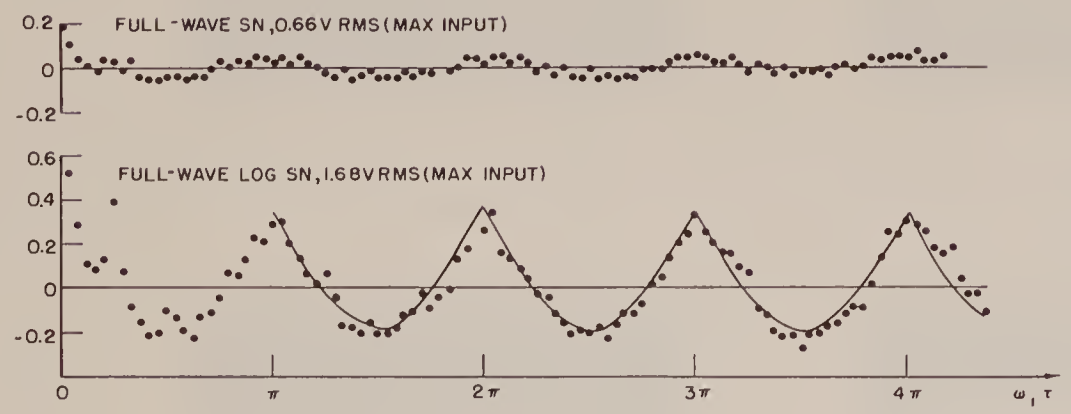

Fig. X-14
$\phi(\tau)$ for full-wave log SN and full-wave SN.

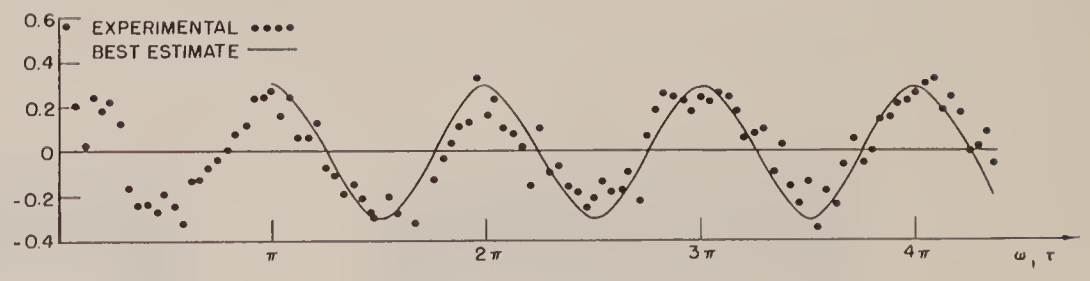

Fig. X-15
$\phi(\tau)$ for full-wave SN.

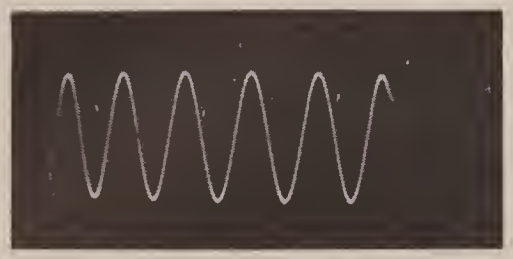

a. S, sine wave.

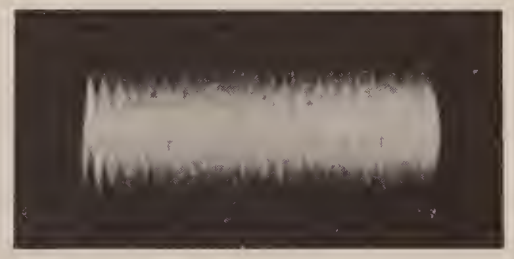

b. N, band-limited noise.

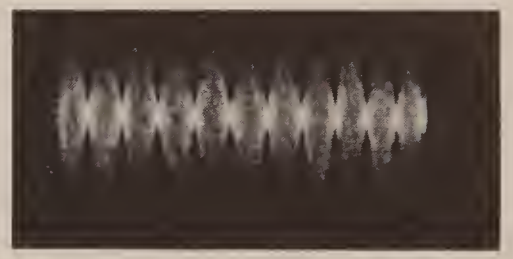

c. SN, sine wave times noise.

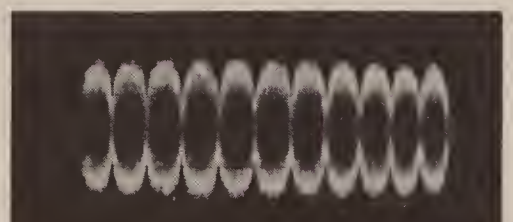

d. Limiter-log SN.

e. Full-wave log SN.

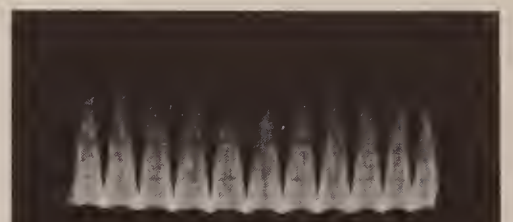

f. Full-wave SN.

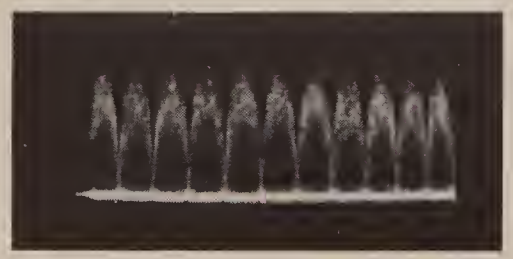

g. Half-wave log SN.

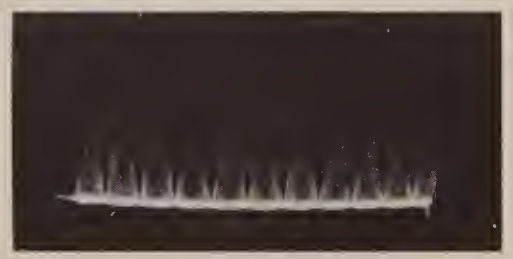

h. Half-wave SN.

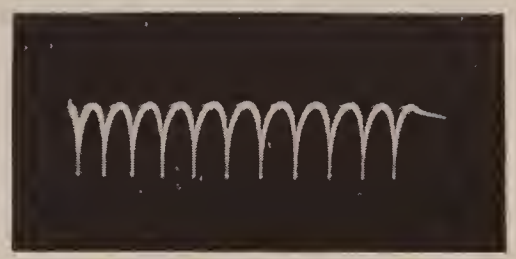

i. Full-wave log S.

Fig. X-16

Oscilloscope photographs: time scale, 1 msec; sine wave, 5.1 kc/sec; noise, 4 kc/sec centered at 21.9 kc/sec.

$$\text{Full-wave (even)} \qquad y = \begin{cases} k_4 \log |k_2 x| & a \leqslant |x| < b \\ |k_5 x| & 0 < |x| \leqslant a \end{cases} \tag{8}$$

$$\text{Full-wave (even)} \qquad y = |k_6 x| \tag{9}$$

If the input of an ideal logarithmic device is $E \sin \omega_1 t$, then the output is $y = B \log_\epsilon |E \sin \omega_1 t|$, and the autocorrelation function of the output is

$$\phi(\tau) = (B \log_\epsilon E)^2 + \frac{B^2 \pi^2}{2} \left[\left(\frac{\omega_1 \tau}{\pi} \right)^2 - \left(\frac{\omega_1 \tau}{\pi} \right) + \frac{1}{6} \right] \tag{10}$$

where B is determined by the characteristics of the log device and the gain of the output amplifiers. The autocorrelation function for the output of a full-wave linear rectifier, $y = |E \sin \omega_1 t|$ is

$$\phi(\tau) = \frac{E^2}{\pi} \left[\left(\frac{\pi}{2} - \omega_1 \tau \right) \cos \omega_1 \tau + \sin \omega_1 \tau \right] \tag{11}$$

Calculated and experimental results are shown in Figs. X-12 and X-13 for these two cases.

Figure X-14 shows the experimentally obtained autocorrelation function for full-wave log SN and full-wave SN for identical correlator control settings. S is a sine wave and N is band-limited gaussian noise. Figure X-15 shows the autocorrelation function for full-wave SN for increased correlator sensitivity (and increased error). The similarity of the curves in Fig. X-12 and X-14 suggests that the factors did separate as indicated by Eq. 3. The autocorrelation function for limiter-log SN does not reveal the periodic component.

Oscilloscope photographs such as those in Fig. X-16 proved to be a valuable aid.

C. E. McGinnis

F. AN IMPROVEMENT IN THE DIGITAL ELECTRONIC CORRELATOR

The correlator employs a compensating circuit to minimize drift error. When processing low-frequency information (dc to 500 cps), this compensating circuit acts upon a reference voltage of zero volts which is applied to the inputs of the correlator in intervals alternate to those during which the signals to be correlated are applied. The intervals are such that samples taken by the machine are alternately signal and reference samples. Difficulty in establishing a constant reference voltage of zero volts during the reference sample intervals has led to the development of a very satisfactory circuit for this purpose.

The circuit previously in use consisted of two tubes in series working between +150 volts and -150 volts. These tubes were alternately gated on and off, and their junction was connected to the input tube of the correlator. A potentiometer in series with the two tubes adjusted the voltage at the junction, during the on time, to zero. During the off time, the grid of the correlator input tube was at high impedance and free to receive the signal fed to it through a series resistor. This method suffered from the obvious difficulty of being very dependent upon the tube characteristics and upon the stability of the plus and minus B supplies.

The improved circuit is shown in Fig. X-17. During the intervals for which both sections of the tube are on, there is a very small resistance (about 150 ohms) between points a and b and the signal, f(t), passes freely to the grid of the correlator input tube. During the intervals for which both sections of the 6AS7 are off, the grid of the correlator tube is isolated from the source f(t), and it returns to zero. This circuit has the advantage of being almost completely independent of changes in the 6AS7 characteristics.

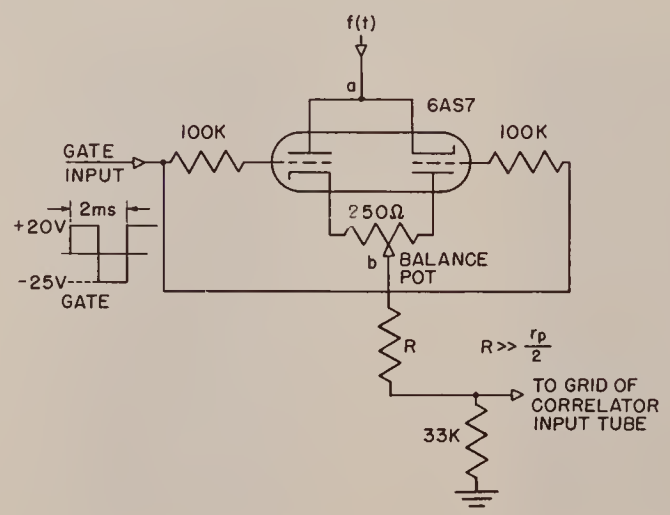

Fig. X-17

Improved circuit for the digital correlator. The time function f(t) is the function to be correlated (10 volts maximum either side of zero). It is to be obtained from a low impedance dc coupled source.

Since there is no B voltage applied to the 6AS7, and since the filament voltage is reduced to minimize hum, the tube life is long. This circuit, in conjunction with the compensator, enables the machine to process low-frequency information with an accuracy of the same order of magnitude as that obtained when the machine is ac coupled and processing higher frequency information.

A. G. Bose

G. MEASUREMENT OF INDUSTRIAL PROCESS BEHAVIOR

Experimental determinations of the transfer function $H(\omega)$ or impulse response $h(t)$ of industrial processes are complicated by the presence of noise and by the difficulty of applying suitable sinusoidal or impulsive driving functions to massive industrial systems. The statistical method of determining system characteristics overcomes these difficulties (1). This method uses as the driving function the random fluctuations already existing in the input variable. The result is not usually affected by random fluctuations originating within the process.

A heat transfer process frequently encountered in industry has been chosen for experimental study. In this process, a liquid flowing through a copper tube is heated by water flowing through a concentric copper shell. Thermocouples are used to measure the temperatures of the liquids. When cold water from the building mains flows through the tube and a mixture of hot and cold water from the same mains flows through the shell, the shell and tube temperatures fluctuate as shown in Fig. X-18.

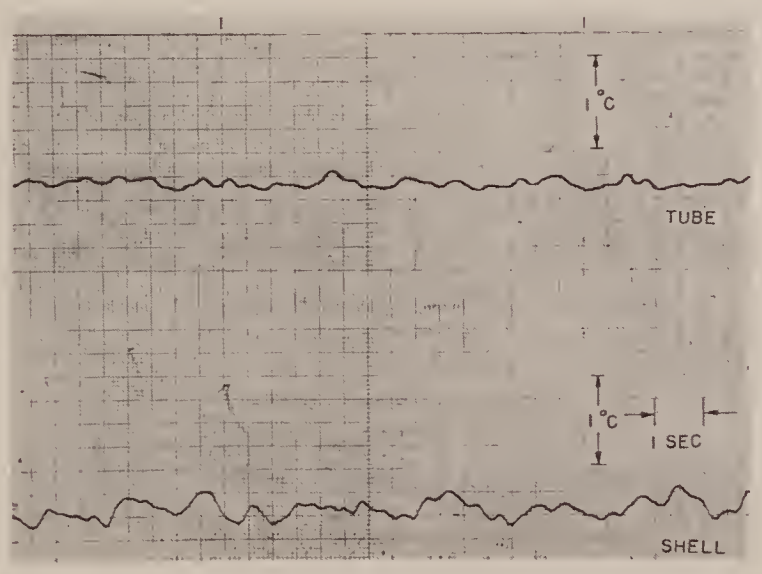

Fig. X-18
Temperature fluctuations in shell and tube of heat exchanger.

Preliminary results obtained with the low-frequency multisignal correlator (2), while encouraging, indicate that practical application of the method must await further refinement of the measuring system.

S. G. Margolis

References

1. Y. W. Lee, Technical Report No. 181, Research Laboratory of Electronics, M.I.T., Sept. 1, 1950.

2. D. G. C. Hare, Final engineering report, Design and construction of low frequency multi-signal correlator for the Air Force Cambridge Research Center, Contract No. AF19(122)-213.

XI. SPEECH ANALYSIS

Prof. M. Halle
G. W. Hughes
J. -P. A. Radley

A. RECOGNITION OF SILENCES

The class of speech sounds known as stops or plosives, e.g., /p/, /k/, /t/, /d/, /b/, and so on, are produced by a complete closure of the vocal tract followed by a sudden opening. During this movement the vocal cords may be vibrating. This vibration distinguishes voiced stops like /b/ and /d/ from voiceless ones like /p/ and /t/.

The acoustic correlate of this articulatory process is an absence of energy in a broad frequency band followed by a rapid onset of energy in all frequencies. For the voiceless stops, the absence of energy is more or less total; for the voiced stops, strong components are usually present in a region below 300 cps but above this region there is hardly any energy. This relative silence is thus one of the cues that permit us to identify stops.

The operation to be performed is that of determining when the input to a device falls below a certain low level and remains there for some minimum time. To recognize a critical level, a Schmitt amplitude discriminator is used after the speech signal, suitably filtered and amplified, has been rectified (full-wave).

In the first method tried, the output of the Schmitt circuit was given a certain amplitude which controlled the onset and timing of a highly unbalanced multivibrator. Impulses from this stage were fed to one side of a flip-flop. When the silence was ended, the flip-flop was returned to its first state and the multivibrator turned off. If a silence did not last long enough, the multivibrator was turned off before emitting its first impulse. In fact, at every half-pitch period, the signal could be expected to reach zero for a short time. It was, however, not possible to reset the multivibrator quickly enough, which led to cumulative timing errors. A new approach was, therefore, developed.

In the second method, the output of the Schmitt stage, a rectangular wave, is used to generate a negative-going triangle whose slope can be varied and which resets very quickly (with respect to audio frequencies) to its origin when the Schmitt tells it to. This triangle is coupled to a "simplified" Multiar (1). A pentode, normally heavily conducting, is cut off by the end of the triangle excursion. In the Multiar a transformer is used in a feedback path for rapid cutoff action, but this is unnecessary in this application, since the tube is cut on rapidly enough by the essentially vertical return of the triangle. It is this rapid return that marks the end of a silence. The location of the beginning of the silence does not have to be known with great accuracy for present purposes.

The circuit was tested with short sentences read by four English speakers (one

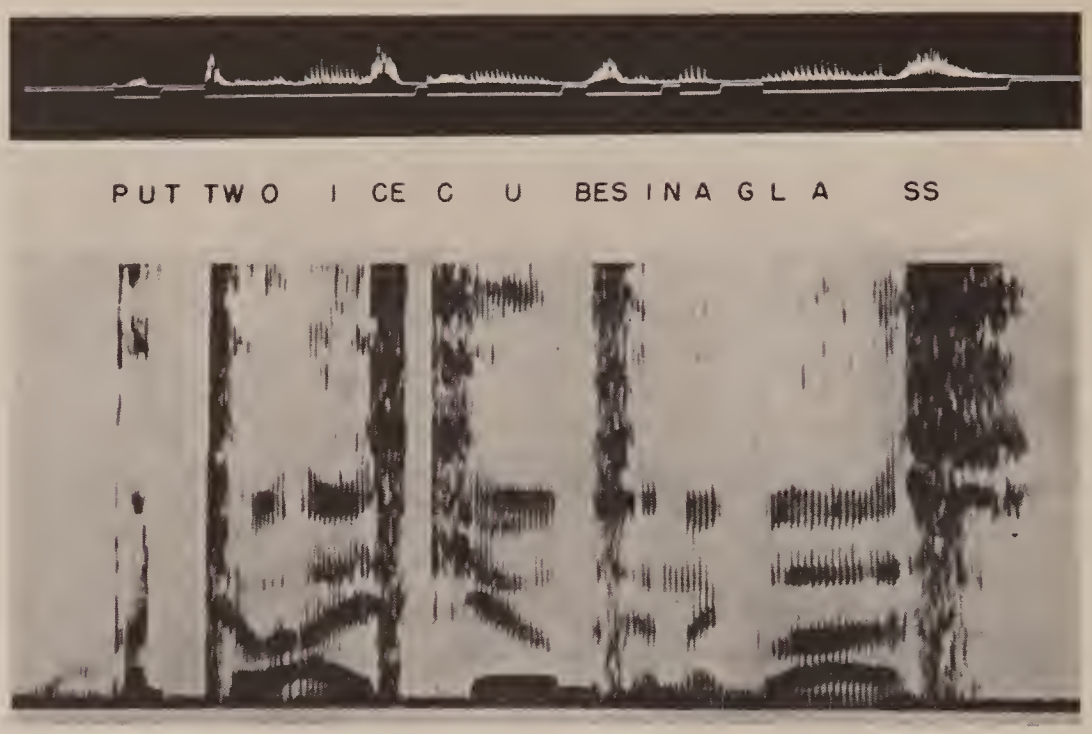

Fig. XI-1

Lower trace signals stops by "end of silence" mark. Note that /n/ is wrongly identified.

female and three male). Because of the relatively gentle slope of the filter available, the signal was highpassed at 1500 cps or 2000 cps to eliminate the voicing component. The critical timing was set at about 16 msec. This is the minimum time for which the amplitude must remain below the critical level before a silence can be noted. In other words, no silence shorter than the critical timing is registered. The hysteresis effects of the Schmitt circuit were arranged to be least for sine waves between 30 cps and 300 cps. A filmed record was made with a dual beam cathode-ray oscilloscope showing a rectified trace of the speech on one trace and the output signal of the "silence recognizer" on the other. See Fig. XI-1.

As expected, the two criteria (level and time) used were necessary but not sufficient for the identification of stops. Different settings will mark silences before, or during, different classes of sounds. Almost all stops in the samples were marked by the end of a silence. Exceptions to this were a few very weak stops that did not reach above the critical amplitude (set just above the noise region) and the flapped /t/ as in "water," in which the silence is extremely short.

On the other hand, because of the very high cutoff frequency of the filter, sounds such as the nasals and the semi-vowels in which most of the energy is located in the low frequencies were judged to be silences. Better filtering might eliminate this.

J. -P. A. Radley

References

1. B. Chance et al., Waveforms, M.I.T. Radiation Laboratory Series, Vol. 19 (McGraw-Hill Book Company, Inc., New York, 1948).

B. THE NASAL CONSONANTS

The nasal consonants have in common with the vowels a spectrum that is dominated by a small number of resonance peaks, the so-called formants. In both the nasals and the vowels the lowest resonances (the first formant) contribute most of the energy. The vowels differ from the nasals in having higher first formants. Furthermore, if the spectrum contains formants above the first formant, these are much less attenuated in the vowels than in the nasals. The first formant of the nasals is generally below 300 cps. The lowest first formant in vowels is found in [i] and [u], where it is located at about 300 cps. The first formant in the other vowels is well above 300 cps. These facts suggested that a comparison of the energy below 300 cps with that above might yield information useful in distinguishing between vowels and nasals.

Our speech samples were isolated syllables consisting of a vowel preceded or followed by a nasal. These syllables had been recorded on tape by one female and two male speakers. Portions 50 msec long were gated out of the nasal and the vowel. The gated portion was passed through a Spencer Kennedy 302 variable electronic filter in which both sections were set either to 300 cps highpass or 300 cps lowpass. This gave us an attenuation of 36 db per octave. We found that a lesser attenuation (18 db per octave) yielded no results of interest. The output of the filter was passed through a variable precision attenuator, integrated and measured.

The following results were obtained: (The numbers in the table are the extreme values found when the lowpass output was subtracted from the highpass output.)

vowels (113 measured)	-8 db to +15 db
[i]	-8 db to +4.5 db
other vowels	-2 db to +15 db
[m] (37)	-15.5 db to -8 db
[n] (37)	-17.5 db to -3 db

If we omit the vowel [i] from consideration it is possible to separate the vowels and the nasals quite well by this criterion: the vowels give positive and moderately negative values, while the nasals give strongly negative values. The vowel [i] could be made to give more positive values if frequencies above 1000 cps were boosted. Such a weighting would affect the nasals but little, because they have very little energy in that region; however, it would greatly improve our chances of separating [i] from the nasals. In the next quarter we intend to investigate this further.

An attempt was also made to establish the difference between the two nasal consonants. For this purpose we measured spectra of these sounds (1). No consistent difference could be found between spectra of [n] and of [m]. See Fig. XI-2.

We pursued this question further and attempted to synthesize some vowels and the

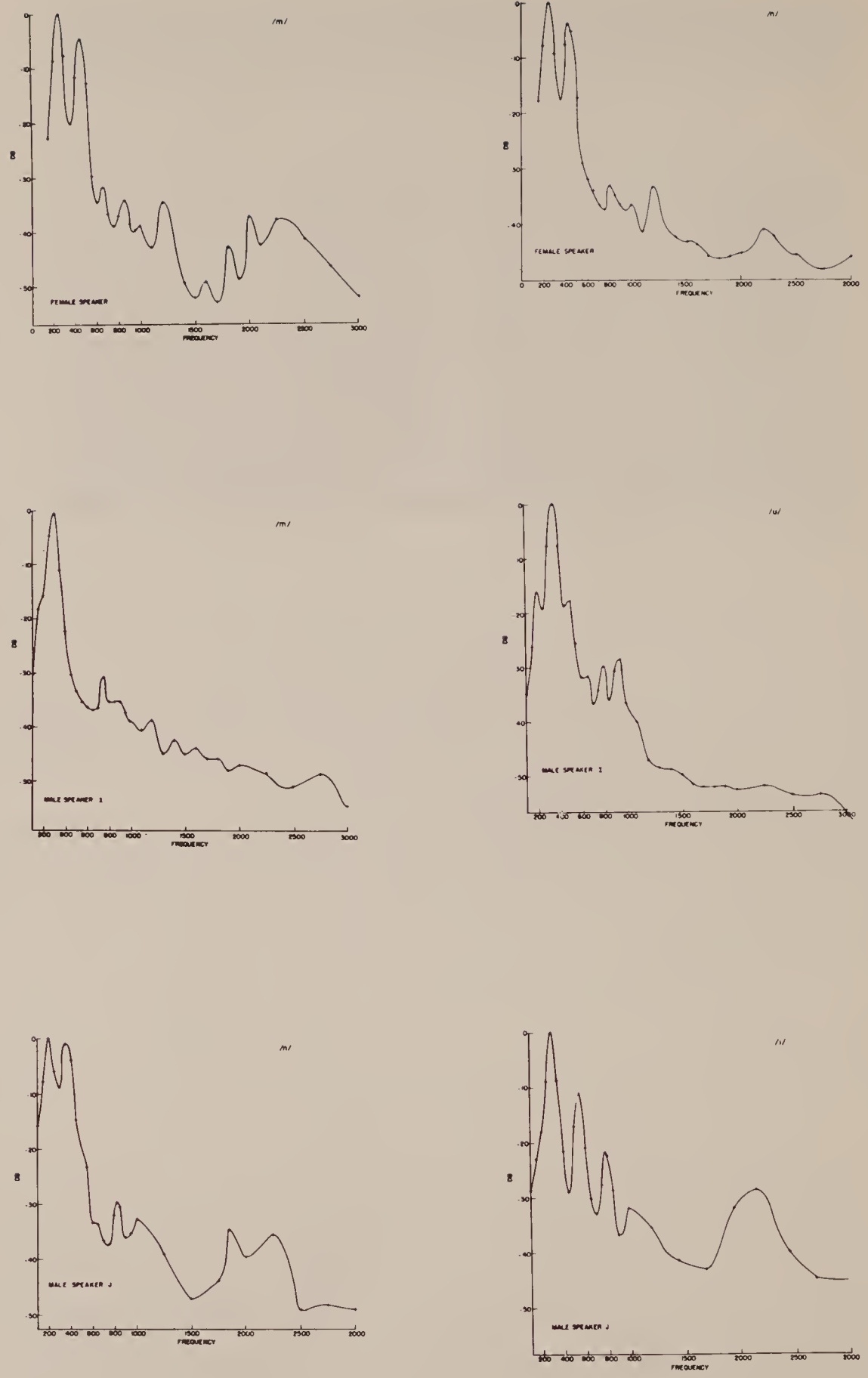

Fig. XI-2

Spectra in the first row were obtained from the syllables /mi/ and /ni/. Spectra in the second and third rows are of the nasal and the vowel in the syllables /mu/ and /ni/, respectively. Note the predominance of the low frequencies in all spectra.

nasals by means of oscillators. A good [m] could be synthesized by a single oscillator tuned at 150 cps. When a second oscillator tuned to 300 cps was added, no appreciable difference was noted until the output of the second oscillator was substantially equal to that of the first. Under these conditions [u] was perceived. In order to obtain [n] it was necessary to introduce a very weak component (-40 db below the fundamental) at about 2300 cps. When this component was increased in intensity to -17 db a sound much like the German [ü] was heard. The best [n] was synthesized by introducing two fairly strong components (-20 db) at 600 cps and 750 cps in addition to the above-mentioned weak component at 2300 cps. It was, however, observed that the 2300 cps component was much more essential in the perception of [n] than the 600 and 750 cps components.

M. Halle, G. W. Hughes

References

1. Quarterly Progress Report, Research Laboratory of Electronics, M.I.T., April 15, 1954; July 15, 1954.

XII. VISUAL REPLACEMENT PROJECTS

Dr. C. M. Witcher
L. Washington, Jr.

A. ACOUSTIC OBSTACLE DETECTION

In the Quarterly Progress Report of April 15, 1954, we described a high-frequency sound pulse projector incorporating automatic scanning. The results obtained with this device were of sufficient interest to warrant the construction of a second model incorporating several improvements. Figure XII-1 is a photograph of the new projector; its circuit is shown schematically in Fig. XII-2. This model, considerably reduced in size, is about 8 1/2 inches long and 3 5/8 inches in diameter. It weighs slightly less than 2 pounds. As in the earlier model, scanning is accomplished by means of a deflecting ellipse, but the motion of the ellipse in the new model takes the form of an angular oscillation rather than a rotation. This motion is achieved with a Scotch crosshead which is driven by the motor near the bottom of the device. The crosshead carries a toothed rack which engages a small spur gear on the shaft of the ellipse. This scanning arrangement is considerably superior to that previously used, since the latter allowed

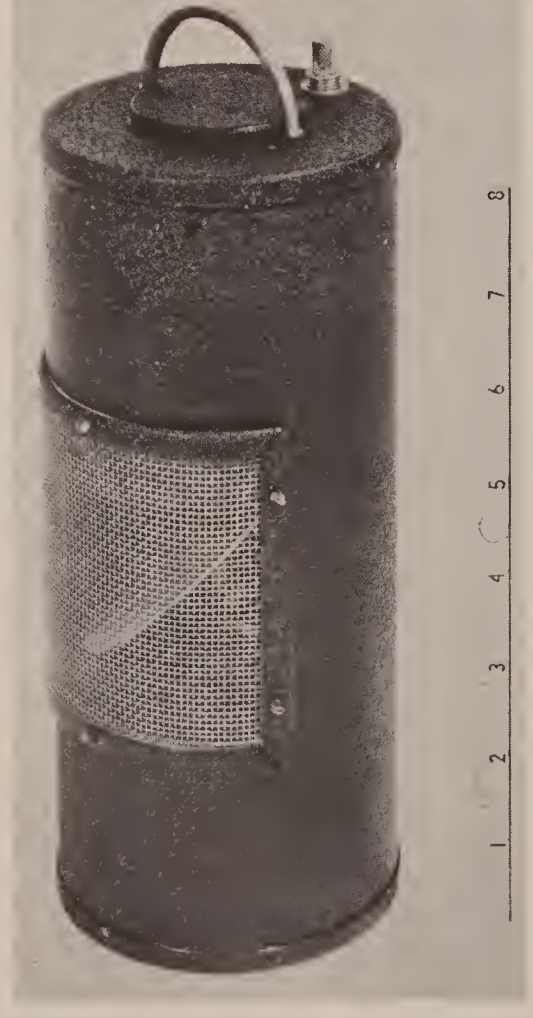

Fig. XII-1
Sound pulse projector.

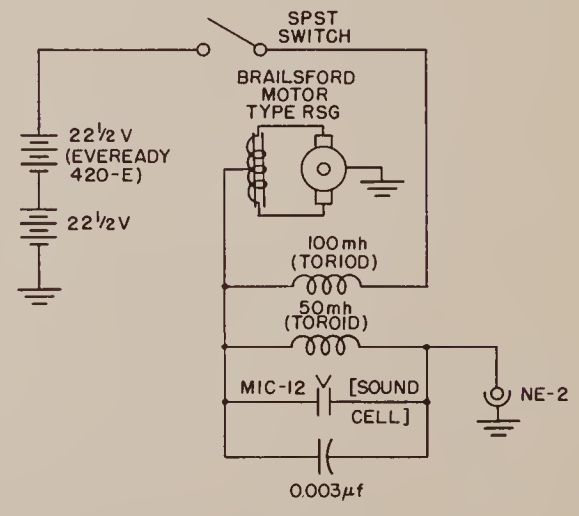

Fig. XII-2
Sound pulse projector schematic.

the sound beam to emerge from the projector for only about half of each scanning cycle. With the oscillating system, the beam is available for obstacle detection at all times. The angular oscillation of the scanning ellipse is almost strictly sinusoidal, having an angular amplitude of 60° and a period of about 1.0 sec. The reduced dimensions of the new model result in one disadvantage, however; the sound beam is more divergent. The motor in the new projector is of the same general type as that used in the older model, but it was made specially for us by the H. D. Brailsford Company, of Rye, New York.

The operation of the electrical circuit is as follows. The inductive "kicks" appearing across the 0.1-henry coil at each break of the motor contacts produce shock excitations of the tuned circuit associated with the crystal transducer through the type NE-2 neon lamp. The neon lamp functions as a switch that disconnects the tuned circuit from the exciting coil during the second half-cycle of oscillation after the arrival of an exciting pulse, so that the tuned circuit is then left free to ring until the next exciting pulse arrives. This scheme has given much more satisfactory sound pulses than were previously obtained. The resonant frequency of the tuned circuit and transducer is 9.0 kc/sec, and its Q is of the order of 10. The amplitude of the sound pulses produced by the new projector has not been measured, but it is apparently greater than that obtained with the old model (104 db above a sound pressure of 0.0002 dyne/cm^2 at distance of 18 inches from the projector).

We have described this projector in considerable detail because it appears to represent a fairly close approach to what can be ideally expected from this type of obstacle detector. Numerous tests conducted with it during the past few months apparently lead to the conclusion that it cannot be expected to serve as a genuinely useful travel aid to the blind except under highly specialized conditions. All obstacles with rough or irregular surfaces yield clearly audible sound reflections at distances up to 15 or 20 ft, but obstacles such as small, smooth, round pipes or columns, as well as smooth walls on which the sound beam is incident obliquely, do not yield reliably detectable sound reflections. A further increase of perhaps 10-15 db in sound intensity might partially eliminate these difficulties, but then the intensity would be so great as to render the user of the instrument unduly conspicuous. We plan to attempt this, however, if and when a more rugged, but sufficiently small, transducer can be found or developed.

The suggestion has been made that a similarly constructed ultrasonic projector together with a pair of ultrasonic receivers (to provide binaural localization) might provide an improved obstacle detection system. The highly satisfactory scanning mechanism developed for the present model, together with its reasonably low total power consumption (about 150 mw), definitely warrants further work along one of the two lines just mentioned.

B. NEW STEP-DOWN DETECTOR

Some months ago it was concluded that a complete redesign of the step-down detector was needed if reliable results were ever to be obtained. The first step, a redesign of the optical system, was carried through, but a delay of several months followed because of difficulties encountered in obtaining the necessary components. The new receiver and light source have now been completed and will be described briefly.

The principal objectives underlying the new design have been: to achieve a considerable improvement in signal-to-noise ratio, and to reduce substantially the blocking effects caused by sunlight-to-shadow transitions, as discussed in the Quarterly Progress Report of January 15, 1954. In designing the optical system, three steps have been taken to further these objectives: (a) Much faster optics have been used in the receiver, permitting a considerable reduction in photocell area; (b) The vibration frequency of the light source has been increased from 30 cps to 160 cps; (c) By use of a specially designed lamp for the source, together with a Schmidt optical system, the beam from the source has been shaped to coincide closely with the receiver image space in the region where the latter "looks at" the terrain.

The optical element in the receiver is a parabolic mirror on a lightweight plastic base, which was generously donated to us by the Polaroid Corporation of Cambridge, Massachusetts. This mirror has a focal length of 1.06 inches and a circle of confusion less than 0.25 mm. The receiver aperture is 2.45 inches, thus giving a speed of F-0.43. The PbS photocell, produced for us by Photoswitch Corporation, is of the evaporated type, enclosed in an evacuated bulb, and the dimensions of its active area are 0.005 by 0.050 inch. This is about 1/15 the area of our previous cells, and hence, for the same amount of incident light energy, it should provide an improvement in signal-to-noise ratio (assuming same signal frequency) of $15^{1/2}$, or 11.8 db.

Since, for a given bandwidth, the noise power from a PbS cell varies inversely with frequency, the increase of 5.3-fold in source vibration frequency should provide an additional improvement of 7.25 db. Thus we may reasonably expect a total improvement in signal-to-noise ratio of about 19 db from the two factors so far considered. Measurements made by the Photoswitch Corporation on the new cells quantitatively confirm this improvement.

The increased source frequency, combined with the use of a more sharply tuned amplifier, must certainly provide some relief from the blocking effects produced by light-to-shadow transitions. For a walking speed of 5 ft/sec and for a receiver image space extending along the surface of the terrain a distance of 1.5 inches in the direction of motion of the detector, the rise times of the pulses produced by light-to-shadow transitions will be of the order of 1.5/60 = 25 msec, so that most of the energy in these pulses will be at frequencies below 320 cps, that is, twice the vibration frequency of the

source. The use of a Polaroid type XRX-40 infrared filter in front of the receiver (short wavelength cutoff 8600 angstroms) further serves to minimize the influence of sunlight.

The greatly improved light concentration from the source should result in a further improvement in signal-to-noise ratio, although this improvement has been sacrificed to some extent by the use of a lower power lamp in the source. The lamp now used was developed especially for us by the lamp division of the General Electric Company, and we are greatly indebted to Clifton Found, of that organization, for contributing several of these lamps. The tungsten filament in the new lamp is in the form of a helix only 0.005 inch in diameter and approximately 0.05 inch long. It is designed to operate at a nominal temperature of 2400°K with an applied voltage of 1.5 volts and a current of 0.25 amp. These lamps have also proved capable of withstanding the vibrational accelerations of the order of 250g to which they are subjected when the source is in operation.

The receiver is housed in a cylindrical bakelite case 2.75 inches in diameter and 2.25 inches long; its total weight is 3.5 oz. The photocell mounting embodies provisions for accurately centering the cell with respect to the axis of the mirror, and a special optical alignment tool has been developed for this purpose.

A photograph of the source assembly is shown in Fig. XII-3. As may be seen, the frame consists of a bakelite box with aluminum corner supports to provide added rigidity. Note that the aluminum ring which holds the Schmidt corrector plate fits snugly into the front end of the box to afford still more rigidity in the neighborhood of the supports for the vibrating element. This element is tuned to mechanical resonance at a frequency of 160 cps and is driven from a small, balanced armature type of headphone unit mounted in the collet assembly on top of the box. The system operates in the manner of an ordinary buzzer, utilizing a make-and-break contact arrangement and a small transformer powered from the same 1.5 volt source which furnishes power for the lamp. The position of the lamp, at the end of the vibrating element toward the mirror, is accurately determined to insure that the filament moves in an arc lying on the focal surface of the Schmidt system. We wish to express our sincere thanks to Harrison J. Merrill, of the Evans Signal Laboratory, Fort Monmouth, New Jersey, for providing us with the optical components for the Schmidt system.

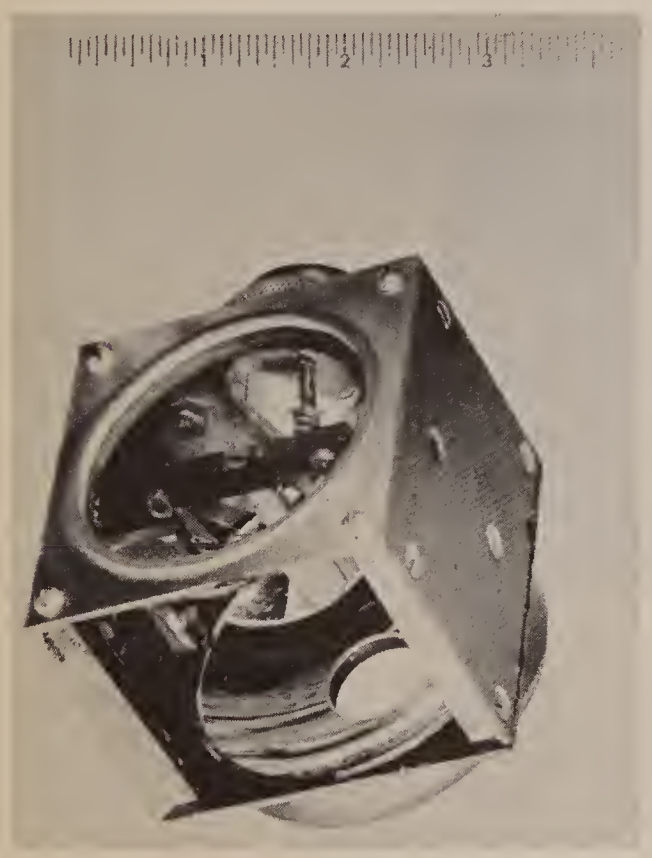

Fig. XII-3
Step-down detector light source.

Considerable development work has been

required to obtain a vibratory system with sufficient rigidity and a sufficiently large mechanical Q to give a vibration amplitude of 4-5° at 160 cps with a power input of not more than 100 mw. These conditions have now been achieved satisfactorily.

As this is written, the complete assembly for the source and receiver has not been finished; we have therefore not had an opportunity to make measurements of the system performance.

XIII. COMMUNICATIONS BIOPHYSICS

Prof. W. A. Rosenblith
Dr. J. S. Barlow*
Dr. M. A. B. Brazier*
Dr. D. H. Raab
Dr. J. R. Hughes
R. M. Brown
L. S. Frishkopf

A. A PROBABILISTIC APPROACH TO CERTAIN NEUROELECTRIC PHENOMENA

1. Basic Data

An acoustic stimulus presented at the ear of an anesthetized cat evokes an electrical response from the auditory nerve of that animal. Our primary stimuli to date have been clicks produced by feeding rectangular pulses of duration 0.1 msec into a PDR-10 earphone. These short stimuli evoke spike-like responses, which are detected by a fine wire electrode placed within the bullar cavity. Suitable electrode placement makes these click responses substantially free of microphonic contamination (1, 2). A typical response is shown in Fig. XIII-1.

The earliest neural component, labeled N_1, can be assumed to represent the synchronous and summated firing of first order auditory neurons. The peak-to-peak amplitude of N_1 (A_{pp}), taken as a measure of total activity, when plotted against the stimulus intensity (S), yields a monotonic function (Fig. XIII-2) referred to hereafter as the intensity function ($A_{pp} = f(S)$) (2). Each datum point represents the average of ten or more measurements.

If the click is presented in a background of continuous white noise (limited by the

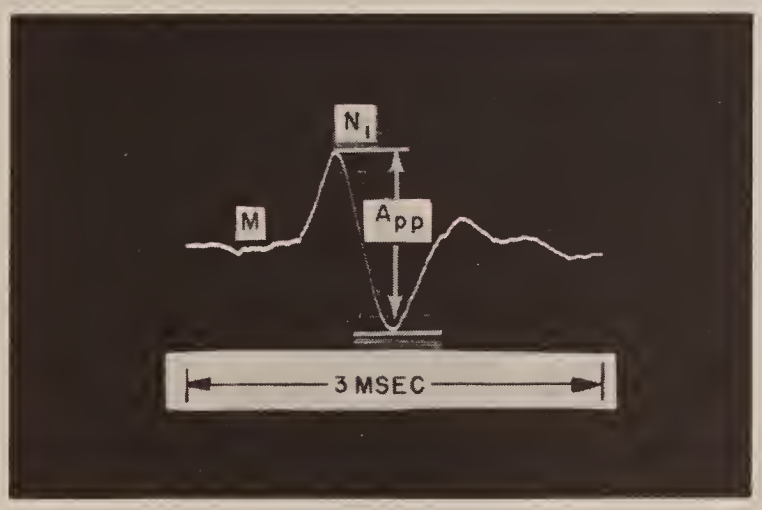

Fig. XIII-1

Typical peripheral response to click (-30 db re 1.29 volts) with very little microphonic content. M, microphonic; N_1, first neural component; A_{pp}, peak-to-peak amplitude.

---

*From the Neurophysiological Laboratory of the Neurology Service of the Massachusetts General Hospital.

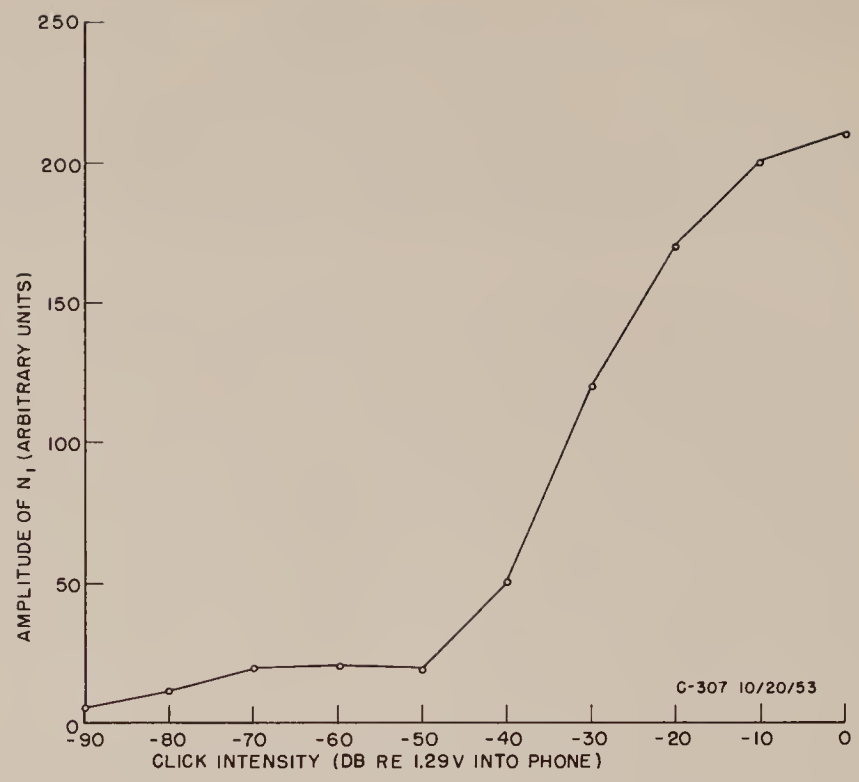

Fig. XIII-2

Intensity function obtained from Cat C-307. This is fairly typical of the functions obtained from animals whose thresholds seem to be normal.

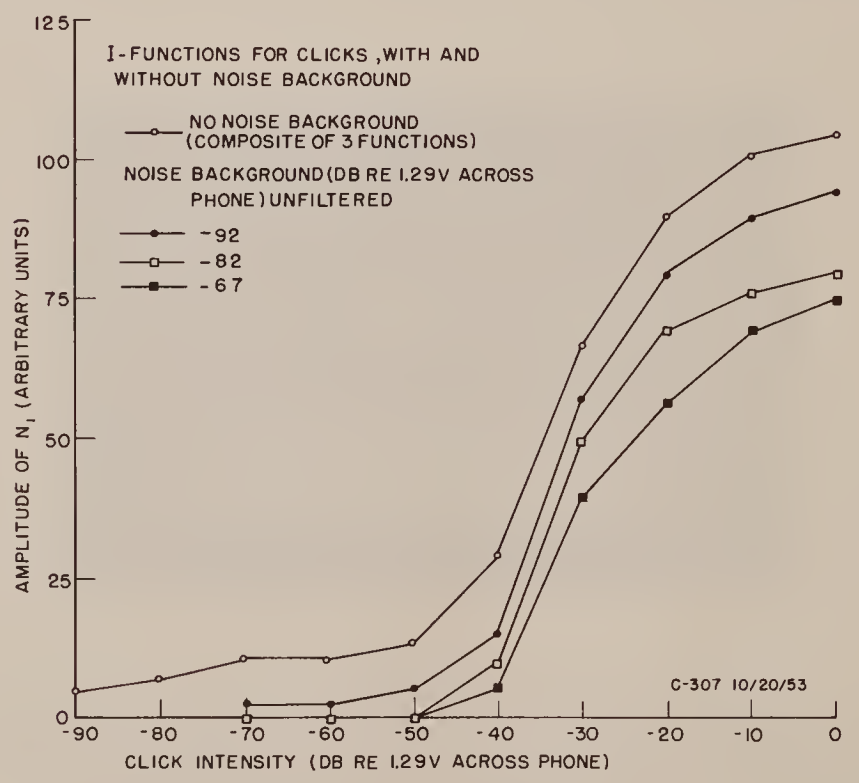

Fig. XIII-3

Masked and unmasked intensity functions.

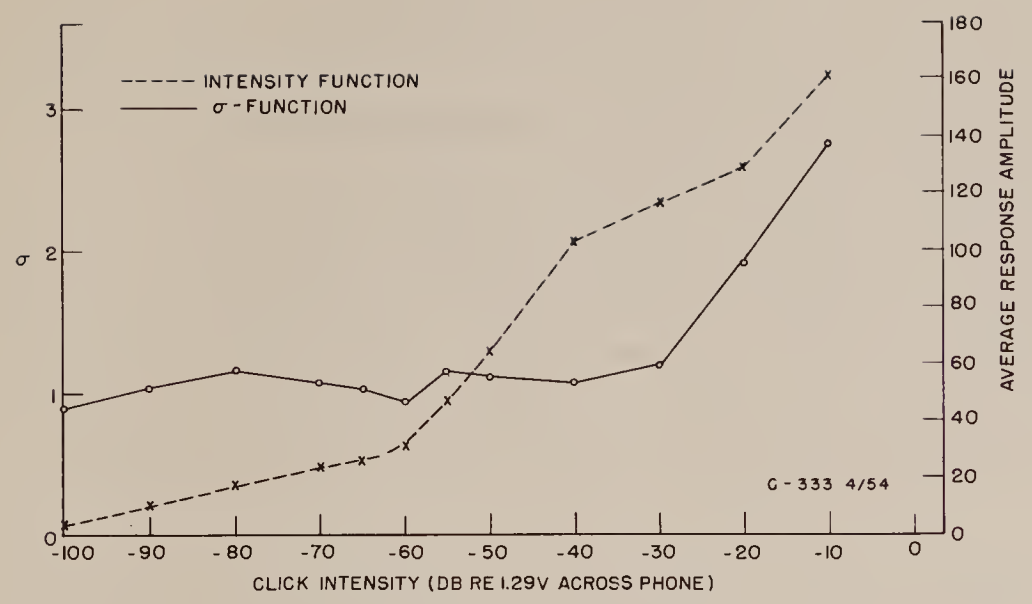

Fig. XIII-4

Standard deviation of response amplitudes to a given stimulus intensity plotted as a function of stimulus intensity. Each point is based on about 100 responses. Plotted with it (dashed line) is the intensity function obtained from the same data.

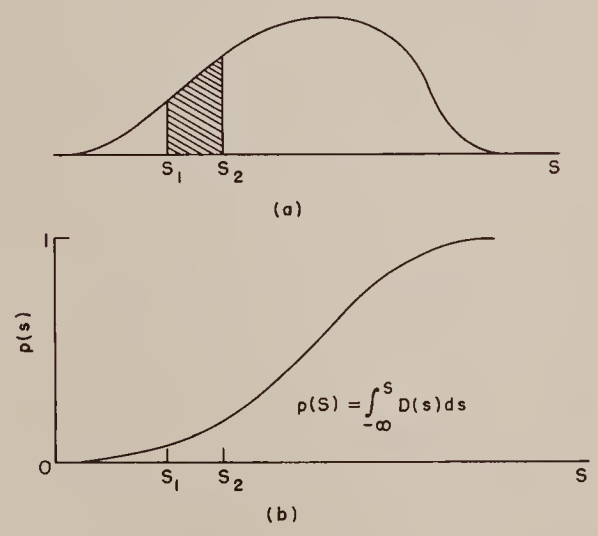

Fig. XIII-5

(a) A possible threshold probability distribution function, D(S). The shaded area equals the probability of finding the threshold in the interval S_1 to S_2. The total area under the curve is 1. (b) p(S), the probability of a unit responding to stimulus S.

characteristics of the system that delivers the acoustic stimulus), the peak-to-peak amplitude of N_1 is reduced. Plotting this amplitude vs. click intensity for a fixed noise level yields (3) a modified, or masked, intensity function, $A_M = f(S, N)$. Several such masked functions for several noise levels, together with the corresponding unmasked functions, are presented in Fig. XIII-3. Each point represents the average of the peak-to-peak amplitude of ten or more responses to identical stimuli.

We have studied the variability of these response amplitudes and have shown (4) that many more than ten responses to a single stimulus intensity were needed to obtain a statistically meaningful measure of variability. From a sequence of 100 responses to a given stimulus setting, the standard deviation of the peak-to-peak amplitudes was determined for a number of stimulus values. The resultant function, $\sigma = f(S)$, is plotted in Fig. XIII-4.

2. The Model

The neural unit is the elemental concept of our model. Its relation to the basic physiological entities, the neuron, the sense-cell, and the junction between them, has been discussed in previous reports (2, 3).

The neural unit has the following properties:

a. It obeys the all-or-none law; that is, it is characterized by only two states, maximal response or no response.

b. Its threshold, or "triggering level" of stimulation, fluctuates in time. No attempt is made to specify the detailed time course of this fluctuation. Rather, the description is limited to a specification of the fraction of the time the unit spends in any threshold interval, i. e., by a threshold probability distribution, Fig. XIII-5. It is, in addition, assumed that the characteristic time of fluctuations is very small compared to the interval (about two seconds) between stimulus presentations.

c. The firing of a unit alters its threshold distribution, which then becomes a function of the time $\Delta\tau$ since firing. For times $\Delta\tau$ that are sufficiently long (greater than 0.1 sec) the unit returns to the resting distribution. For $\Delta\tau$'s that are less than 2 msec the unit will respond to no stimulus, whatever its intensity. This time interval is called the absolute refractory period of the elemental unit.

Our model requires a second concept: a population of neural units; that is, an aggregate of neural units whose properties a, b, and c involve identical parameters.

The present model assumes that at least two populations of neural units are contributing to the peak-to-peak amplitude of the responses. This classification is based mainly on differences in mean threshold values, with each unit labeled as either sensitive or insensitive. It may eventually be found necessary to subdivide one or both of these populations into subpopulations.

No interaction between neural units has been introduced explicitly into the model.

Moreover, the threshold fluctuations occurring in any two units are assumed to be statistically independent.

3. The Model and the Data; Predictions

A single neural unit, presented with a stimulus S, will respond if its threshold is less than or equal to S and not otherwise. If the threshold probability distribution (Fig. XIII-5(a)) is represented by D(S), then the probability of finding the unit with threshold less than S, and therefore the probability that the unit will respond to a stimulus S, is given by (Fig. XIII-5(b))

$$p(S) = \int_{-\infty}^{S} D(s)\, ds \tag{1}$$

A single population of neural units, all of which have the same threshold probability distribution D(S), gives rise to an intensity function

$$A(S) = rN\, p(S) = rN \int_{-\infty}^{S} D(s)\, ds \tag{2}$$

where r is the magnitude of the response of a single unit and N is the number of units in the population. If a single population were involved, the function D(S) could be inferred at once by differentiating the observed intensity function and making use of the normalization

$$\int_{-\infty}^{+\infty} D(s)\, ds = 1 \tag{3}$$

If we are dealing with two independent populations, we obtain

$$A(S) = A_1(S) + A_2(S) = r_1 N_1 \int_{-\infty}^{S} D_1(s)\, ds + r_2 N_2 \int_{-\infty}^{S} D_2(s)\, ds$$

where the subscripts 1 and 2 refer to the two populations. The situation is particularly simple if $D_1(S)$ and $D_2(S)$ are disjoint (Fig. XIII-6). Then again differentiation plus the normalization conditions

$$\int_{-\infty}^{+\infty} D_1(s)\, ds = 1 \quad , \quad \int_{-\infty}^{+\infty} D_2(s)\, ds = 1$$

permit immediate inference of $D_1(S)$ and of $D_2(S)$. If the distributions overlap,

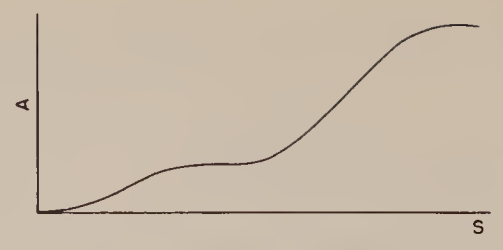

Fig. XIII-6

The type of intensity function obtained from two disjoint, or nearly disjoint, populations.

separation in the region of overlap on the basis of the observed intensity function is no longer possible.

The unmasked intensity functions of Figs. XIII-2 and XIII-3 are of the type shown in Fig. XIII-6 and are, therefore, interpretable within a framework of fluctuating threshold and two populations. Indeed, it was data of this sort that originally suggested the two populations hypothesis.

We now apply the model to the problem of masking. A population characterized by fluctuating thresholds and a period of nonresponsiveness after firing could be rendered nearly incapable of responding to a stimulus, such as a click, by a continuous stimulus such as noise, even at a very low level. This conclusion is reached in the following manner (3): neural units continually drop in threshold below the average level of the masking noise, and fire. The "location" of the noise in the distribution determines the rate at which such firing occurs. The weaker the noise, the less often a unit fires. If threshold fluctuation is sufficiently rapid, nearly all units will have fired in response to even a weak noise in the 2 msec preceding the click. Hence practically all units will be absolutely refractory at the time the click is presented, and none will respond to it.

If a second population is present as well, whose threshold range lies far above the noise level, it will not be affected. As the noise level is further raised, the number of units belonging to this population that respond to the click will also decrease. The data of Fig. XIII-3 support these predictions. They show that a weak noise eliminates the sensitive population completely, leaving the growth of the insensitive portion of the intensity function substantially intact. A still weaker noise permits the appearance of a partial response from the sensitive population. As suggested above, the noise level at which the masked response is, for example, one half as large as the unmasked response, depends on the rate of threshold fluctuation. On the basis of a simple model of fluctuations, involving random transitions between threshold states, this calculation has been carried out and the rate determined (3). The characteristic time of occupancy of a threshold state is found from these data to lie between 0.25 msec and 0.5 msec.

The significant features of the masking curves are thus seen to follow from the assumptions of the model.

Finally, let us inquire as to the variability in response amplitudes expected on the basis of this model. At a given level of stimulation, S, the probability of a unit firing is p(S). The probability that exactly n units out of a population of N will fire is

$$P(n) = \binom{N}{n} p^n (1-p)^{N-n} \tag{4}$$

Plotted as a function of n, P(n) is peaked at n = Np; for sufficiently large N, P(n) may be fitted by a gaussian distribution. Such a fitting procedure yields the result that

$$\sigma = [Np(1-p)]^{1/2} \tag{5}$$

If we introduce now an explicit dependence on S,

$$\sigma(S) = [Np(S)(1 - p(S))]^{1/2}$$

For A = rn, $P^*(A) = P(n)$, where $P^*(A)$ is the probability of a response amplitude A. Since the distributions P(n) and $P^*(A)$ are related by a scale factor r, it follows that the standard deviation of response amplitudes to a stimulus S is given by

$$\sigma^*(S) = r\sigma(S) = r\,[Np(S)(1 - p(S))]^{1/2}$$

The average, and most probable, response is given by

$$A_{av}(S) = rNp(S) \tag{6}$$

This expression is, of course, the intensity function (Eq. 2). Figures XIII-7(a) and XIII-7(b) show an intensity function for one population and the corresponding function $\sigma^*(S)$. Note that for both very strong and very weak stimuli, $\sigma^*(S) = 0$, since for a maximal stimulus (p(S) = 1) all units respond all of the time, while for a minimal stimulus (p(S) = 0) no unit will ever respond. $\sigma(S)$ is maximal for S such that p(S) = 1/2. The relative variability, given by

$$\frac{\sigma^*(S)}{A_{av}(S)} = \frac{1}{N^{1/2}} \left[\frac{1 - p(S)}{p(S)}\right]^{1/2} \tag{7}$$

is determined primarily by the population size.

If, in addition, a stimulus-independent source of variability is present (for instance, amplifier noise) the total standard deviation of the response is

$$\sigma_T(S) = \left[(\sigma^*(S))^2 + \sigma_A^2\right]^{1/2} \tag{8}$$

Here σ_A represents all additional sources of variation and is assumed to be independent of S. Figure XIII-7(c) shows the function σ_T for a given value of σ_A.

If two more or less disjoint populations are involved, one would expect $\sigma_T(S)$ to have

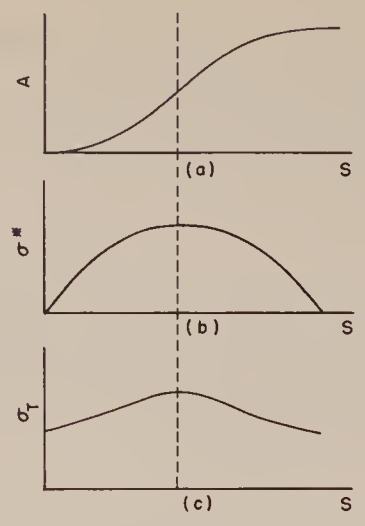

Fig. XIII-7

(a) A one-population intensity function for a gaussian threshold probability distribution. (b) The corresponding function $\sigma^*(S)$ predicted from the model. (c) The function $\sigma_T(S)$ obtained from the model for a given value of σ_A.

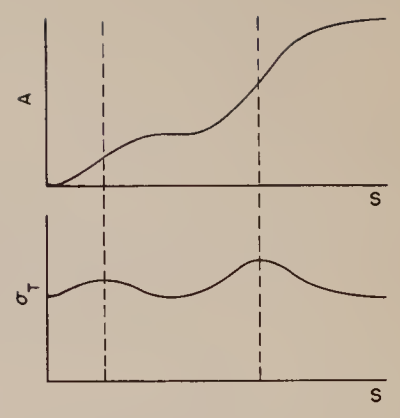

Fig. XIII-8

(a) A two-population intensity function. (b) A corresponding function $\sigma_T(S)$ of the kind predicted by the model.

two peaks. The peaks occur at $p_1(S) = 1/2$ and at $p_2(S) = 1/2$; here the subscripts 1 and 2 refer to the two populations. Figure XIII-8 shows both σ_T and the corresponding intensity function for the two-population case.

If we compare σ_T from Fig. XIII-8 with the variability data of Fig. XIII-4 there is good qualitative agreement with the prediction of the model in the range of the sensitive population. The experimental curve $\sigma(S)$ exhibits a peak at a point where on the basis of the intensity function we conclude that approximately 50 per cent of the units of the sensitive population have contributed. $\sigma(S)$ for the insensitive population does not show the expected behavior. This may be due to our inability to deliver a truly maximal stimulus. Such a stimulus might, of course, overload the mechanical system of the cat's ear.

L. S. Frishkopf, W. A. Rosenblith

References

1. W. A. Rosenblith, M. R. Rosenzweig, Electrical responses to acoustic clicks: influence of electrode location in cats, J. Acoust. Soc. Am. 23, (September 1951).
2. Quarterly Progress Report, Research Laboratory of Electronics, M.I.T., Oct. 15, 1953, pp. 45-50.
3. Quarterly Progress Report, Research Laboratory of Electronics, M.I.T., Jan. 15, 1954, pp. 67-70.
4. Quarterly Progress Report, Research Laboratory of Electronics, M.I.T., July 15, 1954, p. 80.

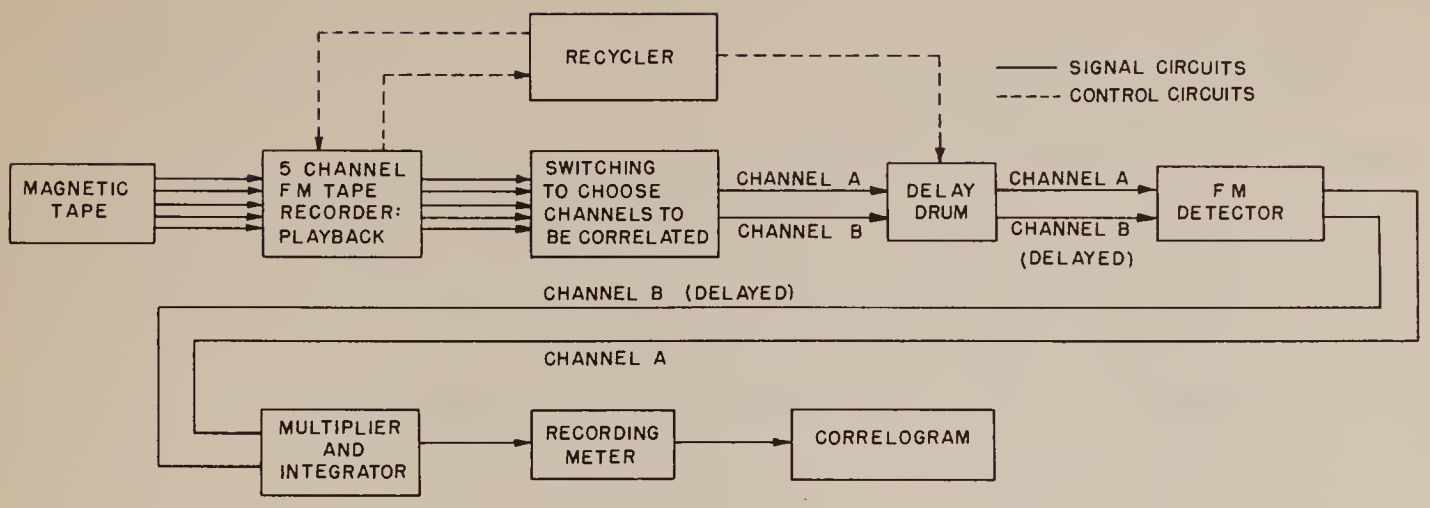

Fig. XIII-9
Block diagram of analog correlator.

B. ANALOG CORRELATOR FOR ELECTROENCEPHALOGRAPHY

With the completion of the recycler and magnetic delay drum (with associated electronics) the analog correlator (Fig. XIII-9) has successfully produced a correlogram from a tape-recorded EEG. The delay drum has already been described (1, 2). The recycler plays through the desired sample of tape, rewinds it to the beginning of the sample and then automatically repeats the play and rewind operations until the correlogram is completed. During each rewinding operation, the recycler advances the movable arm of the drum through one time delay unit ($\Delta\tau$). A piece of silvered tape stuck to the back of the magnetic tape at both ends of the sample to be correlated reflects light into a photocell providing signals for the cycling operations.

A technical report describing the detailed functioning of the complete correlator will be published.

J. S. Barlow, M. A. B. Brazier, R. M. Brown

References

1. Quarterly Progress Report, Research Laboratory of Electronics, M.I.T., Jan. 15, 1954, pp. 71-72.
2. K. Goff, The development of a variable time delay, Proc. I. R. E. 41, 1578-1584 (1953).

XIV. ANALOG COMPUTER RESEARCH

Prof. E. A. Guillemin
Prof. R. E. Scott
N. DeClaris
Y. C. Ho
T. E. Stern

TIME DOMAIN SYNTHESIS BY DELAY LINE TECHNIQUES

Research in the past quarter has resulted in the development of an experimental type of discrete filter and its application to time domain equalization problems in both open- and closed-loop systems.

It has been shown (1, 2) that a discrete filter of the general type

$$D^*(\epsilon^{-sT}) = \sum_{k=0}^{N} a_k \epsilon^{-skT} \tag{1}$$

can be used to approximate the transfer function

$$F(s) = \frac{\sum_{k=0}^{n} b_k s^k}{\sum_{k=0}^{m} c_k s^k} \tag{2}$$

The chief advantage of discrete filters (3) is that mathematically they can be handled easily in time domain, which places in evidence the transient response of a system. Furthermore, discrete filters are more versatile than their conventional counterparts, in the sense that their transfer characteristics can be changed at will after their construction by merely changing the coefficients a_k s in Eq. 1. This property is very useful in practical time domain equalization problems, since experimental adjustment over quite a wide range of transfer characteristics is provided.

Preliminary theoretical study shows that discrete filters can be used to equalize closed loop systems with good results. The approach used is in the time domain and is based on the impulse response of the system.

An experimental discrete filter is being constructed with a magnetic recorder having delayed pick-up heads along a continuous tape loop. The unit will be used in the control loop of a servomultiplier. This will serve not only as an experimental check but also as a test of the practicability of the proposed technique for time domain equalization.

Y. C. Ho

References and Footnote

1. Quarterly Progress Report, Research Laboratory of Electronics, M.I.T., April 15, 1954.
2. Freddy Ba Hli, D. Sc. Thesis, M.I.T., 1953.
3. This filter is essentially a tapped delay line filter that handles continuous input and output signals; thus it differs from the type described in sampled-data systems, although mathematically they are almost equivalent.

XV. NETWORK SYNTHESIS

Prof. E. A. Guillemin
Prof. F. M. Reza
P. M. Lewis II
R. A. Pucel
M. Strieby

VOLTAGE TRANSFER SYNTHESIS – RLC LATTICE

The work on voltage transfer synthesis has been extended to cover the RLC lattice. (The RC lattice was discussed in the Quarterly Progress Report, April 15, 1954.) The necessary and sufficient conditions for a transfer function to be realizable as a lattice have been found, and methods of synthesis have been developed.

1. Theorem

The necessary and sufficient conditions that a voltage transfer function

$$A = \frac{E_2}{E_1} = \frac{K\left(S^n + a_{n-1} S^{n-1} + \ldots + a_1 S + a_0\right)}{S^m + b_{m-1} S^{m-1} + \ldots + b_1 S + b_0} = \frac{KN}{D}$$

be realizable as an RLC lattice are: 1. D is a Hurwitz polynomial; 2. D + KN and D – KN are Hurwitz polynomials. The order of these two polynomials can differ by no more than two. (This condition specifies the maximum value of the parameter K.)

Proof:

(a) The proof of condition 1 is well known and will not be repeated here.

(b) Consider the lattice shown in Fig. XV-1.

The voltage transfer function is

$$A = \frac{KN}{D} = \frac{Z_b - Z_a}{Z_b + Z_a} = \frac{1 - (Z_a/Z_b)}{1 + (Z_a/Z_b)}$$

Solving this equation

$$\frac{Z_a}{Z_b} = \frac{1 - A}{1 + A} = \frac{D - KN}{D + KN}$$

Since the ratio of two positive real impedances must have Hurwitz polynomials in both its numerator and denominator, the theorem is proved.

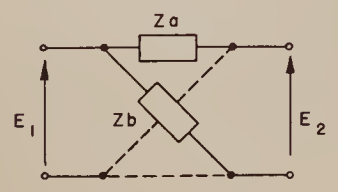

Fig. XV-1
An RLC lattice.

2. Synthesis

Given a voltage transfer function which satisfies the above conditions, one can immediately write

$$\frac{Z_a}{Z_b} = \frac{1 - A}{1 + A} = \frac{D - KN}{D + KN}$$

The problem is then to split Z_a/Z_b into Z_a and Z_b. Three different ways of doing this are suggested.

1. Enough surplus factors can always be added so that Z_a/Z_b can be immediately split into Z_a and Z_b. However, after this is done, the methods of Brune or Bott and Duffin must be used to synthesize the resulting networks. This direct approach may therefore be impractical.

2. If either the odd or the even parts of D + KN and D - KN are proportional, a particularly easy synthesis is possible. The details will be presented for the odd parts proportional. The extension to the other case is obvious.

If

$$\frac{Z_a}{Z_b} = \frac{D - KN}{D + KN} = \frac{m_1 + n_1}{m_2 + kn_1}$$

where m and n are the even and odd parts of the polynomials, then we can write

$$\frac{Z_a}{Z_b} = \frac{1 + (m_1/n_1)}{k + (m_2/n_1)}$$

$$Z_a = 1 + \frac{m_1}{n_1} \quad \text{and} \quad Z_b = k + \frac{m_2}{n_1}$$

Then Z_a and Z_b are realized as lossless networks in series with resistors. Part of this resistance can be removed from the lattice to give a series resistor. If a parallel resistance termination is desired, the function can be split into

$$Z_a = \frac{1}{k + (m_2/n_1)} \quad \text{and} \quad Z_b = \frac{1}{1 + (m_1/n_1)}$$

This type of synthesis will be possible when N is an even or odd polynomial, when D is of the second order, and in certain other particular cases.

3. If the maximum possible gain is not required, a synthesis in terms of partial fractions is possible. Split Z_a/Z_b into

$$Z_a = 1 - A \quad \text{and} \quad Z_b = 1 + A$$

$$\left(\text{or} \quad Z_a = \frac{1}{1 + A} \quad \text{and} \quad Z_b = \frac{1}{1 - A}\right)$$

Expand A in partial fractions. The resulting terms may or may not be realizable as simple RLC circuits. However, those terms that are not, can be made realizable by the addition of a suitable resistance. Consider the 1 in the expressions 1 - A and 1 + A as a one-ohm resistance reservoir that can be used for this purpose. Pick K small enough so that the one ohm is sufficient to make all the terms realizable. The resulting RLC partial fraction canonic forms are well known.

If K is made smaller than is required, some extra resistance will be left over to remove as a series or parallel resistor. Incidentally, the input impedance of this lattice is

$$Z_{in} = \frac{1}{2}(Z_a + Z_b) = \frac{(1-A) + (1+A)}{2} = 1 \text{ ohm}$$

This is particularly convenient for some applications.

P. M. Lewis II

XVI. SWITCHING CONTROL SYSTEMS

Prof. S. H. Caldwell
Prof. D. A. Huffman
Prof. W. K. Linvill
E. J. McCluskey, Jr.

There is a general algebraic method that permits the design of switching circuits to perform according to given specifications (1). For any reasonable set of specifications, it is possible to obtain several appropriate switching circuits.

Often, the design object is to obtain the circuit which, while satisfying the specifications, uses the fewest number of switch contacts or relay springs. The algebraic design method is a great help toward realizing this object; but, since this method always results in a series-parallel type of network, it does not take advantage of possible contact economies that nonseries-parallel (bridge or nonplanar) networks might afford. This report describes a preliminary investigation of switching circuits of the bridge type.

DEFINITIONS

(1) A bridge circuit is defined as a circuit that contains at least one bilateral branch.

(2) A bilateral branch is defined as a branch that contains at least one switch contact and is traversed in both directions in tracing out all possible paths from input to output terminals of the circuit containing the branch. A path is considered to exist even if the occurrence of two complementary transmissions in series prevents signal flow under normal conditions. In other words, the conditions for a branch to be bilateral depend only on the topological properties of the associated network and as such can be determined from the graph (2) of the network.

(3) A bilateral transmission is the transmission function associated with a bilateral branch.

(4) A bridge transmission is any transmission corresponding to a bridge circuit.

(5) A simple bridge circuit is a bridge circuit in which neither the bilateral transmission nor any of its components appear elsewhere in the circuit.

Theorem 1. Any bridge circuit may be realized in the form shown in Fig. XVI-1, where B is the bilateral transmission of one of the bilateral branches.

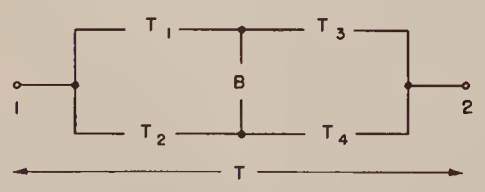

Fig. XVI-1
General form of a bridge circuit.

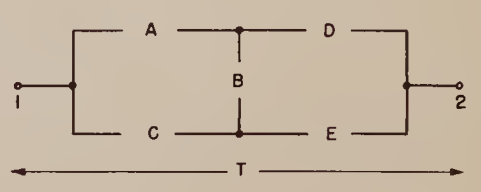

Fig. XVI-2
General form of a simple bridge circuit having bilateral transmission B.

Proof: Any bridge circuit must contain at least one bilateral branch. Let the associated bilateral transmission be denoted by B, and the branch terminals by 3 and 4. Denote the input and output terminals of the circuit by 1 and 2, respectively. By definition there must be a path from 1 to 2, traversing B from 3 to 4; thus there must be a path from 1 to 3 and from 4 to 2. Denote the corresponding transmissions by T_1 and T_4. Similarly a path from 1 to 2 traversing B from 4 to 3 must exist, and hence there must also be transmissions T_2 from 1 to 4, and T_3 from 3 to 2.

Corollary 1. The transmission of any bridge circuit containing a bilateral transmission B can be written in the form:

$$T = B(T_1T_4 + T_2T_3) + T_1T_3 + T_2T_4$$

where $T_1T_3 \not\equiv 0$ or $T_2T_4 \not\equiv 0$, and $BT_2T_3 \not\equiv 0$ or $BT_1T_4 \not\equiv 0$.

(If $T_1T_3 \equiv T_2T_4 \equiv 0$, then $T = B(T_1T_4 + T_2T_3)$, and T may be realized as economically in series-parallel form (without the need for a bilateral transmission B) as in bridge circuit form. Therefore, the requirement that either T_1T_3 or $T_2T_4 \not\equiv 0$ will henceforth be assumed. If $BT_2T_3 \equiv 0$ and $BT_1T_4 \equiv 0$, B is unnecessary; therefore the requirement that $BT_2T_3 \not\equiv 0$ or $BT_1T_4 \not\equiv 0$ will also be assumed.)

Theorem 2. If T is the transmission of a simple bridge circuit with bilateral transmission B, T can be written in the form

$$T = AD + CE + B(AE + CD)$$

where $BAE \not\equiv 0$, or $BCD \not\equiv 0$, AD or $CE \not\equiv 0$, and A, C, D, E are not functions of B.

The corresponding circuit is shown in Fig. XVI-2.

We now proceed to determine under what conditions a transmission $T = f + Bg$ can be realized as a simple bridge circuit with bilateral transmission B.

Expanding A, C, D, E in a standard sum:

$$A = A_0 X_1'X_2'\ldots X_n' + A_1 X_1'X_2'\ldots X_n + \ldots$$

$$C = C_0 X_1'X_2'\ldots X_n' + C_1 X_1'X_2'\ldots X_n + \ldots$$

$$D = D_0 X_1'X_2'\ldots X_n' + D_1 X_1'X_2'\ldots X_n + \ldots$$

$$E = E_0 X_1'X_2'\ldots X_n' + E_1 X_1'X_2'\ldots X_n + \ldots$$

$$AD = A_0D_0 X_1'X_2'\ldots X_n' + A_1D_1 X_1'X_2'\ldots X_n + \ldots$$

$$CE = C_0E_0 X_1'X_2'\ldots X_n' + C_1E_1 X_1'X_2'\ldots X_n + \ldots$$

$$AD + CE = (A_0D_0 + C_0E_0) X_1'X_2'\ldots X_n' + (A_1D_1 + C_1E_1) X_1'X_2'\ldots X_n + \ldots$$

$$f = f_0 X_1' X_2' \ldots X_n' + f_1 X_1' X_2' \ldots X_n + \ldots$$

$$g = g_0 X_1' X_2' \ldots X_n' + g_1 X_1' X_2' \ldots X_n + \ldots$$

It is assumed that T has been simplified by eliminating any terms which appear in both f and g through use of the theorem $X_1^* X_2^* \ldots X_n^* + \left(X_1^* X_2^* \ldots X_n^*\right) B = X_1^* X_2^* \ldots X_n^*$. (The notation X_1^* is used where either X_1 or X_1' may apply.) Thus the situation that $f_i = 1$, and $g_i = 1$ will not occur. In other words, we have either $f_i = g_i'$ or $f_i = 0$ and $g_i = 0$. However, whenever we have $f_i = 1$, g_i may also be set equal to 1 in order to simplify the resulting circuit without changing T. Thus it is sufficient to consider the three possibilities: $f_i = 0$, $g_i = 0$; $f_i = 0$, $g_i = 1$; and $f_i = 0$, $g_i = \phi$, where ϕ signifies that either a 0 or 1 may be assumed to apply.

Now we assume

$$T = f + Bg = AD + CE + B(AE + CD)$$

therefore

$$f = AD + CE, \quad g = AE + CD$$

Equating coefficients of like products $\left(X_1^* X_2^* \ldots X_n^*\right)$ yields

$$A_i D_i + C_i E_i = f_i$$

$$A_i E_i + C_i D_i = g_i$$

(1) Assume $f_i = g_i = 0$

$$A_i D_i + C_i E_i = 0 \qquad \text{either } A_i = C_i = 0$$

$$A_i E_i + C_i D_i = 0 \qquad \text{or } D_i = E_i = 0$$

(2) Assume $f_i = 1$, $g_i = 0$

$$A_i D_i + C_i E_i = 1 \qquad \text{either } A_i = D_i = 1$$

$$A_i E_i + C_i D_i = \phi \qquad \text{or } C_i = E_i = 1$$

(3) Assume $f_i = 0$, $g_i = 1$

$$A_i D_i + C_i E_i = 0 \qquad \text{either } A_i = E_i = 1,\ C_i = D_i = 0$$

$$A_i E_i + C_i D_i = 1 \qquad \text{or } C_i = D_i = 1,\ A_i = E_i = 0$$

Consider the requirement $BAE \neq 0$ or $BCD \neq 0$. This requires $AE \neq 0$ or $CD \neq 0$. But $AE = A_0 E_0 X_1' X_2' \ldots X_n' + A_1 E_1 X_1' X_2' \ldots X_n + \ldots$. So that, if $AE \neq 0$, then $A_i = E_i = 1$

for at least one i. Similar reasoning for BCD $\neq 0$ leads to the requirement that $A_i = E_i = 1$ or $C_i = D_i = 1$ for at least one i.

Now consider the requirement that AD or CE $\neq 0$. This in turn leads to the requirement that $A_i = D_i = 1$ or $C_i = E_i = 1$ for at least one i.

In summary, we require that

$$\left.\begin{array}{ll} \text{(i)} & A_i = E_i = 1 \text{ or } C_i = D_i = 1 \\ \text{(ii)} & A_i = D_i = 1 \text{ or } C_i = E_i = 1 \end{array}\right\} \quad \text{for at least one i}$$

Study of cases 1, 2, and 3 shows that (i) requires that $g_i \neq 0$, and (ii) requires that $f_i \neq 0$.

Theorem 3. If $T = f + gB$ where f and g are not functions of B and $f \neq 0$ and $g \neq 0$, then T may be realized as a simple bridge circuit which contains B only as the bilateral transmission.

Theorem 4. If a transmission T is expanded in a standard sum:

$$T = T_0 X_1' X_2' \ldots X_n' + T_1 X_1' X_2' \ldots X_n + \ldots$$

and if whenever $T_i = 1$ for i even (odd) $T_i + 1 = 1$ ($T_i - 1 = 1$) also (for at least one such i), and if $T_i = 1$ for i odd (even) with $T_i - 1 = 0$ ($T_i + 1 = 0$) (for at least one such i), then T can be realized as a simple bridge circuit having $X_n (X_n')$ as the bilateral transmission.

Example 1.

$$T = xy + x'w + z(w+y)$$

If we let $f = xy + x'w$, $g = w + y$, it is clear that T can be realized as a simple bridge circuit with z bilateral. For the order wxy, $f_i = 1$ for i = 3, 4, 5, 7 and $g_i = 1$ for 1, 6. Thus for i = 1, 6

$$A_1 = E_1 = 1, \quad C_1 = D_1 = 0$$

$$A_6 = E_6 = 0, \quad C_6 = D_6 = 1$$

for i = 3, 4, 5, 7

$$A_i = D_i = 1 \text{ and } C_i = \phi, \; E_i = \phi \text{ or } A_i = \phi, \; D_i = \phi, \text{ and } C_i = E_i = 1$$

for i = 0, 2

$$A_i = C_i = 0 \text{ and } D_i = \phi, \; E_i = \phi \text{ or } D_i = E_i = 0, \; A_i = \phi, \; C_i = \phi$$

Figure XVI-3 shows how the A, C, D, E functions may be simultaneously minimized by the use of Karnaugh charts in accordance with the above constraints. The first row of tables shows the assignment for the $g_i = 1$ case; the second row, the assignment for the $g_i = f_i = 0$ case; the third row, the assignment for the $f_i = 1$ case; and the final row,

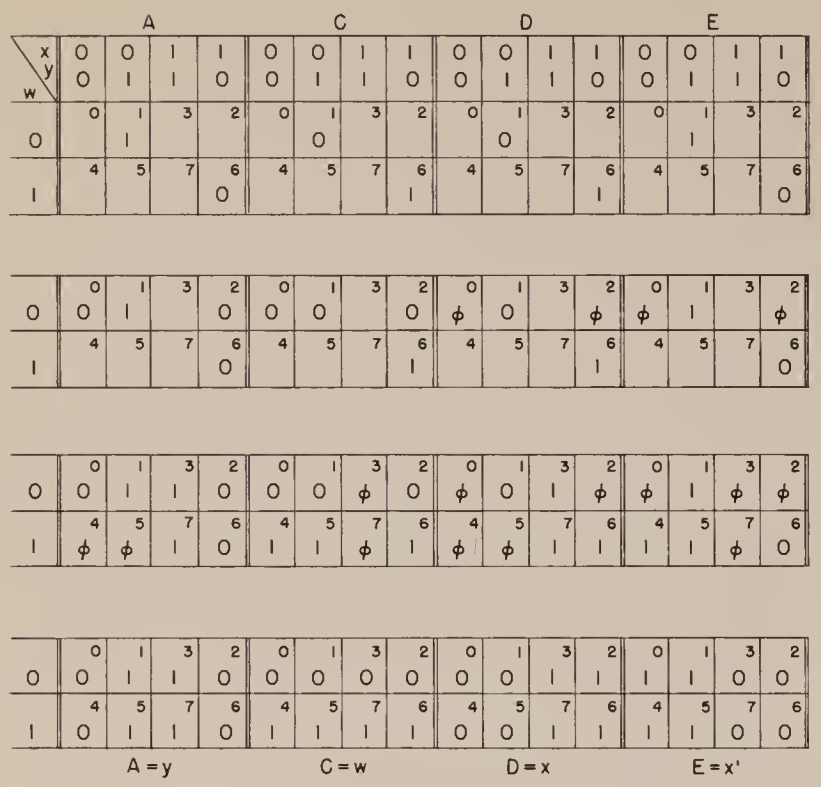

Fig. XVI-3

Karnaugh charts used to minimize A, C, D, and E, simultaneously.

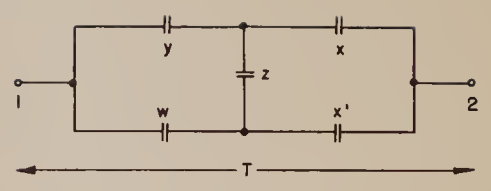

Fig. XVI-4

Bridge circuit realization of transmission T = xy + x'w + z(w+y).

the selection of the ϕ condition used in order to complete the specification.

The resulting bridge circuit is shown in Fig. XVI-4.

Another method by which this circuit could have been realized will be illustrated. By Theorem 2, if z is the bilateral transmission of a simple bridge circuit having transmission T then T can be written: T = AD + CE + z(AE + CD). We now expand the transmission T being considered about z, simplify, and equate the two expressions. Thus we have

$$T = yx + wx' + z(y+w) = AD + CE + B(AE + CD)$$

where B = z, and yx + x'w = AD + CE. Set

$$yx = AD;\ y = A,\ x = D$$

$$wx' = CE;\ w = C,\ x' = E$$

Now form AE + CD = yx' + wx. This clearly is not equal to w + y, but when the complete expression for T is formed

$$T = xy + x'w + z(xw + x'y)$$

and it is noted that

$$w(x' + xz) = w(x' + z) \text{ and } y(x + x'z) = y(x+z)$$

it is evident that T = xy + x'w + z(xw + x'y) does equal xy + x'w + z(w+y), as required. This assignment of A, B, C, and D leads to the circuit shown in Fig. XVI-4. Another possible assignment would have been

$$A = X,\ D = y,\ E = w,\ C = x'$$

This leads to the circuit of Fig. XVI-4 with terminals 1 and 2 interchanged.

E. J. McCluskey, Jr.

References

1. S. H. Caldwell, Teaching Notes, Courses 6.567 and 6.568, M.I.T.
2. E. A. Guillemin, Introductory Circuit Theory (John Wiley and Sons, Inc., New York, 1953) p. 5.